UNIVERSITY OF KWAZULU-NATAL

INYUVESI YAKWAZULU-NATALI

STUDIES ON THE RELATIONSHIP BETWEEN TOTAL ATMOSPHERIC OZONE COLUMN AND SOLAR RADIATION RECEIVED BY VARIOUS REGIONS OF SOUTH AFRICA and AFRICA

By

JEREMIAH AYODELE OGUNNIYI

212562297

A thesis submitted in fulfilment of the academic

Requirements for the degree of

Doctor of Philosophy

In the School of Chemistry and Physics

University of KwaZulu-Natal

Durban

SUPERVISOR: PROFESSOR VENKATARAMAN SIVAKUMAR

NOVEMBER 2018

PREFACE

The work described by this thesis was carried out at the University of KwaZulu-Natal, School of Chemistry and Physics, Durban, from August 2014 until November 2018, under the supervision of Professor Venkataraman Sivakumar

This thesis is entirely, unless specifically contradicted in the text, the work of the author and has not been previously submitted, in whole or in part, to any other tertiary institution. Where use has been made of the work of others, it is duly acknowledged in the text

Signed: ________________________ Jeremiah Ayodele Ogunniyi

Date: _________________________

As the candidate's supervisor, I have/have not approved this thesis/dissertation for submission.

Signed: __________________________ Professor Venkataraman Sivakumar

Date: _________________________

DECLARATION I – PLAGIARISM

I, Jeremiah Ayodele Ogunniyi, declare that

1. The research reported in this thesis, except where otherwise indicated, is my original research.
2. This thesis has not been submitted for any degree or examination at any other university.
3. This thesis does not contain other persons' data, pictures, graphs or other information, unless specifically acknowledged as being sourced from other persons.
4. This thesis does not contain other persons' writing, unless specifically acknowledged as being sourced from other researchers. Where other written sources have been quoted, then:
   a. Their words have been rewritten but the general information attributed to them has been referenced
   b. Where their exact words have been used, then, their writing has been placed in italics and inside quotation marks and referenced
5. This thesis does not contain text, graphics or tables copied and pasted from the internet, unless specifically acknowledged, and the source being detailed in the thesis and in the Reference section

Signed: ______________________________

DECLARATION II – PUBLICATIONS

Ozone climatology and its variability from ground based and satellite observations over Irene, South Africa (25.5^{O}S; 28.1^{O}E) – Part 2: Total Column ozone variations, **J. Ogunniyi** and V. Sivakumar, *Atmósfera, 31(1), 11-24, 2018.*

Ozone climatology and its variability from ground based and satellite observations over Irene, South Africa (25.5^{O}S; 28.1^{O}E) – Part 1: Vertical variations in the troposphere and stratosphere height region, V. Sivakumar and **J. Ogunniyi,** *Atmósfera, 30(4), 337-353,* 2017.

Variations in Temperature, Ultraviolet Aerosol Index, Cloud Pressure and Total Ozone over five South African Cities, **J. Ogunniyi** and V. Sivakumar, *Journal of Energy in Southern Africa* (submitted June 2018)

Interannual and seasonal variation in surface solar radiation, ozone and aerosol over Africa , **J. Ogunniyi** and V. Sivakumar, *Atmósfera* (*In revision – Atmosfera*)

Effects of Aerosol and Clouds on Surface Energy Balance over selected regions of South Africa, **J. Ogunniyi,** K. Raghavendra Kumar and V. Sivakumar, *Meteorology and Atmospheric Physic*s (Submitted July 2018)

Response of Southern Hemisphere midlatitude Ozone during Magnetic Cloud event: A case study, O. Ogunjobi, V. Sivakumar and **J. Ogunniyi,** *Journal of Atmospheric and Solar-Terrestrial Physics* (Submitted November 2018)

ARTICLES IN PEER-REVIEWED NATIONAL/INTERNATIONAL CONFERENCE PROCEEDINGS

Seasonal variation in Global, Direct, Diffuse radiation over South African cities and Namibia, **J. Ogunniyi** and V. Sivakumar, *International conference on solar power system for Namibia, 2018.*

Temporal variation in solar radiation, UV index and its effect on ozone variations over Durban, South Africa – initial result, **J. Ogunniyi**, V. Sivakumar and P. Govender, *Proc. of 31st Annual conference of South African society for atmosphere science, ISBN 978-0-620-67825-4,21-22 September 2015, Hennops River Valley, Pretoria (South Africa), S2b.3, 53-56,* 2015.

Study of aerosol indirect effect and its impact over a coastal city on South Africa, Joseph A. Adesina, V. Sivakumar, Raghavendra K. Kumar, **J. Ogunniyi** and P. Singh, *Proc. of 31st Annual conference of South African society for atmosphere science, ISBN 978-0-620-67825-4,21-22 September 2015, Hennops River Valley, Pretoria (South Africa), P1, 1-4,* 2015.

A new 2-D scan portable Durban LiDAR for atmospheric studies – system description and first scientific result, V. Sivakumar, **J. Ogunniyi**, Joseph A. Adesina, P. Singh and L. Shikwambana *Proc. of 31st Annual conference of South African society for atmosphere science, ISBN 978-0-620-67825-4,21-22 September 2015, Hennops River Valley, Pretoria (South Africa), S1.3, 17-19,* 2015.

Geospatial (Latitudinal and Longitudinal) variability of ozone over South Africa, **J. Ogunniyi** and V. Sivakumar, *Proc. of 30th Annual conference of South African society for atmosphere science, ISBN 978-0-620-62777-1, 01-02 October 2014, Potchefstroom (South Africa), pp, 13-16, 2014.*

DEDICATION

This thesis is dedicated to the Almighty for His mercies and faithfulness, my Saviour and Potentate.

ACKNOWLEDGEMENT

I want to sincerely appreciate the Almighty God for successfully seeing me through my studies. For the gift of life, His protection, provision, preservation and pardon. It is by His mercies that I have not been consumed.

Special thanks to my supervisor Professor Venkataraman Sivakumar who took his time to painstakingly read my thesis and made necessary corrections. His contributions and input to this research work are immense. I also appreciate him for the role he played in providing fund and conducive environment for this study to be a success. I also want to thank the University of KwaZulu Natal for providing an enabling environment for the completion of my studies.

My gratitude also goes to late pastor Adewumi for the part he played in securing my admission to UKZN. I would also like to thank the leadership of Deeper Life Campus Fellowship, Pastor Adesina and Pastor Olusanya for their support. Sis Ruth for the constant supply of food, not making me to worry regarding what to eat. Special thanks also go to other members of DLCF such as Pastor Martins, the Akinolas, Adelekes, Olukanmis, my supporting friends Tunde, Tola, Ayo, Dr and Mrs Merisi, David Adebiyi, Sola, Soji, Nathi, Gabriel and all members of the Deeper Life Bible Church, KZN. Special mention also goes to Onyekachi Esther who came along the way and has become part of my family.

Finally, my appreciation goes to my dad, mum, brother, sister and my beautiful wife for their emotional, financial, moral, spiritual and all-round support from the commencement to the completion of my PhD program.

CONTENTS

List of Figures

List of Tables

List of Acronyms

2AP: Two-Axis Positioner

AIRS: Atmospheric Infrared Sounder

AOD: Aerosol Optical Depth

ARF: Aerosol Radiative Forcing

ARM: Atmospheric Radiation Measurement

BSRN: Baseline Surface Radiation Network

CCD: Charge Couple Device

CERES: Cloud and the Earth's Radiant Energy System

CF: Cloud Fraction

CFCs: Chlorofluorocarbons

CLAES: Cryogenic Limb Array Etalon Spectrometer

DHI: Diffuse Horizontal Irradiance

DNI: Direct Normal Irradiance

DOAS: Differential Optical Absorption Spectroscopy

DSSF: Downwelling Surface Shortwave Radiation

DU: Dobson Units

EBAF: Energy Balanced and Filled

ECMEF: European Centre for Medium-range Weather Forecasts

EOS: Earth Observing System

EPTOMS: Earth Probe Total Ozone Mapping Spectrometer

ERBE: Earth Radiation Budget Experiment

G: Ground heat flux

GHI: Global Horizontal Irradiance

GMAO: Global Modelling and Assimilation Office

GOME: Global Ozone Monitoring Experiment

GOMOS: Global Ozone Monitoring by Occultation of Stars

H: Sensible heat flux

HALOE: Halogen Occultation Experiment

HIRDLS: High Resolution Dynamics Limb Sounder

HRDI: High Resolution Doppler Imager

IASI: Infrared Atmospheric Sounding Interferometer

IMF: International Monetary Fund

ISEA: Integrated Earth System Analysis

JMA: Japan Meteorological Agency

LH: Latent heat flux

LIDAR: Light Detection and Ranging

LIMS: Limb Infrared Monitor of the Stratosphere

LIS: Lightning Imaging Sensor

LW: Longwave flux

MERRA: Modern Era Retrospective Analysis for Research and Application

METOP: Meteorological Operational Satellite Program

MIPAS: Michelson Interferometer for Passive Atmospheric Sounding

MLS: Microwave Limb Sounder

NASA: National Aeronautics and Space Administration

NCEP: National Centres for Environmental Prediction

NIP: Normal Incidence Pyrheliometers

NOAA: National Oceanic and Atmospheric Administration

OMI: Earth Probe Total Ozone Mapping Spectrometer

PBL: Planetary Boundary Layer

PR: Precipitation Radar

PV: Photovoltaics

RADAR: Radio Detection and Ranging

SABER: Sounding of the Atmosphere using Broadband Emission Radiometry

SAURAN: South African Universities Radiometric Network

SAWS: South African Weather Service

SBUV: Solar Backscatter Ultraviolet System

SCIAMACHY: Scanning Imaging Absorption Spectrometer for Atmospheric Chartography

SHADOZ: Southern Hemisphere Additional Ozonesondes

SNPPA: Suomi National Polar-Orbiting Partnership

SURFRAD: National Oceanic and Administration Surface Radiation

SW: Shortwave flux

TMI: TRRM Microwave Imager

TOMS: Total Ozone Mapping Spectrometer

TRMM: Tropical Rainfall Measuring Mission

TRS: Tropospheric Emission Spectrometer

UARS: Upper Atmosphere Research Satellite

UV: Ultraviolet

UVAI: Ultraviolet Aerosol Index

VIRS: Visible Infrared Radiometer

WLS: White Light Source

ABSTRACT

The importance and need for solar energy man and living organisms cannot be overemphasised. It is therefore necessary to estimate the amount of solar radiation incident on South African surfaces and how it can be harnessed for solar energy application. The amount of solar radiation received by a surface depends on solar elevation, weather patterns, geographical location, cloud cover, aerosols, time of the day as well as surface reflectivity. Some of these factors influencing the amount of solar radiation are studied in this thesis. We made use of measurements from the South African Universities Radiometric Network (SAURAN), Ozone Monitoring Instrument (OMI), Clouds and the Earth's Radiant Energy System (CERES) and the Modern Era Retrospective Analysis for Research and Application (MERRA) over different South African surfaces by extension, Africa.

Measurements from the SAURAN network were used to study the seasonal variation in global horizontal irradiance (GHI), direct normal irradiance (DNI) and diffuse horizontal irradiance (DHI) over South African cities and Namibian city from 2013 to 2017. The selected South African cites are Alexander Bay, Durban, Bloemfontein, Pretoria and Port Elizabeth while Windhoek was selected in Namibia. Over a longer period, we examined the trend in shortwave flux and total cloud fraction over the same surfaces using MERRA data. The results reveal summer maximum and winter minimum for GHI, DNI and DHI. We observed that measurements of GHI, DNI and DHI from Durban and Port Elizabeth were much higher than other locations. For shortwave flux over the surfaces, the result showed that the North-western region received the highest amount of solar radiation while the South-eastern region received the least. This decrease down east was linked with low cloud fraction in the Northwest while the cloud fraction in the Southeast was very high. However, the amount of solar energy received in the South-eastern part of South Africa is still higher than the amount received in the United States and several European countries who are maximizing solar energy potential. The result revealed that South Africa received good amount of solar radiation throughout the year and this must be harnessed more. We obtained a statistically significant trend in shortwave flux of 2.65 Wm^{-2} per decade over Alexander Bay between 2009 and 2017 while a significant trend of 2.34 Wm^{-2} per decade was obtained in Port Elizabeth between 2000 and 2009.

We then investigated the seasonal variation in temperature, ultraviolet aerosol index (UVAI) and total column ozone over different geographic zones of South Africa using datasets from OMI from 2004 to 2016. Cape Town was selected for the southern region, Springbok in the west, Durban for east while Irene and Johannesburg were selected for the Northern region. The results indicated the influence of warm Agulhas current on Durban temperature and cold Benguela current on Cape Town temperature. The result of seasonal variation in UVAI showed a spring time maximum attributed to biomass burning. High UVAI in Durban was linked to significant emissions from local sugar cane burning while that of Cape Town was attributed to marine aerosols. Ozone seasonality shows the well-established spring time

maximum and autumn minimum for southern mid-latitudes. We then used second order Fourier decomposition to determine the increasing and decreasing trend in UVAI and total ozone.

This study was then extended over Africa as we estimated the interannual and seasonal variation in shortwave flux, ozone and aerosol index over Africa. The results reveal that Eastern, Central and Southern Africa received more solar radiation compared to Northern and Western Africa. However, all regions received good amount of radiation which makes Africa a potential place for solar energy exploration. In the eastern part of Africa, high ozone was observed in Malindi which was attributed to its unique location while a systematic increase in total ozone was observed in Ethiopia. For western regions of Gambia and Senegal, ozone trends were similar and its precursors were suggested to be from natural sources with little anthropogenic contributions. High ozone in Mozambique was attributed to the atmosphere being rich in carbon dioxide, carbon monoxide, methane, organic and inorganic particles as well as biomass burning. Total ozone in Algeria was low compared to other North African regions. This was attributed to the injection of cold and dry air from higher latitudes to southern Spain and Algeria which creates vortex on the Algerian coast and the formation of cyclone. However, in Morocco, ozone was very high and it was linked to the presence of high-level volatile organic compounds from forests made up of Eucalyptus and Pine trees. The result of the Aerosol Index (AI) showed very high absorption properties in Namibia being one of the three places on earth with persistent low-level cloud and the only location with steady supply of tiny aerosol particles from inland fires. High aerosols index observed in Algeria linked to high desert fires resulting in pollutions while high aerosol index in Congo was attributed to high mineral dust concentration from the Sahara and high nitric acid concentrations from biomass burning in the Congo basin.

We also assessed the effect of aerosols and clouds on surface energy budget over eight South African regions using MERRA and CERES datasets. Both datasets showed similar pattern in climatology and interannual variability of both shortwave and longwave radiation. We determined aerosol forcing on both shortwave and longwave flux and showed that it had more effects on shortwave compared to longwave which results in dimming. We obtained the Bowen ratio and it showed a strong negative correlation with aerosol effect anomaly in winter and spring which indicates that as aerosol effect increases, less radiation reaches the earth.

CHAPTER ONE

1.0 INTRODUCTION

1.1 The Earth's Atmosphere

The earth's atmosphere consists of gases such as Nitrogen (78 %), Oxygen (21 %) and trace gases (1 %) from different sources which surround the earth (Seinfeld and Pandis, 2016). The earth is believed to be the only planet that can sustain life in the solar system, although it has been discovered that living things can survive in Mars. The atmosphere is a very thin layer which wraps around the earth. It is much more than just the air we breathe in as it serves as a buffer which prevents meteorites from striking the earth, and harmful radiation from penetrating making earth's temperature comfortable (Aucamp, 2007).

The earth's atmosphere is divided into five layers based on temperature variations, the troposphere, stratosphere, mesosphere, thermosphere and exosphere. The atmosphere thins out with height until the gases dissipate in space. The troposphere is the closet layer to the earth surface and is 7 km to 18 km thick. It extends to about 18 km at the equator but is thinner at the polar regions. In this height region, temperature decreases with increasing height (Turner and Overland, 2009). This layer is basically composed of 70% Nitrogen, 21 % Oxygen as well as almost all atmospheric water vapour. Most clouds are found in the troposphere due to the abundance of water vapour (Christensen et al., 2013). The tropopause, which marks transition between the troposphere and stratosphere is a region where temperature no longer decreases with height and could be as low as -57^{o}C (Wang et al., 2018).

The stratosphere lies just above the troposphere and is separated from the troposphere by the tropopause. The stratosphere may extend to about 50 km in altitude. In this layer, we have the abundance of ozone which absorbs harmful radiation from the sun, thereby heating the atmosphere (Sivakumar et al., 2007). Stratospheric air is very dry with relative humidity of $\leq$ 5 % and is about a thousand times less dense than air at sea level (Trickl et al., 2018). Due to the less dense of the air in this region, weather balloons and jet aircrafts reach their operational altitude. It contains a very limited amount of water vapours resulting in the presence of very few clouds found. However, polar stratospheric clouds are formed within stratospheric heights in the poles when temperature goes below -81^{o}C (Tabazadeh et al., 1994). This results in the formation of the ozone hole. In contrast to the troposphere, temperature increases with increasing height in the stratosphere.

The mesosphere is directly above the stratospheric layer of the earth's atmosphere and extends from 50 km to 85 km The mesosphere and the stratosphere are sometimes referred to collectively as the middle atmosphere. This region is the coldest in the earth's atmosphere. As in the troposphere, temperature decreases with increasing height here. Near the top of this layer, temperature is about -90^{o}C. This layer is quite difficult to study as weather balloons and aircrafts cannot fly high enough to reach it. Fan et al (2007) opined that satellite instruments are not sufficient for mesospheric measurements especially when the solar zenith angle exceeds 92^{o} as their orbit is located above the mesosphere. However, other researchers have shown that satellite instruments such as The Halogen Occultation Experiment (HALOE), Sounding of the Atmosphere using Broadband Emission Radiometry (SABER), the High Resolution Doppler Imager (HRDI), Michelson Interferometer for Passive Atmospheric Sounding (MIPAS), the Global Ozone Monitoring by Occultation of Stars (GOMOS) can accurately measure in the mesosphere (Bertaux et al., 2010; Marsh et al., 2002; Remsberg, 2008; Smith et al., 2013; Strelnikov et al., 2013). Sounding rockets, Light Detection and Ranging (LIDAR) and Radio Detection and Ranging (RADAR) are also used for measurements in this region. There is high iron and metal concentration in the mesosphere due to meteors that do not vaporise lingering in this layer (Plane et al., 2015). High altitude clouds such as Noctilucent clouds are formed in the mesosphere.

The thermosphere extends from about 85 km to between 500 km and 1000 km. It is the layer directly above the mesosphere and below the exosphere. In the lower thermosphere, below 300 km altitude, there is an increase in temperature after which temperature decreases steadily with increasing height. Thermospheric temperatures are greatly influenced by solar activities (Yigit and Medvedev, 2010). Temperature is about 500^{o}C hotter when the sun is very active than when it is not and about 200^{o}C hotter in the day than in the night. During the period when the sun is very active, high energy radiations are emitted which expands the thermosphere (Lei et al., 2010). This expansion makes the height of the thermopause to vary between 500 km and 1000 km. This heating and expansion results in changes in the density of air which generates a drag force on satellites found in this region. It is necessary for engineers to take this into account when calculating orbits as they may need to boost the satellites to offset the effects of the drag force (Lei et al., 2010). The main components of air in the upper thermosphere are atomic oxygen, atomic nitrogen and helium. The aurora occurs in the thermosphere. When charged particles from space collide with atoms and molecules at high latitudes, they are excited to a higher energy state. This results in colourful aurora display as these atoms and molecules shed the excess energy by emitting photons of light (Shematovich et al., 2006).

The uppermost layer of the earth's atmosphere is the exosphere. Some scientists consider the thermosphere to be the uppermost layer of the earth's atmosphere as they believe that the exosphere is in space while other scientists believe that the exosphere is actually part of our planet's atmosphere. Depending on the activity of the sun, the exosphere may extend from 500 km or 1000 km to about 190,000 km which is about half way to the Moon. Geocorona, a region of ultraviolet radiation glow formed by scattered hydrogen atoms around 100,000 km have been detected by satellites (Shematovich et al., 2006). Air in the exosphere is so thin that it can be likened to the airless void of outer space that they rarely collide. Most atoms and molecules escape to the outer space from the exosphere.

1.2 Atmospheric Ozone

Aquatic organisms make use of solar energy to split molecules of water vapour (H_2O) and carbon dioxide (CO_2), then recombine them to form molecular oxygen (O_2) (NASA). This process is referred to as photosynthesis. Some of the created oxygen combines with organic carbon to form carbon dioxide while remaining oxygen atoms accumulate in the atmosphere. In the stratospheric height region, molecular oxygen absorbs ultraviolet radiation which splits them to oxygen atoms. The atoms then combine with oxygen molecules which results in ozone. Ozone in this region absorbs dangerous ultraviolet radiation and prevents it from reaching the earth. Ozone's ability to absorb ultraviolet radiation leads to its destruction. During ozone's absorption of ultraviolet radiation, it dissociates to molecular oxygen and then to oxygen atom. These molecular and atomic oxygens gain kinetic energy produce, heat during the dissociation process, thereby increasing the atmospheric temperature (Mlynczak et al., 2013).

Apart from solar radiation affecting the amount of ozone in the atmosphere, compounds containing either chlorine (CFCs) or bromine have the capacity to alter ozone levels in the atmosphere (McCormick et al., 1995). Chlorofluorocarbons (CFCs) are harmless and unreactive with materials in the troposphere, they were created to reduce occupational hazards of compressor explosions and as substitutes for toxic refrigerant gases. Since CFCs are unreactive and insoluble in water, after years of accumulation in the troposphere, they have gradually moved to the stratosphere where they are broken by photodissociation when high ultraviolet radiation breaks them down. Atomic chlorine, a catalyst for ozone depletion is released during photodissociation, leading to massive ozone depletion when it reacts with ozone (Solomon, 1999).This process continues and only stops when there is insufficient amount of atomic chlorine to fuel the process.

The control of ozone depletion started in the early 1970s when concerns were raised over emissions from aerosol spray cans and supersonic transport. The United States government then banned the use of CFCs in aerosols when it was made known to them that CFCs depleted stratospheric ozone, which increased the possibility of skin cancer (Velders et al., 2007).

Below the stratosphere, in the troposphere, ozone is harmful and dangerous to living organisms. It acts as a pollutant and a strong photochemical oxidant which damages rubber, plastics, plants and animals. The ratio of protective and destructive ozone in the atmosphere however depends on the processes that create and destroy them. As ozone depletion continued, it became an international issue which led to the United Nations Environmental Program to sign an agreement in September 1985 to cut back the production of CFC by 50%. Since the enactment of the Montreal Protocol, ozone has experienced gradual recovery (Newchurch et al., 2003).

It is important to note however that over the years, natural processes have regulated the amount of atmospheric ozone. Seasons, time of solar activity, wind direction often change ozone level in the atmosphere (Shindell et al., 1999). Natural disasters such as volcanic eruptions also affect atmospheric ozone concentrations. The most significant change in ozone concentration is observed in the south pole (Oltmans et al., 2008). During long polar nights, there is the formation of cold stratospheric air which stays within this polar vortex during winter resulting in the formation of polar stratospheric clouds. After the long polar winter, the arrival of sunlight makes ozone very vulnerable which results in major ozone loss in the southern hemisphere (Steele et al., 1983; Toon et al., 1990). This region with the greatest ozone depletion is known as the ozone hole which appears in southern spring after the coldest season. However, in the northern hemisphere, the polar vortex is not as strong as the one in the southern hemisphere, thereby breaking and reforming during winter months (James et al., 2000).

1.3 Ozone Measurement

The measurement of ozone has started around 1913. Few years later, British meteorologists, Dobson developed a spectrophotometer later named after him for ozone measurement (NOAA). Since then, improvements in the instrument as well as the development of satellite instruments have taken place. Ground-based instruments such as the Dobson spectrophotometer and more recently, in the late 1980s the automated Brewer spectrometer have provided long-term monitoring of ozone (Kerr et al., 1988; McPeters and Komhyr, 1991). Other instruments such as the Light Detection and Ranging (Lidar) and ozonesondes have been used in measuring ozone. The Dobson and Brewer spectrometers measure the total column of ozone in the atmosphere while Lidar and ozonesondes measure the vertical distribution of ozone. These ground-based instruments are very effective and accurate in their ozone estimation. Series of campaign measurements have taken place over time in order to study ozone due to its importance in energy balance. However, lack of consistency in ozonesonde launches have limited research in this area. This brought about the Southern Hemisphere Additional Ozonesondes (SHADOZ) project which aimed at correcting the inconsistency in ozonesonde launches at operational sites (Thompson et al., 2003). Though the SHADOZ project helped improve ozone knowledge in operational sites, the cost of maintenance has been very high which led to a stop in ozonesonde launches in some sites. Despite the effectiveness and accuracy of ground-based instruments, they have the limitation of global coverage as they can only measure the points where they are being launched. This necessitated the need for satellite instruments that can provide global coverage (Bowman and Krueger, 1985; Fioletov et al., 2002). Satellite instruments have been effective in atmospheric chemistry by providing wide range of knowledge about the atmosphere. Some of the satellite instruments which have enhanced knowledge about ozone include the Total Ozone Mapping Spectrometer (TOMS) – being the first satellite instrument launched October 24, 1978 to measure ozone (NASA). Its operation was discontinued in May 1993. Meteor-3 was launched in 1991 though its overpass was for a short time. Over the years, other satellite instruments have been launched such as the Solar Backscatter Ultraviolet

System (SBUV), the Limb Infrared Monitor of the Stratosphere (LIMS). Both of these instruments were on board the Nimbus-7 aircraft upon which the TOMS instrument was launched. The Upper Atmosphere Research Satellite (UARS) was launched 12th September 1991 carrying 10 instruments. The Cryogenic Limb Array Etalon Spectrometer (CLAES), The Halogen Occultation Experiment (HALOE) were both on board. The Earth Probe Total Ozone Mapping Spectrometer (EPTOMS) was launched 2nd July 1996 and was operational till December 2005. The Ozone Monitoring Instrument (OMI) measuring total column ozone was launched October 2004 with the Microwave Limb Sounder (MLS) measuring ozone vertical profile on the Aura satellite and it is still in operational till now. The High Resolution Dynamics Limb Sounder (HIRDLS) was also on board the Aura satellite. The Global Ozone Monitoring Experiment I (GOME-1) was launched April 1995 and was in operational till 2003. An improved version GOME-2A was launched in 2007 while GOME-2B, an improved version of GOME-2A was launched in 2012. The Infrared Atmospheric Sounding Interferometer (IASI) was first launched on board the Meteorological Operational Satellite Program-A (METOP-A) 19th October 2006 while the second program was launched in 2012. All these instruments have provided a global view on both the vertical profile (very few) as well as the total column concentration of atmospheric ozone (Ogunniyi 2015).

Due to the importance of ozone and its effect on the energy budget and balance of the earth, different researches have looked at its variability and climatology on local, regional and global scales. Several researchers have studied ozone on a global stage (Fioletov et al., 2002; McPeters and Labow, 1996; McPeters et al., 1997; McPeters et al., 2007; Ziemke et al., 2011) while (Chandra et al., 1996; Mahendranth and Bharathi, 2012; Nair et al., 2013) have studied ozone in the northern hemisphere. Few researchers (Bodeker et al., 2007; Sivakumar et al., 2007; Thompson et al., 2003) have studied ozone in the southern hemisphere; while in South Africa, most studies have concentrated over Irene (Ogunniyi and Sivakumar, 2018; Sivakumar and Ogunniyi, 2017; Semane et al., 2006).

1.4 Earth's Energy Budget

The knowledge of energy entering and leaving the earth provides information on the earth's warming. Only about 51 % of incoming solar radiation reaches the earth. 19 % (16 % by atmospheric gases and 3 % by clouds) are absorbed by the atmosphere while the remaining 30 % are reflected to space (6 % by air, 20 % by clouds and 4 % by the earth's surface) (Nahar Sultana, 2008). The shortest wavelengths of solar radiation in the ultraviolet range are absorbed by ozone while visible radiation penetrates unhindered. When solar radiation reaches the ground, reflection takes place either by scattering through air molecules, reflection by clouds or reflection by the ground itself. Dark coloured surfaces such as rocks, forests, snow reflect very little solar radiation that incident on them compared to light coloured surfaces such as snow and ice which reflects almost all the solar radiation they receive. This amount of energy reflected by a surface is known as albedo. The combined albedo of different surfaces is called planetary albedo. The earth's planetary albedo is about 0.29 which means about a third of incoming radiation is reflected out and two-thirds absorbed (Kiehl and Trenberth, 1997).

1.4.1 Solar Radiation

Solar radiation is the amount of energy and light that comes directly from the sun. The total amount of this energy is referred to as global solar radiation. Global solar radiation is then the total incoming radiation or insolation. It is the combination of the direct, diffuse and reflected radiation. Solar radiation is measured with the use of a Pyranometer. The direct solar radiation is the radiation from the sun to the earth surface traveling in a straight line. It is also referred to as beam radiation. The diffuse solar radiation is the radiation from the sun that is scattered by molecules, aerosols and clouds in the atmosphere. Diffuse solar radiation is also referred to as sky radiation because the scattering occurs from all regions of the sky. There is also the reflected solar radiation which is the radiation that gets to the earth surface but are reflected by non-atmospheric things like the ground. On snowing days, reflected radiations are quite high because snows are good reflectors of solar radiation (Grenfell et al., 1994). On sunny days when the sky is clear, about 85 % of the solar radiation received is in the direct form while the remaining 15 % is diffused in the atmosphere. However, as the sun goes lower in the sky, the amount of diffuse radiation increases and may be up to 40 % when the sun is about 10^o above the horizon. There are extreme overcast days when larger percentage of the solar radiation is diffuse radiation. It is important to note that in higher latitudes, colder regions, larger percentage of the solar radiation is diffused while in hotter places in the lower latitude, most radiation there are direct. Also, during winter when there is very little sunshine, the percentage of diffuse radiation is much more than the direct radiation (Urban et al., 2007). There is also the normal radiation which describes the radiation that penetrates the earth's surface 90^o to the sun's rays.

1.4.2 Importance of Solar radiation

The earth receives large amount of energy from the sun in the form of solar radiation. When properly harnessed, and converted to usable energy, we would be able to meet the energy demand of most countries. A number of solar energy technologies are being developed to utilize the sun's energy. In their book Shining on, (Dunlap et al., (1992) highlighted six technologies using solar radiation: 'solar electric (photovoltaic) for converting sunlight directly into electricity, solar heat (thermal) for heating water for industrial and household uses, solar thermal electric for producing steam to run turbines that generate electricity, solar fuel technologies for converting biomass (plants, crops and trees) into fuels and by products, passive solar for lighting and heating buildings and solar detoxification for destroying hazardous waste with concentrated sunlight'. They further stated that these technologies depend on the operational cost of building the instruments, the amount of solar radiation that can be converted to the desired energy product as well as the amount of solar radiation present in the location. If there is not enough solar radiation to power the instruments, the performance and goals for which the instrument is built will not be met. Therefore, it is important that the amount of solar radiation present and the solar energy needed by the instruments is similar for effectiveness and economic goals to be met.

Since the amount of solar radiation received on the earth's surface is not constant but changes throughout the day due to the position of the sun, weather patterns, geographic position, it is important to have energy storage systems that can provide enough energy to power the instruments on cloudy days as well as during night period when there is little or no solar radiation (Proszak-Miasik and Rabczak, 2017). Generally, more solar radiation is received during the day especially at mid-day. The sun is positioned high in the sky with very little radiation scattered or absorbed making most of the incoming radiation penetrate to the earth. The knowledge of this information is important in building the solar energy technologies. Also clouds, large lakes, oceans, mountains also influence the amount of solar radiation received on the earth surface (Rathod et al., 2016). Plains receive more solar radiation than mountains because the winds blowing against mountains force the air surrounding the mountain to rise, resulting in the formation of clouds which scatters incoming solar radiation. Another consideration in building energy panels are anthropogenic activities and natural occurrences. Human activities such as pollutions and biomass burning reduce the amount of solar radiation by either scattering or absorbing incoming radiation while natural occurrence such as airborne ash from volcanic activity will also scatter and absorb incoming radiation, thereby reducing the amount of solar radiation reaching the earth. Figures 1.1 shows the global energy flow.

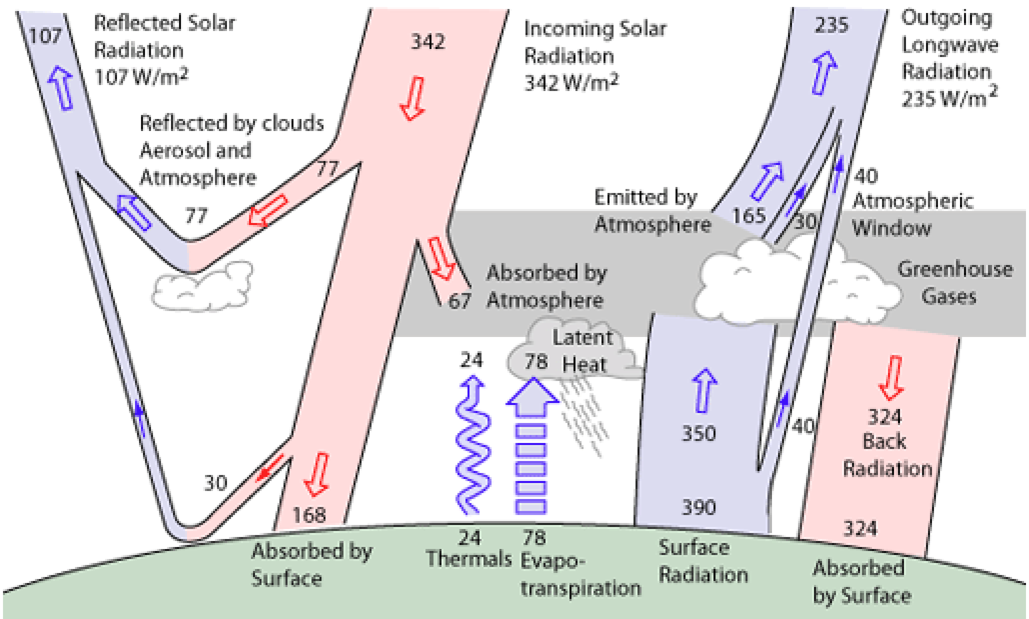

Figure 1.1: Global energy flow (obtained from Kiehl and Trenberth, 1997)

The atmosphere, clouds and the earth's surface emit radiation of infrared and near infrared wavelengths. These outgoing radiations are absorbed by water vapour and carbon dioxide, thereby making the earth's surface temperature warmer. If the amount of incoming and outgoing energy is equal, the earth's energy is said to be balanced. This state is called radiative equilibrium. If they are not equal, then the earth will either experience warm or cold.

1.4.3 Terminologies used in Solar Radiation study

Irradiance: This is the amount of radiant energy that is incident on a surface per unit area per unit time.

Direct Normal Irradiance: This is the amount of radiant energy incident on a surface held perpendicular to sun rays.

Diffuse Horizontal Irradiance: This is the amount of solar radiation incident on a horizontal surface due to sky radiation only.

Global Horizontal Irradiance: This is the amount of solar radiation incident on a horizontal surface due to both direct rays and diffuse sky radiation.

Reflected Solar Irradiance: This is the amount of upward radiant energy that exits the atmosphere in the shortwave range.

Net Terrestrial Radiation: This is the difference between the upward irradiance and downward irradiance in the longwave range through a horizontal surface near the earth surface.

Net Total Irradiance: This is the difference between the downward irradiance and upward irradiance in the entire spectrum.

Incident energy: The energy that reaches the earth's ground surface.

1.5 Atmospheric Aerosol

Aerosols are small particles either solid or liquids suspended in the atmosphere with diameters between 0.002 µm and 100 µm. Aerosols vary in size, chemical composition, source, in their amount and distribution in the atmosphere (Kumar et al., 2011). When they are large enough, they scatter and absorb sunlight. Atmospheric aerosols influence the earth radiation budget. They can either scatter sunlight back into space or modify the size of cloud particles, change how cloud absorb and reflect sunlight in the lower atmosphere. Therefore, aerosols have significant impact on local, regional and global scales (Yuan et al., 2014; Urankar et al., 2012; Zhou et al., 2005). They can lead to urban air pollution from vehicular emissions, industrial processes, wood burning, fires on local scales while regionally, they can be transported to areas of clean air, thereby contaminating the air there.

Atmospheric aerosols are from two sources: the primary and the secondary. Primary sources are also referred to as natural sources such as dust storms, sea spray, volcanic dust, botanical debris, forest fires, grassland fires, smoke and soot. Secondary aerosols are formed by gas to particle conversion processes like sulphates and nitrates (Kroll and Seinfeld, 2008).

Three basic types of aerosols have significant effects on the earth's climate: the volcanic aerosol, desert dust and human-made aerosols. A significant example of volcanic aerosol is the layer formed in the stratosphere in 1991 during Mt. Pinatubo's volcanic eruption. Once this type of aerosol is formed, it stays in the stratosphere for about two years, reflecting sunlight and reducing the amount of energy reaching the earth. Desert dust is composed of minerals that absorb and scatter sunlight (Power and Mills, 2005). When they absorb sunlight, they warm the atmospheric layer where they reside which inhibits the formation of storm clouds. Through this suppression, they further desert expansion. Additional absorption of sunlight by clouds has been attributed to desert aerosols. The third type which is human made are from anthropogenic activities. This is mostly seen in highly industrial areas. It is believed that anthropogenic sulphates are more produced than naturally produced sulphates (NASA). When these sulphates rise in the atmosphere and enter the cloud, they increase cloud droplets but reduce their sizes. The resultant effect of this is that they make the clouds to reflect more sunlight than they would without sulphate aerosols.

Anthropogenic aerosols are from human activities such as industrial and vehicular emissions, biomass and fossil fuel burning. The net effect of these is the release of sulphates, nitrates and carbonaceous aerosols also known as soot to the atmosphere. Sulphates are basically produced from oil refining and smelting, coal and oil combustion with about 72 % from fossil fuel burning, 19 % from phytoplankton, 7 % from volcanic eruptions and the remaining 2 % from biomass burning. Nitrates originates from biomass burning, fertilizers and bacterial actions, with ammonium nitrate being the predominat nitrate. The most significant sunlight absorbing aerosol are the carbonaceous aerosols which also serves as catalysts for some chemical reactions in the atmosphere. Carbonaceous aerosols are formed from a complex mixture of organic and elemental carbons (Li et al., 2017).

Based on nature and source of production, there are six types of aerosols: Soil, sea-salt, polar, rural continental, urban and extra-terrestrial aerosols. Soil aerosols are formed from soil weathering in arid areas and are transported by wind through convection currents. Soil aerosols are predominantly found in the troposphere. Sea-salt aerosols, either crystalline or solution droplets are associated with the bursting of whitecap bubbles while polar aerosols are influenced by the Arctic haze. The rural continental aerosols are mainly found in the rural areas and they are of natural sources as there are little or no industrial activities going on there. The urban aerosols are found in cities and can be in form of dust and sea-salt, nucleation mode from reactions from nitrates, ammonium, sulphates or from combustion sources.

Atmospheric aerosols are important for heterogeneous chemistry, air quality, human health, visibility, acid deposition, cloud formation and climate. Acid deposition can catalyse deterioration of building materials, destroy vegetation, damage the aquatic ecosystem, increase mortality rate in humans due to breathing problems. According to Adesina (2015), aerosols effects are both health and non-health related. Its effects on health are determined by the toxicity of concentration, susceptibility of individuals and the duration of exposure. This results in respiratory hazards, cardio-vascular diseases, carcinogenic effects, morphological changes and increase in mortality and morbidity. When people have asthma, respiratory and cardiovascular problems, the effects are more pronounced. Its non-health effects are visibility impairment and vegetation damage.

1.6 Atmospheric Cloud

Clouds are formed when water vapour condenses to droplets or ice crystals. The study of clouds and their characteristics helps in the understanding of climate change. Low, thick clouds help in cooling the earth as they reflect incoming solar radiation while high clouds transmit incoming solar radiation, traps and radiates emitted infrared radiation by the earth which results in warming of the earth (Salgueiro et al., 2014). Cloud altitude, size and particles that make up the cloud determine whether the cloud will heat or cool the surface of the earth. Clouds are classified either by their height in the sky or by their shapes. Based on their occurrence heights, clouds are classified into three: high-level, middle level and low-level clouds. Tropospheric clouds with their height regions is shown in figure 1.2.

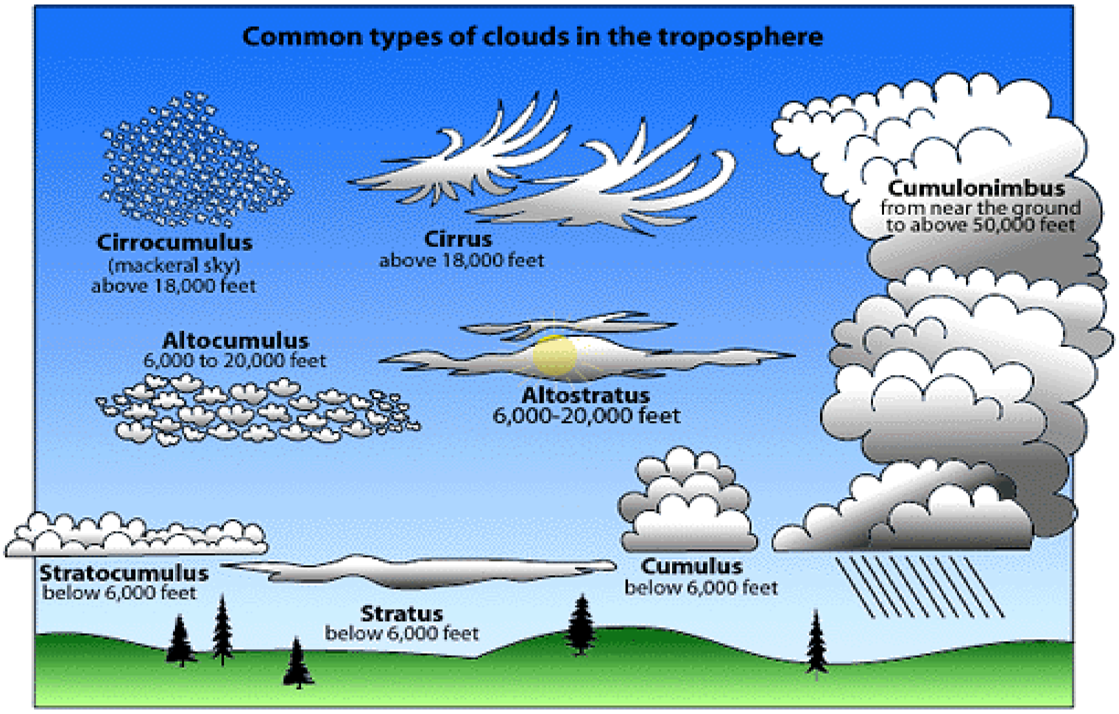

Figure 1.2: Tropospheric clouds with height region (Obtained from Puiu Tibi, 2017).

1.6.1 High-level clouds

High level clouds are clouds that reach between 5 km and 13 km above sea level. Examples are the Cirrus, Cirrostratus and Cirrocumulus clouds. Cirrus clouds are recognised with their white patches, narrow bands and hair-like appearance as shown in figure 1.3. They are transparent and are composed of ice crystals. They are often bright yellow or red before sunrise and after sunset which makes them different from other types of clouds. They also mostly predict fair weather and can be seen mostly throughout the year.

Cirrostratus is quite similar to the Cirrus, but it is transparent, has a smooth appearance and always ends by covering the whole sky. When they are purely white, it indicates that they have stored moisture. If they descend to lower altitudes, they may turn to altostratus clouds. Figure 1.4 shows the Cirrostratus cloud.

Cirrocumulus is a white patch layered cloud with arranged ripples usually formed about 5 km above the surface as presented in figure 1.5. It usually appears less than 24 hours before a rain or snow storm. Cirrocumulus is an uncommon cloud as its mostly the degraded form of either Cirrus or Cirrostratus. If it covers the sky, it is referred to as mackerel sky because the sky would look like the scales of a fish.

Figure 1.3: Cirrus cloud (Puiu Tibi 2017).

Figure 1.4: Cirrostratus cloud (Obtained from PuiuTibi 2017).

Figure 1.5: Cirrocumulus cloud (Puiu Tibi 2017).

1.6.2 Mid-level clouds

Mid-level clouds are found in the height region of 2 km and 5 km. The mid-level clouds are Altostratus, Altocumulus and Nimbostratus. The Altostratus is a bluish or grey cloud layer that totally or partially covers the sky. Their thin nature makes it possible to see the sun through them. They are mostly linked with light rain or snow. Figure 1.6 shows an Altostratus cloud.

Mostly, the Altocumulus appears with other cloud types especially cumulonimbus clouds. They are often made up of water droplets because they are found in lower altitudes. They appear like white sheet of layered clouds. When the edge of an Altocumulus cloud lies infront of either the sun or the moon, a corona appears. If an Altocumulus cloud appears in the morning, it is very likely that there would be thunderstorms by late afternoon. An Altocumulus cloud is shown in figure 1.7.

The Nimbostratus is a thick cloud which blots out the sun as shown in figure 1.8. It is mainly referred to as the continuous rain cloud. They are formed when moisture accumulate over a large area. They can also be formed from other cloud types such as when altostratus descends or from the spreading of cumulonimbus.

Figure 1.6: Altostratus cloud (Puiu Tibi 2017).

Figure 1.7: Altocumulus cloud (Puiu Tibi 2017).

Figure 1.8: Nimbostratus cloud (Puiu Tibi 2017).

1.6.3 Low-level clouds

Low-level clouds consist of Cumulus, Stratus, Cumulonimbus and the Stratocumulus. They are found between 0 and 2 km above the surface. Cumulus clouds are generally dense clouds with sharp outlines like domes and bulging upper parts as presented in figure 1.9. They appear mostly in the morning on clear sky days. They are mostly white in the parts that the sun pass through while other parts are relatively dark. Cumulus clouds indicate fair weather.

The Stratus clouds are thick clouds in the form of ice prisms shown in figure 1.10. When one of its layers breaks up, the sky is seen to be blue. They are formed when large air masses rising in the atmosphere condense. They are mostly found in coastal and mountainous regions.

Cumulonimbus clouds are also referred to as the thunderstorm clouds and they are always in form of mountains or huge towers. They are made up of water droplets at low altitudes and ice crystals at high altitudes. They basically produce precipitations and sometimes could also produce hails and tornadoes. They are mostly seen during summer and spring when the earth releases heat. An example is shown in figure 1.11.

The last in this category are the Stratocumulus clouds. They are common in the coastlines. Sunsets appear reddish in colour as airborne particles absorb shorter wavelengths of light. Figure 1.12 shows a Stratocumulus cloud.

Figure 1.9: Cumulus cloud (Puiu Tibi 2017).

Figure 1.10: Stratus cloud (Puiu Tibi 2017).

Figure 1.11: Cumulonimbus cloud (Puiu Tibi 2017).

Figure 1.12: Stratocumulus cloud (Puiu Tibi 2017).

There are other cloud types that are quite unusual such as the Lenticular, Kelvin-Helmholtz and the Mammatus cloud as shown in figures 1.13, 1.14 and 1.15 respectively. Lenticular are formed on the downwind side of mountains. When winds blow most cloud types across the sky, Lenticular clouds remain in their position. They are formed when air moves up over a mountain and are evaporated on the side that is farther away from the mountain. When wind blows over a barrier like a mountain, the air continues flowing in the atmosphere in a wave-like pattern, Kelvin-Helmholtz clouds are formed. Basically, they are formed when there is a difference in wind speed or direction between two wind currents in the atmosphere while the Mammatus clouds are clouds that hang underneath the base of another cloud.

Figure 1.13: Lenticular cloud (Courtesy Metoffice 2016).

https://www.metoffice.gov.uk/learning/learn-about-the-weather/clouds/lenticular-clouds

Figure 1.14: Kelvin-Helmholtz cloud (Eleanor Imster 2017).

Figure 1.15: Mammatus Cloud (Puiu Tibi 2017).

1.7 Research Aims

The current research work focuses on;

i. to determine the relationship between ozone and solar radiation over various regions of South Africa.
ii. to examine the solar potential of South African cities for solar energy application.
iii. to investigate the effects of aerosol and/or cloud forcing on different South African cities.
iv. to estimate the earth's radiation budget over South African cities
v. to analyse the relationship between ozone and aerosol index over South African cities.
vi. to understand the climatology and variation of ozone, aerosol over Africa

1.8 Geographical information of South Africa

South Africa (latitudes 21.8ºS and 35.5ºS and longitudes 16ºE and 33ºE) is in the southernmost part of the African continent. It shares its northern boundaries with Namibia and Botswana while it is bounded in the north-eastern part with Zimbabwe, Mozambique and Swaziland as shown in figure 1.16. South Africa is bounded with the Indian Ocean on the east and Atlantic Ocean on the west. These Oceans meet at Cape Agulhas, the southernmost tip of the continent. South Africa is the 25th largest country in the world based on land area, the 24th most populous nation in the world with almost 60 million people and second largest economy in Africa behind Nigeria according to the International Monetary Fund

(IMF). South Africa's interior consists of almost flat plateau of about 2134 m in the east which gradually reduces in the south-west. South Africa has 9 provinces with each having its own legislative, premier and executive council, economy, climate, population and landscape. The number of people living in each province varies and does not depend on the land area. Gauteng province, though the smallest in terms of land area has the highest population and contributes most to the national economy while the northern cape province, which takes about 30 % of the land area has a population of just 2 % of South Africa's population.

South Africa, located in the subtropical region of the African continent has warm temperate condition due to the altitude of the interior plateau and the surrounding oceans. However, its average temperatures of 16ºC to 26ºC are higher compared to most countries in this latitudinal band such as Australia, 13ºC to 23ºC (25.3ºS and 33.5ºS), Uruguay, 11ºC to 24ºC (30.6ºS and 34.9ºS), Argentina, 12ºC to 25ºC (24.1ºS and 41.2ºS), Brazil 22ºC to 26ºC (5.8ºN and 34.5ºS) and Chile 21ºC (17.1ºS and 55.9ºS). South Africa experience the four seasons: Summer (December, January, February), Autumn (March, April, May), Winter (June, July, August) and Spring (September, October and November). The climatic condition in the west and east may vary extremely due to the cold and warm ocean currents on the west and east coasts. El Nino Southern Oscillation (ENSO) also influences South African weather (Kane 2009).

Figure 1.16: Map of South Africa showing the nine provinces and surrounding countries (Courtesy http://onlineresize.club/news-club.html, last visited 9th February 2019).

1.9 Thesis Outline

This work focuses on the relationship between ozone and solar radiation over South Africa and Africa. The influence of aerosol was also examined. This work begins by introducing the earth's atmosphere, atmospheric constituents examined in this work such as ozone, aerosols, clouds and the earth's radiation budget. The various instruments used for the study are presented in chapter two. Both ground-based instruments, satellite instruments and reanalysis data were employed for this work. The ground-based data used were obtained from the South African Universities Radiometric Network (SAURAN). They make use of Pyranometer and Pyrheliometers for irradiance measurements. Satellite instrument, Ozone Monitoring Instrument (OMI) was used to obtain total ozone and ultraviolet aerosol index measurements while the Cloud and the Earth's Radiant Energy System (CERES) was used for shortwave and longwave radiation measurements. The results were compared to reanalysis measurements from the Modern Era Retrospective Analysis for Research and Application (MERRA). In chapter 3, the seasonal variation in global, direct, diffuse radiation over South African cities and Namibia was studied using measurements from the SAURAN network. The corresponding results were submitted for the journal publication. We analysed the seasonal variation in global, direct and diffuse irradiance over the various cities. We also analysed the variation in shortwave and total cloud fraction and observed that Durban and Port Elizabeth received the least amount of radiation, linked to high cloud fraction.

Chapter 3 is to be cited as

Ogunniyi, J. & Sivakumar, V. (2018). Seasonal variation in global, direct, diffuse radiation over South African cities and Namibia. *International conference on solar power systems for Namibia*.

In chapter 4, we studied the variation in temperature, ultraviolet aerosol index and total ozone over five South African cities from 2004 to 2016 using OMI measurements. The study shows the influence of Agulhas current and Benguela current on Durban and Cape Town temperatures respectively. The study also linked the local sugar cane burning in Durban with the high absorbing aerosol while low aerosol in Cape Town was linked with the presence of marine aerosol.

Chapter 4 is to be cited as

Ogunniyi, J. & Sivakumar, V. (2018). Variations in Temperature, Ultraviolet Aerosol Index and Total Ozone over Five South African Cities (*Submitted for publication – Journal of Energy in Southern Africa*)

In chapter 5, the variation in solar radiation, ozone and aerosol was analysed over Africa. The results reveal high solar energy potential in Africa. High ozone observed in Morocco and Mozambique was linked with the presence of volatile organic compounds and high concentration of CO and biomass burning respectively.

Chapter 5 is to be cited as

Ogunniyi, J. & Sivakumar, V. (2018). Interannual and Seasonal Variation in Surface Solar Radiation, Ozone and Aerosol over Africa (*In revision – Atmosfera*)

Chapter 6 examines the effect of aerosol and clouds on the surface energy balance for selected regions of South Africa using datasets from CERES and MERRA 2. Both instruments show similar patterns in the interannual variability of shortwave and longwave radiation. Over cold semi-arid surface, there was a significant trend in shortwave radiation during spring. The effect of aerosol forcing on shortwave and longwave radiation was also determined.

Chapter 6 is to be cited as

Ogunniyi, J. Ruchith, R.D. & Sivakumar, V. (2018). Effects of Aerosol and Clouds on Surface Energy Balance over selected regions of South Africa (*Submitted to – Meteorology and Atmospheric Physics*)

Chapter 7 presents the summary of the results and recommendations for future work.

1.10 References

Adesina A. Joseph (2015). Aerosol characteristics over different regions of Southern Africa-using sunphotometer and satellite measuremnts. PhD thesis submitted to univeristy of KwaZulu natal, South Africa.

Aucamp, P. J. (2007). Questions and answers about the effects of the depletion of the ozone layer on humans and the environment. *Photochemical & Photobiological Sciences, 6*(3), 319-330.

Bertaux, J.L., Kyrola, E., Fussen, D. Hauchecorne, A., Dalaudier, F., Sofieva,V., Tamminen, J., Vanhellemont, F., Fanton d'Andon, O., Barrot, G., Mangin, A., Blanot,L., Lebrum, J.C., Perot, K., Fehr, T., Saavedra, L., Leppelmeier, G.W., & Fraisse, R. (2010). Global ozone monitoring by occultation of stars: an overview of GOMOS measurements on ENVISAT. *Atmos.Chem.Phys.,* 10, 12091-12148.

Bodeker, G., Garny, H., Smale, D., Dameris, M., & Deckert, R. (2007). The 1985 Southern Hemisphere mid-latitude total column ozone anomaly. *Atmospheric Chemistry and Physics, 7*(21), 5625-5637.

Bowman, K. P., & Krueger, A. J. (1985). A global climatology of total ozone from the Nimbus 7 total ozone mapping spectrometer. *Journal of Geophysical Research: Atmospheres, 90*(D5), 7967-7976.

Chandra, S., Varotsos, C., & Flynn, L. (1996). The mid-latitude total ozone trends in the northern hemisphere. *Geophysical Research Letters, 23*(5), 555-558.

Christensen, M.W. Carrio, G.G. Stephens, G.L. & Cotton, W.R. Radiative impacts of free-tropospheric clouds on the properties of marine stratocumulus. Journal of the atmospheric sciences, Vol. 70, 3102-3118.

Dunlap, M., Cook, G., Marion, B., Riordan, C., & Renne, D. (1992). Shining on: A primer on solar radiation data: National Renewable Energy Lab., Golden, CO (United States).

Fan, Z.Y. Plane, J.M.C. Gumbel, J. Stegman, J. & Llewellyn, E.J. (2007). Satellite measurements of the global mesospheric sodium layer. Atmos. Chem. Phys, 7, 4107-4155.

Fioletov, V., Bodeker, G., Miller, A., McPeters, R., & Stolarski, R. (2002). Global and zonal total ozone variations estimated from ground-based and satellite measurements: 1964–2000. *Journal of Geophysical Research: Atmospheres, 107*(D22).

Grenfell, T. C., Warren, S. G., & Mullen, P. C. (1994). Reflection of solar radiation by the Antarctic snow surface at ultraviolet, visible, and near-infrared wavelengths. *Journal of Geophysical Research: Atmospheres, 99*(D9), 18669-18684.

James, P., Peters, D., & Waugh, D. (2000). Very low ozone episodes due to polar vortex displacement. *Tellus B, 52*(4), 1123-1137.

Kane, R.P. (2009). Periodicities, ENSO effects and trends of some South African rainfall series: an update. South African journal of science, 105, 199-207.

Kerr, J., Asbridge, I., & Evans, W. (1988). Intercomparison of total ozone measured by the Brewer and Dobson spectrophotometers at Toronto. *Journal of Geophysical Research: Atmospheres, 93*(D9), 11129-11140.

Kiehl, J. T., & Trenberth, K. E. (1997). Earth's annual global mean energy budget. *Bulletin of the American Meteorological Society, 78*(2), 197-208.

Kroll, J.H. & Seinfeld, J.H. (2008). Chemistry of secondary organic aerosol. Formationa nd evolution of low-volatility organics in the atmosphere. Atmospheric environment, 42, 3593-3624.

Kumar, A. Saxena, D. & Yadav, R. (2011). Measurements of atmospheric aerosol concentration of various sizes during monsoon season at Roorkee, India. Atmospheric science letters, 12, 345-350.

Lei, J. Thayer, J.P. Burns, A.G. Lu, G. & Deng, Y. (2010). Wind and temperature effects on theremopshere mass density response to the November 2004 geomagnetic storm. Journal of geophysical research, Vol. 115, A5.

Li, G. Bei, N. Cao, J. Huang, R. Wu, J. Feng, T. Wang,Y. Suixin, L. Zhang,Q. Tie, X. & MolinaL.T. (2017). A possible pathway for rapid growth of sulfate during haze days in China. Atmos. Chem. Phys, 17, 3301-3316.

Mahendranth, B., & Bharathi, G. (2012). Interannual variability and temporal variations of total column ozone in Visakhapatnam from ground based observations. *Asia-Pacific Journal of Atmospheric Sciences, 48*(2), 191-195.

Marsh, D.R., Skinner, W.R., Marshall, A.R., Hays, P.B., Ortland, D.A., & Yee, J. (2002). High Resolution Doppler Imager observations of ozone in the mesosphere and lower thermosphere. Journal of geophysical research, Vol. 107, D19.

McCormick, M. P., Thomason, L. W., & Trepte, C. R. (1995). Atmospheric effects of the Mt Pinatubo eruption. *Nature, 373*(6513), 399-404.

McPeters, R., & Labow, G. (1996). Assessment of the accuracy of 14. 5 years of Nimbus 7 TOMS Version 7 ozone data by comparison with the Dobson network. *Geophysical Research Letters, 23*(25), 3695-3698.

McPeters, R., Labow, G., & Johnson, B. (1997). A satellite-derived ozone climatology for balloonsonde estimation of total column ozone. *Journal of Geophysical Research: Atmospheres, 102*(D7), 8875-8885.

McPeters, R. D., & Komhyr, W. (1991). Long-term changes in the total ozone mapping spectrometer relative to world primary standard Dobson spectrometer 83. *Journal of Geophysical Research: Atmospheres, 96*(D2), 2987-2993.

McPeters, R. D., Labow, G. J., & Logan, J. A. (2007). Ozone climatological profiles for satellite retrieval algorithms. *Journal of Geophysical Research: Atmospheres, 112*(D5).

Mlynczak M.G. Hunt, L.A. Mast J.C. Marshall, T. Russell III, .M. Smith, A.K. Siskind, D.E. Yee, J.H. Mertens, C.J. Martin-Torres, F.J. Thompson, R.E. Drob, D.P. & Gordley, L.L. (2013). Atomic oxygen in the mesosphere and lower thermosphere derived from SABER: Algorithm theoretical basis and measurement uncertainty. Journal of geophysical research: Atmospheres, Vol. 118, 5724-5735.

Nair, P. J., Godin-Beekmann, S., Kuttippurath, J., Ancellet, G., Goutail, F., Pazmino, A., . . . Wang, H. (2013). Ozone trends derived from the total column and vertical profiles at a northern mid-latitude station. *Atmospheric Chemistry and Physics*, *13*(20), 10373-10384.

Nahar N. Sultana (2008). Solar irradiation of the earth's atmosphere. International symposium on climate change and food security of South Asia, August 24-29.

Newchurch, M., Yang, E. S., Cunnold, D., Reinsel, G. C., Zawodny, J., & Russell, J. M. (2003). Evidence for slowdown in stratospheric ozone loss: First stage of ozone recovery. *Journal of Geophysical Research: Atmospheres, 108*(D16).

Ogunniyi, J. & Sivakumar, V. (2018). Ozone climatology and its variability from ground based and satellite observations over Irene, South Africa (25.5^{o} S; 28.1^{o} E) - Part 2: Total column ozone variations. Atmosfera, 31(1), 11-24.

Oltmans, S.J. Johnson, B.J. & Helmig, D. (2008). Episodes of high surface-ozone amounts at South Pole during summer and their impact on the long-term surface-ozone variation. Atmospheric environment, 42 2804-2816.

Plane, J.M.C. Feng, W. & Dawkins, C.M. (2015). The mesosphere and metals: chemistry and changes. American chemical society, 4497-4534

Power, H.C. & Mills D.M. (2005). Solar radiation climate change over Southern Africa and an assessment of the radiative impact of volcanic eruptions. International journal of climatology, 25, 295-318.

Proszak-Miasik, D. & Rabczak, S. (2017). Impact of solar radiation change on the collector efficiency. Journal of ecological engineering, Vol. 18, 268-272.

Puiu Tibi (2017). The types of clouds: everything you need to know. ZME science.

Rathod, A.P.S. Mittal, P. & Kumar, B. (2016). Analysis of factors affecting solar radiation received by any region. IEEE.

Remsberg, E.E. (2008). On the response of Halogen Occultation Experiment (HALOE) stratospheric ozone and temperature to the 11-year solar cycle forcing. Journal of geophysical research: Atmospheres, Vol. 113, D22.

Salgueiro, V. Costa, M.J. Silva, A.M. & Bortoli, D. (2014). Variability of the daily-mean shortwave cloud radiative forcing at the surface at a midlatitude site in southwestern Europe. Journal of climate, Vol. 27, 7769-7780.

Seinfeld, J. H., & Pandis, S. N. (2016). *Atmospheric chemistry and physics: from air pollution to climate change*: John Wiley & Sons.

Semane, N., Bencherif, H., Morel, B., Hauchecorne, A., & Diab, R. (2006). An unusual stratospheric ozone decrease in the Southern Hemisphere subtropics linked to isentropic air-mass transport as observed over Irene (25.5 S, 28.1 E) in mid-May 2002. *Atmospheric Chemistry and Physics, 6*(7), 1927-1936.

Shematovich, V.I. Bisikalo, D.V. & Gerard, J.C. (2006). Energetic oxygen atoms in the polar geocorona. Journal of geophysical research, vol. 111, A10301.

Shindell, D., Rind, D., Balachandran, N., Lean, J., & Lonergan, P. (1999). Solar cycle variability, ozone, and climate. *Science, 284*(5412), 305-308.

Sivakumar, V. & Ogunniyi, J. (2017). Ozone climatology and variability over Irene, South Africa determined by ground based and satellite observations. Part 1: Vertical variations in the troposphere and stratosphere. Atmosfera 30(4), 337-353.

Sivakumar, V., Portafaix, T., Bencherif, H., Godin-Beekmann, S., & Baldy, S. (2007). *Stratospheric ozone climatology and variability over a southern subtropical site: Reunion Island (21 S; 55 E).* Paper presented at the Annales geophysicae.

Smith, A.K., Harvey, V.L., Mlynczak, M.G., Funke, B., Garcia-Comas, M., Hervig, M., Kaufmann, M., Kyrola, E., Lopez-Puertas, M., McDade, I., Randall, C.E., Russell, J.M., Sheese, P.E., Shitotani, M., Skinner, W.R., Suzuki, M., & Walker, K.A. (2013). Satellite observations of ozone in the upper mesosphere. Journal of geophysical research: Atmospheres, Vol. 118.

Solomon, S. (1999). Stratospheric ozone depletion: A review of concepts and history. *Reviews of Geophysics, 37*(3), 275-316.

Steele, H., Hamill, P., McCormick, M., & Swissler, T. (1983). The formation of polar stratospheric clouds. *Journal of the Atmospheric Sciences, 40*(8), 2055-2068.

Strelnikov, B., Rapp, M., & Lubken, F. (2013). In-situ density measurements in the mesosphere/lower thermosphere region with the TOTAL and CONE instruments. An introduction to space instrumentation, 1-11.

Tabazadeh, A. Turco, R.P. Drdla, K. & Jacobson, M.Z. (1994). A study of type I polar stratospheric cloud formation. Geophysical research letters. Vol. 21, 1619-1622.

Thompson, A. M., Witte, J. C., McPeters, R. D., Oltmans, S. J., Schmidlin, F. J., Logan, J. A., . . . Coetzee, G. J. (2003). Southern Hemisphere Additional Ozonesondes (SHADOZ) 1998–2000 tropical ozone climatology 1. Comparison with Total Ozone Mapping Spectrometer (TOMS) and ground-based measurements. *Journal of Geophysical Research: Atmospheres, 108*(D2).

Toon, O. B., Browell, E., Kinne, S., & Jordan, J. (1990). An analysis of lidar observations of polar stratospheric clouds. *Geophysical Research Letters, 17*(4), 393-396.

Trickl, T. Vogelmann, H. Ries, L. Scheel, H.E. & Sprenger, M. (2018). The underestimated role of stratosphere-to-troposphere transport on tropospheric ozone. Atmos. Chems. Phys. Discuss. doi.org/10.5194.

Turner, J. & Overland, J. (2009). Contrasting climate change in the two polar regions. Norwegian polar institute, doi:10.1111, 146-164.

Urankar, G. Prabha, T.V. Pandithurai, G. Achuthavarier, D. & Goswami, B.N. (2012). Aerosol and cloud feedbacks on surface energy balance ober selected regions of the Indian subcontinent. Journal of geophysical research, Vol. 117, doi:10.1029.

Urban, O., JANOUŠ, D., Acosta, M., CZERNÝ, R., Markova, I., NavrATil, M., . . . Zhang, R. (2007). Ecophysiological controls over the net ecosystem exchange of mountain spruce stand. Comparison of the response in direct vs. diffuse solar radiation. *Global Change Biology, 13*(1), 157-168.

Velders, G. J., Andersen, S. O., Daniel, J. S., Fahey, D. W., & McFarland, M. (2007). The importance of the Montreal Protocol in protecting climate. *Proceedings of the National Academy of Sciences, 104*(12), 4814-4819.

Wang, K. Wu, Y. Lin, J.T. & Tan, P.H. (2018). Temperature properties in the tropical tropopause layer and their correlations with outgoing longwave radiation: FORMOSAT-3/COSMIC observations.

Yigit E. & Medvedev, A.S. (2010). Internal gravity waves in the thermosphere during low and high solar activity: simulation study. Journal of geophysical reaseach, Vol. 115, doi:10.1029.

Yuan, Y. Huang, X. Shuai, Y. & Mao, Q.J. (2014). Study on the influence of aerosol radiation balance in one-dimensional atmospheric medium using P_n- approximation method. Hindawi publishing corporation, doi.org/10.1155

Zhou, M. Yu, H. Dickinson, R.E. Dubovik, O. & Holben, B.N. (2005). A normalized description of the direct effect of key aerosol types on solar radiation as estimated from Aerosol Robotic Network aerosols and Moderate Resolution Imaging Spectroradiometer albedos. Journal of geophysical research, Vol. 110, doi:10.1029.

Ziemke, J., Chandra, S., Labow, G., Bhartia, P., Froidevaux, L., & Witte, J. (2011). A global climatology of tropospheric and stratospheric ozone derived from Aura OMI and MLS measurements. *Atmospheric Chemistry and Physics, 11*(17), 9237-9251.

IMF: https://www.iol.co.za/business-report/economy/these-are-the-biggest-economies-in-africa-imf-15929339

CHAPTER TWO
DATA AND INSTRUMENTATION

The importance of solar radiation to man cannot be over emphasised. Change in the amount of energy that reaches the earth has implications on man. It is therefore important to estimate this energy and to predict changes that may occur. Ground based instruments are known to estimate solar energy better than satellite instruments, however, the sparseness of instruments and cost of procuring and maintaining the instruments have limited its coverage. Another challenge with ground-based instruments is the unavailability of long-term data sets, data gap, though they are simple, reliable and useful in validating satellite retrievals. This brings about the introduction of satellite and reanalysis data for analysis and predictions (Fioletov et al., 2008).

2.1 Remote Sensing Techniques

Remote sensing is the process of acquiring information/measurements without direct contact with the sensor. This is made possible through electromagnetic radiation or acoustical waves from the target of interest. Remote sensing can either be active or passive. When a remote sensing instrument depends on an external source of energy, it is passive, but when it provides its own source of energy, it is active. Remote sensing instruments and reanalysis datasets that are used in the present studies are discussed in this chapter.

2.2 Radiation Instruments

2.2.1 Pyranometer

A pyranometer is used to measure global and diffuse solar irradiance on a planar surface (Martinez et al., 2009). It is designed to measure solar radiation flux density within a wavelength range of 0.3 µm to 3 µm. There are basically three types of pyranometers: the thermopile pyranometers designed for measuring the broadband of solar radiation flux from 180^{o} field of view, the photodiode-based pyranometer also called silicon pyranometer which measures in 400 nm to 900 nm band and the photovoltaic pyranometer mostly used in solar simulators. The most common is the thermopile which comprises several thermocouples connected in series, an outer and inner dome which limits the spectral response to a range of 300 nm to 2800 nm and also shields the thermopile sensor from convection, a sensing element drying cartridge, reference element and a black coating which absorbs solar radiation and converts it to heat. Thermopile pyranometers can be divided into three, based on their precision: the second class, the first class and the secondary standard, with the secondary standard being the most accurate and normally used in high quality measurements at weather stations and solar energy projects. They also have long-term stability as well as low error rates compared to others. The silicon cell pyranometers are most common. The schematic of a typical pyranometer is shown in figure 2.1. An Eppley precision pyranometer is shown in figure 2.2 has a temperature dependence of ± 1 % over ambient temperature range of 20 ºC to 40 ºC, sensitivity of approximately 9 µV/Wm^2, an impedance of about 650 ohms. It has a linearity of ± 0.5 % from 0 to 2800 Wm^2 and a response time of 1 s. For a pyranometer to function effectively, there must be absence of zero drift and it must not be wavelength selective. Its calibration factor must be independent of the intensity, time and temperature. Its response time should be small, and temperature minimum with the cosine and azimuthal response of the detector also minimum. However, its sensitivity should be as large as possible. Pyranometers only measure a portion of the solar radiation spectrum and do not respond to longwave radiation. The CMP21 pyranometer measures in the wavelength regions of 0.285 µm to 2.8 µm. Pyranometer calibrations are from the World Radiometric Reference established by the World Meteorological Organization.

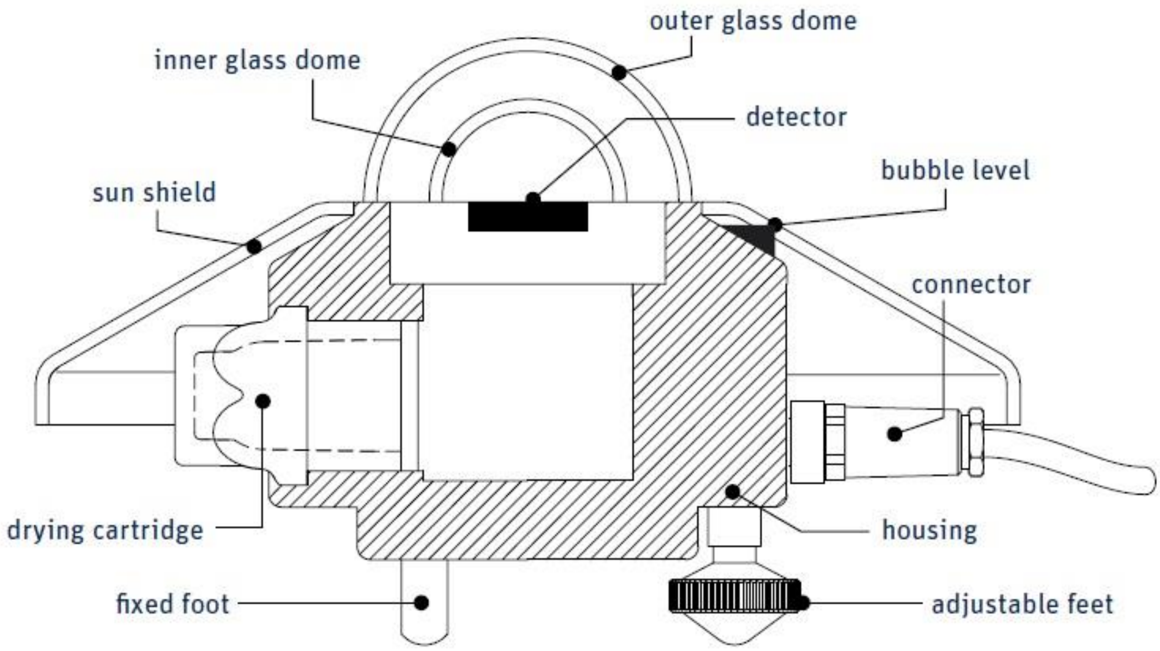

Figure 2.1: Schematic of a SMP 10 pyranometer (Courtesy Omni instruments)

Figure 2.2: A global precision pyranometer (Courtesy Eppley laboratory)

2.2.2 Albedometer

An albedometer is an instrument used to measure solar albedo (reflectance). It consists of two pyranometers with thermopile sensors in opposite direction (one facing up and the other facing down). The one facing up measures the global solar irradiance while the other facing down measures the reflected solar radiation. Figure 2.3 shows a typical albedometer. The albedometers available in market are the CMP 6 and the CMP11 albedometers.

Figure 2.3: A typical SRA01 Albedometer (Courtesy Hukseflux thermal sensors)

2.2.3 UV Radiometers

UV radiometers are used to measure solar irradiance in the ultraviolet and infrared spectrum. They are mostly used to complement solar radiation measurements with pyranometers. There are different types of UV radiometers depending on what they are designed for. The CUV 5 radiometer is a general-purpose instrument used to measure total uv irradiance under all-weather conditions while the UVS-A-T is used to measure only UVA, and example is shown in figure 2.4. The UVS-B-T is used for measuring UVB irradiances with precise temperature correction. The UVS-E-T for erythemally active UV irradiance while the UVS-AB-T is used to measure both UVA (315 nm to 400 nm) and UVB (280 nm to 315 nm)irradiance. UVA and erythemally active UV irradiance are measured with the UVS-AE-T radiometer.

Figure 2.4: UVS-A-T UV radiometer (Kipp and Zonen)

2.2.4 Net Radiometers

Net radiometers are used to measure net radiation on earth’s surface. It has a thermopile sensor with two receivers connected at a junction, one to measure warm temperature and the other to measure cold temperature. The temperature difference between the two receivers gives the net irradiance. There are two types of net radiometer available in market today. The first is the NR lite 2 and the CNR4 net radiometer which has a ventilation and heating unit. The NR lite 2 and CNR4 net radiometers are shown in figures 2.5a and 2.5b respectively.

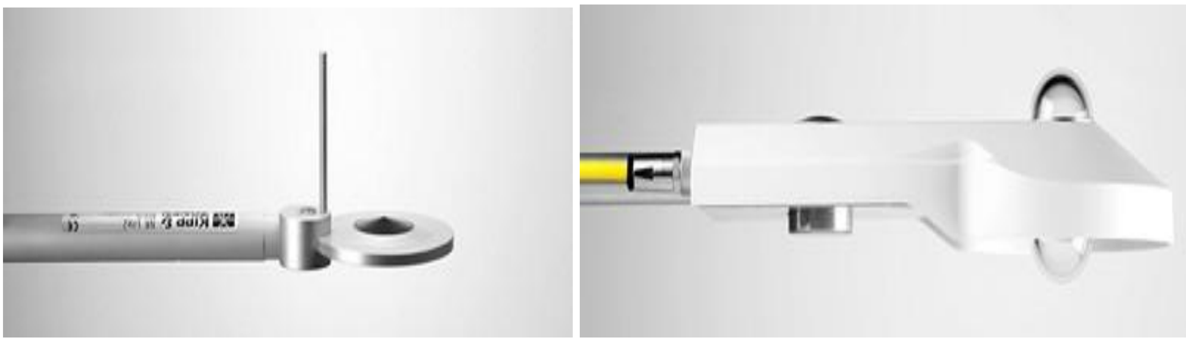

Figure 2.5: (a) NR Lite 2 Net Radiometer (Kipp& Zonen) (b) CNR4 Net Radiometer (Kipp & Zonen)

2.2.5 Pyrheliometer

A pyrheliometer is used to measure direct normal irradiance. Figure 2.6 shows a CHP1 pyrheliometer. It is used with a solar tracking system to keep the instrument aimed at the sun and mostly setup with a pyranometer. It also helps in the assessment of the efficiency of solar panels and photovoltaic devices. Pyrheliometers are also used for climate observations, material testing research and scientific meteorology (Thakkar Vanita, 2014). When sunlight enters the pyrheliometer through a window, it is directed on a thermopile which then converts heat energy to an electrical signal that can be recorded. This signal is then converted to measure in Wm^{-2}. Pyrheliometers are also classified into three, standard, first class and second class pyrheliometers. Examples of standard pyrheliometers are the absolute cavity radiometer, abbot silver disk pyrheliometer and the angstrom electrical compensation pyrheliometers. Michelson bimetallic pyrheliometer, new eppley pyrheliometer, Yanishevsky thermoelectric pyrheliometer and the Linke Feussner iron clad pyrheliometers are examples of first class pyrheliometers while the Moll-Gorczynski and Old Eppley are second class pyrheliometers.

Pyrheliometers have a linearity response time cosine of ± 0.5 % from 0 to 2800 Wm^{-2}, ± 1 % normalization 0 to 70^{o}, temperature dependence of ± 1 % over ambient temperature range of -20 ^{o}C to 40 ^{o}C. The instrument has 9 $\mu V/Wm^{-2}$ and 650 ohms sensitivity impedance receiver.

Figure 2.6: A CHP1 pyrheliometer (Kipp & Zonen)

2.2.6 Pyrgeometer

A pyrgeometer is used for measuring infrared radiation in the atmosphere. It is used for measuring longwave radiation as well as atmospheric radiations from clouds, water vapour and carbon dioxide. It works on the principle of converting radiant energy to heat energy, measurable with a thermopile. A pyrgeometer has a silicon dome which isolates longwave radiation from shortwave radiation. It also has a vacuum deposited interference filter which minimizes the heating of the instrument due to solar radiation. CGR3 developed by Kipp and Zonen and IR02 developed by Hukseflux Thermal sensors are the common pyrgeometers available in market. The IR02 has the advantage of better accuracy and prevention of dew deposition compared to the CGR3. The IR02 and CGR3 pyrgeometer are shown in figures 2.7a and 2.7b respectively.

Figure 2.7: (a) The CGR3 pyrgeometer (Kipp & Zonen) (b) The IR02 pyrgeometer (Hukseflux)

2.2.7 Sun Trackers

Sun trackers are used for monitoring the direct, diffuse and global irradiance. They are also used in atmospheric chemistry research as well as for forecasting pollution and material testing. There are three types of sun trackers, the SOLYS 2 sun tracker has an advantage of being cheap, possesses integrated GPS which configures location and time data automatically. Figure 2.8 shows the Solys 2 sun tracker. It is easy to install, does not need regular maintenance and has the Baseline Surface Radiation Network (BSRN) performance and reliability. SOLYS gear drive sun tracker has the best performance and widest temperature range of – 50 ^{o}C to + 60 ^{o}C. It does not require regular maintenance and has the advantage of carrying heavy instruments up to 80 kg. The Two-Axis Positioner (2AP) sun tracker is an all-weather and reliable instrument with active sun tracking capabilities.

Figure 2.8: A Solys2 sun tracker (Omni instruments)

2.3 South African Universities Radiometric Network (SAURAN)

Solar radiation measurement in South Africa commenced in 1907 in Johannesburg at the Transvaal observatory (Drummond and Kirsten, 1951). These measurements lasted for few years and comprised of total sun and sky radiation received on horizontal surface. Some years later, in 1937, Drummond and Kirsten, (1951) reported the solar radiation survey carried out at six stations in South Africa. After the second world war, the survey continued with focus now on how solar radiation affected organic matter. It was first in 1949 that there was a homogeneous record of solar radiation made possible through the establishment of the South Africa's Weather Bureau. Despite these early measurements, there were challenges such as transportation of equipments to regions of measurements, remoteness of the sites, climatic influence on instrumentations and the various stages of development in Africa (Drummond and Vowinckel, 1957). Satellite instruments have then been introduced for global coverage. However, ground based instruments have been found to be more accurate especially in the lower atmosphere. The need for building high quality, long-term datasets of high temporal resolution for public use brought the South African Universities Radiometric Network (SAURAN) initiative (Brooks et al., 2015). SAURAN was an initiative of Stellenbosch University and University of KwaZulu Natal. Its initial phase consisted of six Universities and four farms in rural settlements. The Universities are Nelson Mandela Metropolitan University, University of KwaZulu Natal (Westville and Howard college), University of Free state, University of Pretoria and Stellenbosch University while the farmlands are in Vanrhynsdorps in western cape, Vryheid in KwaZulu Natal, Graaff-Reinet in Eastern Cape and Alexander Bay near Richtersveld in Sothern cape province. The second phase includes stations within and outside South Africa. The stations in the second phase are University of Venda, Mangosuthu University of Technology, University of Fort Hare. Stations outside South Africa include, Namibian University of Science and Technology, Gaborone in Botswana and University of Reunion in Reunion Island. Currently, the SAURAN network exists in twenty stations (17 South African and 3 outside South

Africa) and in seven of the nine South Africa provinces. Most of these stations use Kipp and Zonen radiometers to provide direct normal irradiance, global horizontal irradiance and diffuse horizontal irradiance at 1-minute, hourly and daily time averaged intervals.

2.4 Modern Era Retrospective Analysis for Research and Application (MERRA)

Reanalysis is the process whereby an unchanging data assimilation system is used to provide consistent reprocessing of meteorological observations over an extended period of the historical data (Gelaro et al., 2017). Reanalysis products have been used for climate monitoring and in the atmospheric research community. The National Oceanic and Atmospheric Administration (NOAA)/National Centres for Environmental Prediction (NCEP), the European Centre for Medium-range Weather Forecasts (ECMEF), the National Aeronautics and Space Administration (NASA), Global Modelling and Assimilation Office (GMAO) and the Japan Meteorological Agency (JMA) have all provided recent reanalysis. The primary goals of MERRA was to provide complete information for earth radiation budget studies and to significantly improve on the previous generation of reanalyses in the representation of the atmospheric branch of the hydrological cycle. These objectives were achieved and was found to have good quality when compared with reanalysis from NCEP and ECMWF (Rienecker et al., 2011). Though MERRA reanalysis are from 1979 to 2016, towards the end of its termination in 2016, it suffered some deficiencies such as unphysical jumps and trends in precipitation response to changes in the observing system, biases and imbalances in certain atmospheric and land surface hydrological quantities as well as poor representation of the upper stratosphere (Bosilovich et al., 2017).

MEERA 2 was then provided to replace MERRA as well as to sustain GMAO's commitment of providing on-going near-real time climate analysis. MERRA 2 was developed to also show the progress towards the development of a future Integrated Earth System Analysis (ISEA) capability. These objectives have been achieved in the assimilation of satellite observations not available to MERRA, reduction in bias and imbalance in water cycle, reduction in trends and jumps in precipitation related to changes in the observing system (Gelaro et al., 2017). MERRA 2 has basically the same features with MERRA but with updates such as a forecast model, analysis algorithm, observing system, radiance assimilation, bias correction of aircraft observations, mass conservation and water balance, precipitation used to force the land surface and drive wet aerosol deposition, boundary conditions for sea surface temperature and sea ice concentration as well as reanalysis production. Aerosol data assimilation and improved representations of cryosphere and stratosphere are other benefits of MERRA 2 compared with MERRA. However, despite these advantages, the preparation and improvement of inputs conventional data types received little attention. This was due to the rapid development schedule to replace MERRA. This resulted in increased warm bias in the upper troposphere as well as excessive precipitation in the tropics and sometimes in northern high latitudes where the topography is high. MERRA 2 is still ongoing developments in aspects of modelling and data similation which aims at providing benefits for future reanalysis. MEERA products are presented in Table 2.1.

Table 2.1: MERRA data products (Courtesy: US Department of Transportation, Federal Highway Administration).

Abbreviation	Description	Unit
CF	Total cloud fraction	Fraction
PPT	Precipitation flux incident upon the ground surface	Kg H_2O m^2 s^{-1}
PS	Surface pressure at 2 m above ground surface	Pa
Q	Specific humidity at 2 m above ground level	Kg H_2O Kg $^{-1}$ air
Rsw	Shortwave radiation incident upon the ground surface	Wm^{-2}
Rtoa	Shortwave radiation incident at the top of atmosphere	Wm^{-2}
T	Air temperature at 2 m and 10 m above ground surface	K
U	Eastward wind at 2 m and 10 m above ground surface	ms^{-1}
V	Northward wind at 2 m and 10 m above ground surface	ms^{-1}
PRMC	Total profile soil moisture content	m^3 s^{-3}
RZMC	Root zone soil moisture content	m^3 s^{-3}
SFMC	Top soil layer soil moisture content	m^3 s^{-3}
TSURF	Mean land surface temperature (including snow)	K
TSOIL	Soil temperature in layer (available for 6 soil layers)	K
PRECSNO	Surface Snowfall	Kg m^{-2} s^{-1}
SNOMAS	Snow mass	Kg m^{-2}
SNODP	Snow depth	M
EVPSOIL	Bare soil evaporation	W m^{-2}
EVPTRNS	Transpiration	W m^{-2}
EVPSBLN	Sublimation	W m^{-2}
QINFIL	Snow water infiltration rate	Kg m^{-2} s^{-1}
SHLAND	Sensible heat flux from land	W m^{-2}
LHLAND	Latent heat flux from land	W m^{-2}
EVLAND	Evaporation from land	Kg m^{-2} s^{-1}
LWLAND	Net downward longwave flux over land	W m^{-2}
SWLAND	Net downward shortwave flux over land	W m^{-2}
EMIS	Surface emissivity	Fraction
ALBEDO	Surface albedo	Fraction

2.5 Satellite Instruments

2.5.1 Clouds and the Earth's Radiant Energy System (CERES)

The Clouds and the Earth's Radiant Energy System is one of the five instruments onboard the Tropical Rainfall Measuring Mission (TRMM) observatory. However, due to onboard circuit failure, the system stopped operation few months after its launch. Other instruments onboard were the Visible Infrared Radiometer (VIRS), TRRM Microwave Imager (TMI), Precipitation Radar (PR) and the Lightning Imaging Sensor (LIS). After flying onboard TRMM, it has also flown on the Earth Observing System (EOS)-AM and the EOS-PM and more recently both terra and aqua Suomi National Polar-Orbiting Partnership (SNPPA) as well as the National Oceanic and Atmospheric Administration (NOAA) 20 satellites. Terra is a descending sun-synchronous orbit with an equator crossing time to 10.30 AM local time while Aqua is an ascending sun-synchronous orbit with an equator crossing time of 1.30 PM local time. Each of these instruments measure filtered radiances in the shortwave wavelength of 0.3 µm and 5 µm, total irradiance in the wavelength of 0.3 µm and 200 µm (Loeb et al., 2018). CERES goals were to produce long-term integrated global climate data record for detecting decadal changes in the earth's radiation budget from the surface to the top of the atmosphere together with associated cloud and aerosol properties; to enable improved understanding of earth's radiation budget variability and the roles aerosols and clouds play in the variability; and to provide datasets for climate model evaluation and improvement (Loeb et al., 2017). Datasets from CERES are expected to provide top of the atmosphere fluxes with a factor of 2 or 3 fewer errors compared to the Earth Radiation Budget Experiment (ERBE) data (Wielicki et al., 1995). The schematic of the CERES instrument is shown in figure 2.9.

CERES instruments provide daily datasets on global scale. Despite its excellent spatial and temporal coverage, some uncertainties are discovered in its measurements. Instrumental error due to calibration in CERES is estimated to be about 1 % for shortwave and 0.75 % for longwave radiation (Loeb et al., 2018). Loeb et al (2018) also noted errors due to radiance to flux conversion as well as uncertainties from time interpolation. To address these shortcomings, the CERES Energy Balanced and Filled (EBAF) is used by adjusting the shortwave and longwave top of the atmosphere fluxes within their ranges of uncertainties. This process removes the uncertainties in the measurements. The CERES EBAF also helps in observing cloud free conditions at CERES footprint. An improved instrument calibration, cloud properties, angular distribution models for radiance to flux conversion, use of 1 hourly geostationary imager data for time interpolation has been made possible using CERES EBAF Edition 4.0 (Loeb et al., 2018).

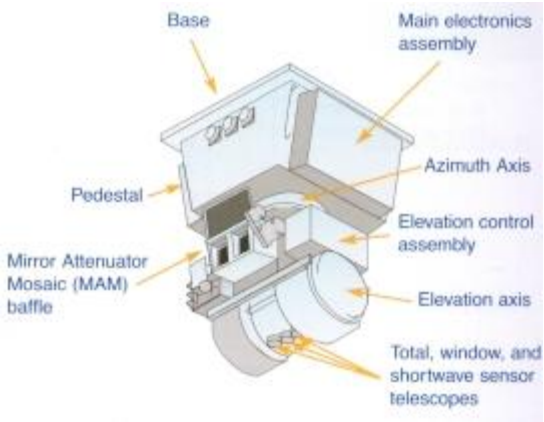

Figure 2.9: Schematic of the CERES instrument (NASA)

2.5.2 Ozone Monitoring Instrument (OMI)

The Ozone Monitoring Instrument was launched on July 15, 2004 onboard the Aura spacecraft in California from the Vandenberg Air Force base. Other instruments onboard Aura are the Microwave Limb Sounder (MLS), the High Resolution Dynamics Limb Sounder (HIRDLS) and the Tropospheric Emission Spectrometer (TRS). OMI is a sun-synchronous polar orbit at 705 km, inclination angle of 98.2^o and a local afternoon equator crossing time of 13:45 (Levelt et al., 2006). Being a more recent instrument compared with the Global Ozone Monitoring Experiment (GOME), the Scanning Imaging Absorption Spectrometer for Atmospheric Chartography (SCIAMACHY) and the Total Ozone Mapping Spectrometer (TOMS), it combines all their advantages by measuring the complete spectrum in the ultraviolet and visible range with a high spatial resolution of 13 km x 24 km on daily global coverage. It measures in a wavelength range from 270 nm to 500 nm. It uses UV/VIS spectrometers to measure the solar irradiance scattered and absorbed in the atmosphere with the aid of a 2-D charge couple device (CCD) detector. This detector enables OMI to measure the complete atmosphere on a global basis daily and with high spatial resolution (Levelt et al., 2006).

After fourteen years in space, Levelt et al (2018) assessed the performance of the instrument. They noted that OMI exceed expectations in air quality measurements and estimation of emissions and monitoring of trends due to its frequent observations of nitrogen dioxide, sulphur dioxide and formaldehyde. They also assessed the science objective of OMI with regards to its contribution to climate research by observing tropospheric ozone and aerosols. They stated that OMI also exceeded expectations with regards to its ability to detect trends as part of longer multi-instrument data records.

OMI standard products include: Radiances and solar irradiances (OML1BRUG, OML1BRVG, OML1BRR), Aerosol absorption optical depth, single scattering albedo (UV), (OMAERUV), BrO columns (OMBRO), OClO slant column (OMCLO), Cloud product O_2-O_2 absorption (OMCLDO2), Cloud product rational Raman (OMCLDRR), HCHO columns (OMHCHO), NO_2 column (standard) (OMNO2), NO_2 columns (DOMINO), O_3 total column, aerosol index (TOMS) (OMTO3), O_3 total column (DOAS) (OMDOSO3), O_3 profile (OMO3PR), pixel corners (OMPIXCOR), SO_2 columns (OMSO2), OMI MODIS merged cloud (OMMYDCLD), OMI indices collocated to MODIS aerosol products (OMMYDAGEO), Surface reflectance climatology (OMLER), Surface UVB (OMUVB), Total O_3, Effective cloud fraction UV index, erythemal UV index, erythemal daily UV dose, SO_2 index and Aerosol index. All these products are available from 2004 to present (Levelt et al., 2018).

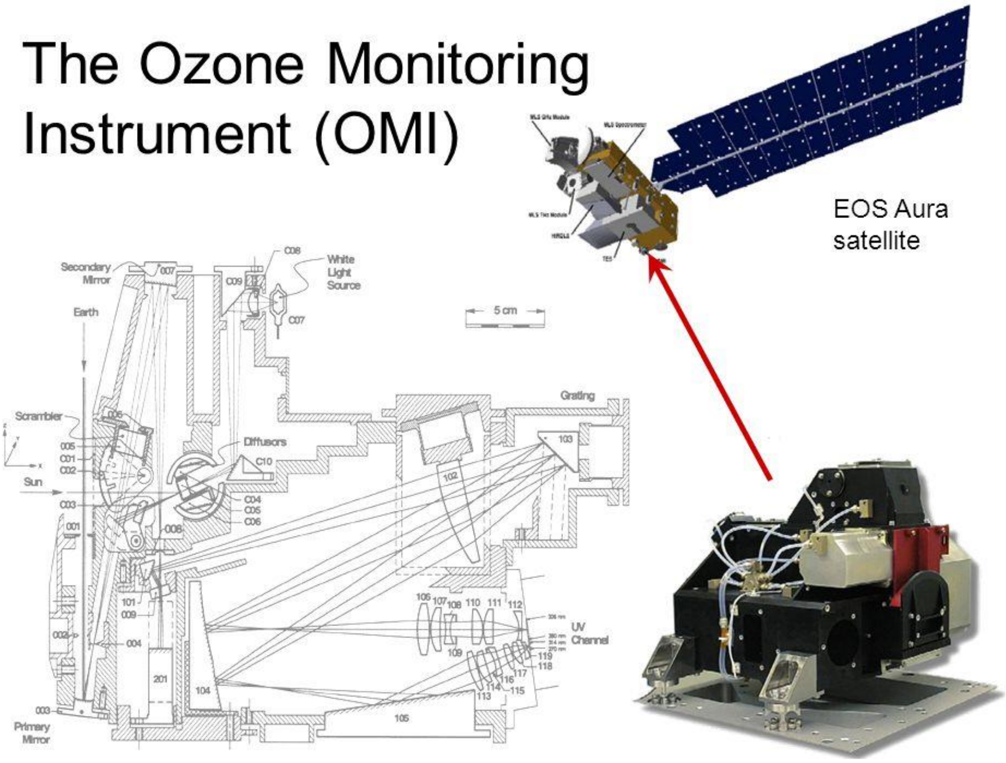

Figure 2.10: OMI instrument (Mijling Bas & van der A Ronald 2014)

2.6 Ultraviolet Aerosol Index (UVAI)

Aerosols can directly influence the earth's radiation balance by either scattering or absorbing incoming solar radiation, which results in uncertainties in climate radiative forcing (Chen & Bond, 2010). Absorbing aerosol index is a measure of how much the wavelength dependence of backscattered UV radiation from an atmosphere containing aerosols (Mie scattering) differs from that a pure molecular atmosphere (Rayleigh scattering). It indicates the amount of elevated absorbing aerosols in the troposphere (de Graaf et al., 2005).

Mathematically, aerosol index is defined as

$AI = 100 \log_{10} (I_{360\text{-measured}}/I_{360\text{-calculated}})$

Where I_{360}measured is the measured 360 nm OMI radiance and

I_{360}calculated is the calculated 360 nm OMI radiance for a Rayleigh atmosphere.

UVAI is used in detecting aerosol absorption using satellite measurements. It is calculated by separating the spectral contrast of radiances due to aerosol effects from radiances due to Rayleigh scattering (Hammer et al., 2016). They stated two attributes of UVAI method which are that aerosol optical properties are more readily detected over surfaces with low reflectance and that the strong interaction between aerosol absorption and molecular scattering in the near UV increases the sensitivity of UV radiances to aerosol absorption. An increasing number of observations show evidence of significant absorption of a form of organic carbon known as brown carbon (Chen & Bond, 2010). Brown carbon decreases in the visible and near infrared regions is strongest in the ultraviolet region. This brown carbon has been found to significantly contribute to the overall absorption by biomass burning aerosol especially in the UV region (Hoffer et al., 2016; Kirchstetter & Thatcher, 2012). TOMS have provided long-term datasets for AI which have been used extensively to investigate aerosol impact on climate and to study biomass burning, volcanic eruption events and heavy dust. More recently, OMI measures UVAI using the OMI near UV algorithm (OMAERUV) which uses the 354 nm and 388 nm radiances measured to calculate it. When UVAI is positive, it signifies the presence of desert dust, volcanic ash and carbonaceous aerosols which indicates the presence absorbing aerosols. When UVAI is near zero, it implies either clouds or minimal aerosol or other non-aerosol related effects such as unaccounted land surface albedo wavelength dependence, ocean colour effects or specula ocean reflection (Hammer et al., 2016).

$UVAI = -100 \log_{10} (I_{354}^{meas}/I_{354}^{cal} (R^*_{354}))$ Equation (1)

Where I_{354}^{meas} is the top of the atmosphere at 354 nm measured by OMI

I_{354}^{cal} is the radiance at 354 nm calculated for a purely Rayleigh scattering atmosphere bounded by a Lambertian surface of reflectance

R^*_{354} is the adjusted Lambert equivalent reflectivity which is calculated by correcting the Lambert equivalent reflectivity at 388 (R^*_{388}) for the spectral dependence of the surface reflectance at 354 nm.

When UVAI is positive, it signifies the presence of desert dust, volcanic ash and carbonaceous aerosols which indicates the presence absorbing aerosols. When UVAI is near zero, it implies either clouds or minimal aerosol or other non-aerosol related effects such as unaccounted land surface albedo wavelength dependence, ocean colour effects or specula ocean reflection (Hammer et al., 2016).

2.7 Reference

Bosilovich, M.G. Robertson, F.R. Takacs, L. Molod, A. & Mocko, D. (2017). Atmospheric water balance and variability in the MERRA-2 reanalysis. Journal of climate, Vol. 30, 1177-1196.

Brooks, M.J. du Clou, S. van Niekerk, W.L. Gauche, P. Leonard, C. Mouzouris, M.J. Meyer R. van der Westhuizen, N. van Dyk, E.E. & Vorster, F.J. (2015). SAURAN: A new resource for solar radiometric data in Southern Africa. Journal of energy in Southern Africa. Vol. 26.

Chen, Y. & Bond, T.C. (2010). Light absorption by organic carbon from wood combustion. Atmos. Chem. Phys., 10, 1773-1787.

de Graaf, M. Stammes, P. Torres, O. Koelemeijer, R.B.A. (2005). Absorbing aerosol index: sensitivity analysis, application to GOME and comparison with TOMS. Journal of geophysical research, Vol. 110, d01201.

Drummond, A.J. & Kirsten, M.K. (1951). The measurement of solar radiation in South Africa. South African journal of science, 48, 103-110.

Drummond, A.J. & Vowinckel, E. (1957). The distribution of solar radiation throughout southern Africa. journal of meteorology 14(4):343-353.

Fioletov, V.E. Labow, G. Evans, R. Hare, E.W. Kohler, U. McElroy, C.T. Miyagawa, K. Redondas, A. Savastiouk, V. Shalamyansky, A.M. Staehelin, J. Vanicek, K. & Weber, M. (2008). Performance of the ground-based total ozone network assessed using satellite data. Journal of geophysical research, Vol. 113, D14313.

Gelaro, R. McCarty, W. Suarez, M.J. Todling, R. Molod, A. Takacs, L. Randles, C.A. Darmenov, A. Bosilovich, M.G. Reichle, R. Wargan, K. Coy, L. Cullather, R. Draper, C. Akella, S. Buchard, V. Conaty, A. da Silva, A.M. Gu, W. Kim, G.K. Koster, R. Lucchesi, R. Merkova, D. Nielsen, J.E. Partyka, G. Pawson, S. Putman, W. Rienecker, M. Schubert, S.D. Sienkiewicz, M. & Zhao, B. (2017). The Modern-Era Retrospective Analysis for Research and Applications Version 2 (MERRA-2). American meteorological society, Vol. 30, 5419-5454.

Hammer, M.S. Martin, R.V. van Donkelaar, A. Buchard, V. Torres, O. Ridley, D.A & Spurr, J.D. (2016). Interpreting the ultraviolet aerosol index observed with the OMI satellite instrument to understand absorption by organic aerosols: implications for atmospheric oxidation and direct radiative effects. Atmos. Chem. Phys., 16, 2507-2523.

Hoffer, A. Toth, A. Posfai, M. Chung, C.E. & Gelencser, A. (2016). Brown carbon absorption in the red and near infrared spectral region. Atmos. Chem. Phys. Discuss. doi:10.5194.

Kirchstetter, T.W. & Thatcher, T.L. (2012). Contribution of organic carbon to wood smoke particulate matter absorption of solar radiation. Atmos. Chem. Phys., 12, 6067-6072.

Levelt, P.F. Joiner, J. Tamminen, J. Veefkind, J.P. Bhartia, P.K. Zweers, D.C.S. Duncan, B.N. Streets, D.G. Eskes, H. van der A, R. McLinden, C. Fioletov, V. Carn, S. de Laat, J. DeLand, M. Marchenko, S. McPeters, R. Ziemke, J. Fu, D. Liu, X. Pickering, K. Apituley, A. Abad, G.G. Arola, A. Boersma, F. Miller, C.C. Chance, K. de Graaf, M. Hakkarainen, J. Hassinen, S. Ialongo I. Kleipool, Q. Krotkov, N. Li, C. Lamsal, L. Newman, P. Nowlan, C. Suleiman, R. Tilstra, L.G. Torres, O. Wang, H. & Wargan, K. (2018). The Ozone Monitoring Instrument: overview of 14 years in space. Atmos.Chem.Phys. 18, 5699-5745.

Levelt, P.F. van den Oord G.H.J. Dobber, M.R. Malkki, A. Visser, H. de Vries, J. Stammes, P. Lundell, J.O.V. & Saari, H. (2006). The Ozone Monitoring Instrument. IEEE transactions on geoscience and remote sensing, Vol. 33, 1093-1101.

Loeb, N.G. Doelling, R. Wang, H. Su, W. Nguyen, C. Corbett, J.G. Liang, L. Mitrescu, C. Rose, F.G. & Kato, S. (2017). Clouds and the Earth's Radiant Energy System (CERES) Energy Balanced And Filled (EBAF) Top of Atmosphere (TOA) Edition 4.0 data product. Journal of climate. Vol. 31. doi 10:1175.

Martinez, M.A. Andujar, J.M. & Enrique J.M. (2009). A new and inexpensive pyranometer for the visible spectral range. Sensors, 9, 4615-4634.

Mijling, B. & van der A, R. (2014). Emission symposium. Royal Netherland Meteorological Institute, ministry of infrastructure and the environment.

Sudarshan, B.S. Solar energy irradiation measurements.

Rienecker, M.M. Suarez, M.J. Gelaro, R. Todling, R. Bacmeister, J. Liu, E. Bosilocich, M.G. Schubert, S.D. Takacs, L. Kim, G.K., Bloom, S. Chen, J. Collins, D. Conaty, A. da Silva, A. Gu, W. Joiner, J. Koster, R.D. Lucchesi, R. Molod, A. Owens, T. Pawson, S. Pegion, P. Redder, C.R. Reichle, R. Robertson, F.R., Ruddick, A.G. Sienkiewicz, M. & Woollen, J. (2011). MERRA: NASA's Modern-Era Retrospective Analysis for Research and Applications. Journal of Climate, Vol. 24, 3624-3648.

Thakkar Vanita (2014). Solar radiation measurement. Babaria institute of technology, Varnama, Vadodara.

Wielicki, B.A. Barkstrom, B.R. Harrison, E.F. Lee, R.B. Smith, G.L. & Cooper, J.E. (1995). Clouds and the Earth's Radiant Energy System (CERES): an earth observing system experiment. Bulletin of the American Meteorological Society. Vol. 7 853-868.

Figure links

CERES instrument https://ceres.larc.nasa.gov/aqua_pictures.php (last visited 26th May 2018)

CGR3 pyrgeometer http://www.kippzonen.com/Product/16/CGR3-Pyrgeometer#.Ww-rpEiFNPY (last visited 26th May 2018)

CHP1 pyrheliometer http://www.essearth.com/product/pyrheliometers-from-kipp-zonen/ (last visited 26th May 2018)

CNR4 Net Radiometer http://www.kippzonen.com/Product/85/CNR4-Net-Radiometer#.Ww-pGkiFNPY (last visited 26th May 2018)

Global precision pyranometer http://www.eppleylab.com/instrument-list/global-precision-pyranometer/ (last visited 26th May 2018)

IR02 pyrgeometer https://www.hukseflux.com/product/ir02-pyrgeometer (last visited 26th May 2018)

NR Lite 2 Net Radiometer http://www.kippzonen.com/Product/31/NR-Lite2-Net-Radiometer#.Ww-pDUiFNPY (last visited 26th May 2018)

Schematic of a SMP 10 pyranometer http://www.omniinstruments.co.uk/smp10-smart-pyranometers.html (last visited 26th May 2018)

Solys2 sun tracker http://www.omniinstruments.co.uk/solys-2-sun-tracker.html (last visited 26th May 2018)

SRA01 Albedometer https://www.hukseflux.com/product/sra01-albedometer (last visited 26th May 2018)

UVS-A-T UV radiometer http://www.kippzonen.com/Product/26/UVS-A-T-UV-Radiometer#.Ww-odEiFNPY (last visited 26th May 2018)

file:///C:/Users/Dell/Downloads/KippZonen_Brochure_UV_Radiometers_V1508.pdf (last visited 26th May 2018)

CHAPTER THREE

SEASONAL VARIATION IN GLOBAL, DIRECT, DIFFUSE RADIATION OVER SOUTH AFRICAN CITIES AND NAMIBIA

This chapter to be cited as:

Ogunniyi, J. & Sivakumar, V. (2018). Seasonal variation in global, direct, diffuse radiation over South African cities and Namibia. International Conference on Solar Power Systems for Namibia, 16-18 May 2018, University of Namibia.

Seasonal variation in Global, Direct, Diffuse radiation over South African cities and Namibia

Jeremiah Ogunniyi[1] and Venkataraman Sivakumar[1]

School of Chemistry and Physics, Discipline of Physics, University of KwaZulu Nata, Westville, Durban 4000, South Africa

Abstract

The seasonal variation in global, direct and diffuse irradiance over five South African stations (Alexander Bay, Durban, Bloemfontein, Pretoria and Port Elizabeth) and one in Namibia (Windhoek) was evaluated from 2013 to 2017 using datasets from the Southern African Universities Radiometric Network (SAURAN). The result of the seasonal variation in global, direct and diffuse irradiance shows winter minimum and summer maximum. Measurements in Durban and Port Elizabeth from the SAURAN network were uncharacteristically higher than the expected averaged values and were thus, neglected in further analysis. Pretoria station had the least global and direct irradiance but the highest diffuse irradiance while Windhoek and Alexander Bay had the least diffuse irradiance. Modern-Era Retrospective Analysis for Research and Applications (MERRA 2) was used to analyse the variation in surface incident shortwave flux over the sites. The climatological mean of shortwave flux reveals winter minimum and summer maximum with Windhoek and Alexander Bay having the highest radiation while Durban and Port Elizabeth received the least amount of solar radiation. Low solar radiation in Durban and Port Elizabeth was linked to high total cloud fraction while the low cloud cover measured in Alexander Bay could be attributed to high solar radiation in the station. From the incident shortwave analysis, South Africa and Namibia have good solar energy potential throughout the year for solar energy application.

Keywords: solar radiation, solar energy, summer, winter, measurements

3.1 Introduction

Solar radiation is the major and best source of renewable energy with least negative impact on our atmosphere (Jyotsna Singh 2016). It reaches the earth surface mainly in form of shortwave radiation. With the growing scarcity of fossil fuels and availability of cheap and abundant solar radiation, the need to harness solar energy has increased. Though solar energy is readily available, converting it to meet the human's need is expensive. It is therefore important to analyse solar radiation data to determine the solar potential of a location in order to install of photovoltaics (PV) and solar thermal. For the installation of PV, global horizontal irradiance datasets are needed while direct normal irradiance datasets are used for solar power (Singh, 2016). The amount of energy the sun radiates in a second is more than the energy people have ever used (Solangi et al., 2011). Therefore, change in the amount of solar radiation entering the earth has implications on water, agriculture, architectural design as well as solar thermal devices. Southern Africa and Africa receives sunshine all year round which makes Africa local resource high. In fact, according to the Department of Energy, South Africa, South Africa receives an annual average of 220 Wm^{-2} compared to some parts of USA and Europe that receive 150 Wm^{-2} and 100 Wm^{-2} respectively and are making the most of the limited solar radiation they receive. Most solar energy studies require global horizontal irradiance, direct normal irradiance and diffuse horizontal irradiance datasets (Singh and Kruger 2017). However, procuring radiometric instruments such as shaded and unshaded pyranometers and pyrheliometers is expensive. This brought about the SAURAN network with the aim of providing long-term measurements of Global Horizontal Irradiance (GHI), Direct Normal Irradiance (DNI) and Diffuse Horizontal Irradiance (DHI). This study examines the seasonal variability in global, diffuse and direct irradiance over South Africa and Namibia. Solar radiation as well as cloud fraction were also studied over the selected locations.

3.2 Datasets

The global, direct and diffuse radiation datasets used for this study is obtained from the South African Universities Radiometric Network (SAURAN). The primary aim of the SAURAN network is to provide long-term datasets in regions with high solar technology potentials. The SAURAN network uses the Kipp & Zonen CMP11 pyranometers for global and diffuse irradiance measurement while the CHP1 Normal Incidence Pyrheliometers (NIP) is used for direct radiation measurements. All these instruments are mounted on a Solys2 automatic sun tracker with a data sampling rate of 1 second. The shortwave flux and total cloud fraction were obtained from MERRA-2 from 1980 to 2017. The locations, latitudes, longitudes, elevations and period of measurements are presented in Table 3.1.

Table 3.1: Latitude, longitude, elevation and period of observation for the selected SAURAN stations

Locations	Latitude (°S)	Longitude (°E)	Elevation (m)	Period
Alexander Bay	28.56	16.76	141	2014-2017
Bloemfontein	29.11	26.19	1491	2013-2017
Durban	29.82	30.94	200	2013-2017
Port Elizabeth	34.01	25.67	35	2014-2017
Pretoria	25.75	28.23	1410	2013-2017
Windhoek	22.57	17.08	1683	2016-2017

Figure 3.1: Map showing the study locations

3.3 Results and Discussion

3.3.1 Seasonal variation in global, direct and diffuse irradiance

Figure 3.2 shows the seasonal variation in global, direct and diffuse irradiances. The result reveals that stations in the eastern part of South Africa (Durban and Port Elizabeth) have the highest global irradiance. The average global mean ranges from 230.2 Wm^2 in Pretoria to 953.9 Wm^2 in Port Elizabeth while the average direct normal irradiance ranges from 250.6 Wm^2 in Pretoria to 775.1 Wm^2 in Port Elizabeth. For diffuse irradiance, 51.0 Wm^2 was measured in Alexander Bay with Port Elizabeth having a mean of 493.9 Wm^2. The result reveals seasonal variation with summer months having the highest global, direct and diffuse irradiances and winter months having the least. Power and Mills (2005) assessed solar radiation and climate change over eight South African stations and two stations in Namibia. They observed decrease in global and direct irradiances from northwest to southeast while they observed increase in diffuse irradiance towards the east. They attributed the presence of tropical temperate troughs associated with cloud bands to the increase and decrease. However, compared to results Power and Mills (2005) obtained and when compared to other stations within the SAURAN network, irradiances measured in Durban and Port Elizabeth are very high. The reason behind this high discrepancy was not addressed in this work. This discrepancy is further confirmed in the long-term measurement of solar radiation presented in session 3.2 where Durban and Port Elizabeth had the least amount of radiation. When measurements from Durban and Port Elizabeth are neglected, further analysis shows that the mean global irradiance was 230.2 Wm^{-2} in Pretoria and 268.4 Wm^{-2} in Windhoek. For all locations, minimum global irradiance was measured in June corresponding to 147.4 Wm^{-2}, 153.5 Wm^{-2}, 166.9 Wm^{-2} and 197.1 Wm^{-2} in Alexander Bay, Bloemfontein, Pretoria and Windhoek respectively while maximum global irradiance was observed in December in Alexander Bay and Bloemfontein corresponding to 368.6 Wm^{-2} and 329.6 Wm^{-2}, maximum was observed in November in Pretoria and Windhoek corresponding to 279.6 Wm^{-2} and 318.4 Wm^{-2}. Minimum direct irradiance of 234.3 Wm^{-2} and 265.3 Wm^{-2} were measured in June for Alexander Bay and Bloemfontein while their maximum of 413.1 Wm^{-2} and 361.9 Wm^{-2} were recorded in December and November respectively. The seasonal variation in Pretoria and Windhoek were different as minimum direct irradiance corresponding to 206.8 Wm^{-2} and 219.3 Wm^{-2} were observed in March and February and maximum of 298.1 Wm^{-2} and 341.9 Wm^{-2} were measured in August and July respectively. In Bloemfontein and Pretoria, minimum diffuse radiation of 30.8 Wm^{-2} and 33.5 Wm^{-2} were recorded in June and maximum of 84.4 Wm^{-2} and 108.8 Wm^{-2} recorded in December while in Alexander Bay and Windhoek, minimum diffuse radiation of 35.7 Wm^{-2} and 28.2 Wm^{-2} were measured in May and July while their maximum of 70.7 Wm^{-2} and 107.1 Wm^{-2} were measured in November and January respectively. Minimum global and direct irradiance was measured during winter in Pretoria which also had the highest diffuse radiation while Alexander Bay which had the highest direct and global irradiance had the least diffuse irradiance. In their work, Power and Mills (2005) also reported that highest diffuse irradiance was observed in Pretoria with only Port Elizbeth having a statistically significant trend. Also, in their work, they showed that there was statistically significant trend in global irradiance in Bloemfontein, Durban and Pretoria.

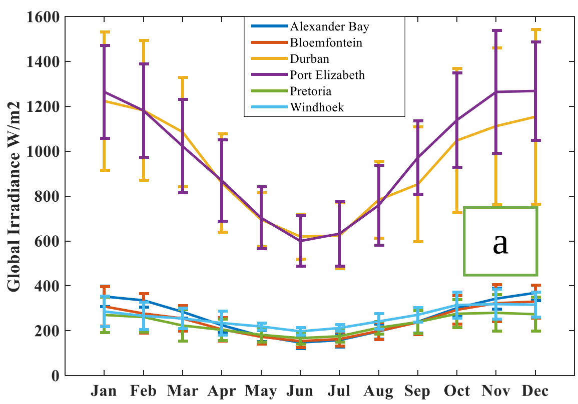

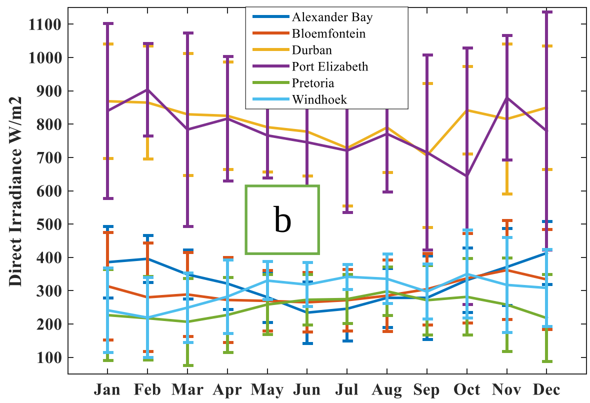

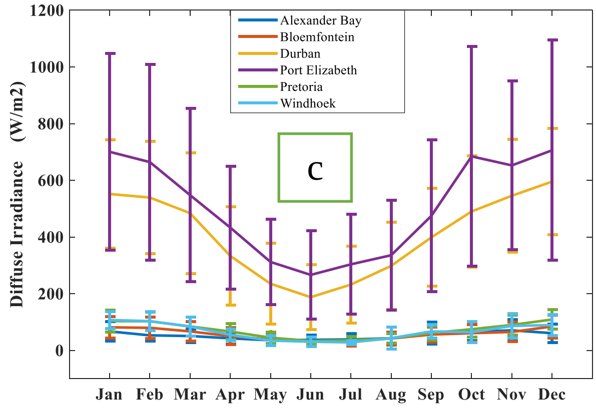

Figure 3.2: Seasonal variation in (a) global horizontal irradiance (b) direct normal irradiance (c) diffuse horizontal irradiance

3.3.2 Variations in Shortwave radiation and total cloud fraction

The amount of solar radiation received in a particular location depends on the altitude, cloud cover and sunshine duration in that location. Figure 3a shows the seasonal variation in shortwave incident radiation from 1980 to 2017. It is observed that the north-western regions (Windhoek and Alexander Bay) received more solar radiation compared to stations in south-east (Durban and Port Elizabeth). This may be attributed to the amount of cloud cover in these regions. The total cloud fraction in Port Elizabeth and Durban were higher compared to other locations as seen in Figure 3b. This results in the scattering of incoming solar radiation before reaching the earth thus reducing solar radiation, while in Windhoek, total cloud fraction is least, thereby allowing more radiation to penetrate. This is consistent with the results obtained by Power and Mills (2005) where they observed that Namibia and three inland locations in South Africa had the least annual diffuse irradiance. The result of the seasonal variation in solar radiation reveals summer maximum and winter minimum.

Table 3.2 presents the decadal mean and trend in solar radiation with Durban having received the lowest and Windhoek the highest amount of radiation. This was consistent through the four decades. The mean radiation received in Durban was 233.1 Wm^{-2} while that of Windhoek was 279.4 Wm^{-2}. The least amount of solar radiation was received between 2000 and 2009 except in Pretoria and Alexander Bay. The trend results reveal decreasing radiation in Pretoria at a decreasing rate. However, the only statistically significant trend was observed between 2000 and 2009 in Port Elizabeth and between 2009 and 2017 in Alexander Bay where the trends were estimated at 2.34 Wm^{-2} and 2.65 Wm^{-2} per decade. Between 1980 and 1989, decreasing trend in solar radiation was observed in Alexander Bay, Port Elizabeth, Pretoria and Windhoek while between 2009 and 2017, decreasing trend was only observed in Pretoria. Also, of the six stations, only Bloemfontein had a consistent positive trend for the four decades while in Windhoek, the only decreasing trend was observed between 1980 and 1989 after which there has been an increasing trend.

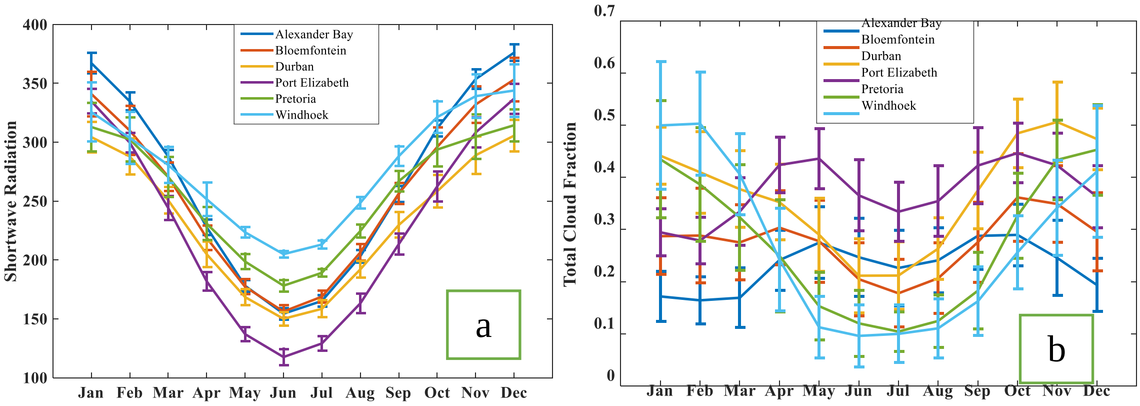

Figure 3.3: Figure showing the seasonal variation in (a) shortwave radiation (b) total cloud fraction

Table 3.2: Decadal mean in shortwave radiation and the decadal trends for the selected locations. * indicates statistically significant trend.

	1980-1989		1990-1999		2000-2009		2009-2017	
	Mean	Trend	Mean	Trend	Mean	Trend	Mean	Trend
Alexander Bay	270.1	-0.99	267.8	-0.38	267.4	-1.94	266.5	2.65**
Bloemfontein	255.7	0.23	258.8	1.00	255.5	0.24	257.3	0.08
Durban	232.4	0.31	234.5	-0.99	232.0	-0.74	233.4	0.06
Port Elizabeth	230.5	-1.40	226.6	-1.75	227.1	2.34*	225.7	1.45
Pretoria	253.8	-1.78	259.4	-0.75	256.5	-1.54	257.0	-0.55
Windhoek	286.5	-0.68	279.3	0.39	275.9	0.93	275.9	1.86

3.4 Summary

This chapter examined the seasonal variability in GHI, DNI, DHI, solar radiation and total cloud fraction over five South African cities and one Namibia city. Following are the main summary of the results noted:

- Recorded values of GHI, DNI and DHI for Durban and Port Elizabeth were very high for all seasons attributed to instrumentation. The seasonal variability in GHI, DNI, DHI and solar radiation reveal winter minimum and summer maximum. Alexander Bay had the highest global and direct irradiance and least diffuse irradiance while Pretoria which had the least global and direct irradiance had the highest diffuse irradiance.
- The result of solar radiation analysis shows the north-western part having the highest radiation with the minimum observed in the south-eastern part. This was attributed to low cloud fraction in the north-western part and high cloud fraction in the south-eastern part.
- The decadal trend reveals statistically significant trend in Port Elizabeth between 2000 and 2009 and in Alexander Bay between 2010 and 2017.

Acknowledgement

The authors of this work would like to acknowledge the Giovanni online data system maintained by NASA as well as SAURAN network for the availability of data, and University of KwaZulu Natal for providing an enabling environment to conduct this research work.

References

Brooks M.J., du Clou S., van Niekerk J.L., Gauche P., Leonard C., Mouzouris M.J., Meyer A.J., van der Westhuizen N., van Dyk E.E. and Vorster F. (2015). SAURAN: A new resource for solar radiometric data in Southern Africa. *J. Energy in southern Africa, 26, 2-10*

Jyotsna Singh (2016). Ranking South African provinces on the basis of MERRA 2D surface incident shortwave flux. *J. Energy in southern Africa 27(3) 50-57*

Solangi K.H., Islam M.R., Saidur R., Rahim N.A., and Fayaz H. (2011). A review on global solar energy policy. *Renewable and Sustainable energy reviews,15, 2149-2163*

Singh J. and Kruger A. (2017). Is the summer season losing potential for solar energy applications in South Africa? *J. Energy in southern Africa, 28, 52-60*

Power, H., & Mills, D. (2005). Solar radiation climate change over Southern Africa and an assessment of the radiative impact of volcanic eruptions. *International journal of climatology, 25*(3), 295-318.http://www.energy.gov.za/files/esources/renewables/r_solar.html

(Last visited ????)

CHAPTER FOUR

VARIATIONS IN TEMPERATURE, ULTRAVIOLET AEROSOL INDEX AND TOTAL OZONE OVER FIVE SOUTH AFRICAN CITIES

This chapter is to be cited as

Ogunniyi, J. & Sivakumar, V. (2018). Variations in Temperature, Ultraviolet Aerosol Index and Total Ozone over five South African Cities – Part 1 (Submitted for review – Journal of Energy in Southern Africa)

Manuscript URL: https://journals.assaf.org.za/index.php/jesa/authorDashboard/submission/5772

Variations in Temperature, Ultraviolet Aerosol Index and Total Ozone over Five South African Cities

J. Ogunniyi[1]and V. Sivakumar[1]

School of Chemistry and Physics, Discipline of Physics, University of KwaZulu Natal, Westville, Durban 4000, South Africa

Corresponding author: jerryogunniyi@yahoo.com

Abstract

This study investigates the seasonal variability of temperature, ultraviolet aerosol index (UVAI) and total column ozone over five South African cities: Irene, Johannesburg (Northern region of South Africa), Durban (Eastern region), Cape Town (Southern region) and Springbok (Western region) using data from the Ozone Monitoring Instrument (OMI) for the period October 2004 to September 2016. The results show the influence of the warm Agulhas current on temperatures in Durban and the cold Benguela current on temperatures in Cape Town. UVAI peaks in spring due to the presence of strong absorbing dust and particles resulting from biomass burning. High UVAI values recorded in Durban can be attributed to significant emissions of strongly absorbing aerosols from local sugar cane burning while low values recorded in Cape Town are probably due to the presence of marine aerosols. Low total column ozone values were recorded in 2006 as a direct consequence of the considerable size of the Antarctic ozone hole. Ozone levels were relatively high in 2012 as this was the year with the second smallest ozone hole measured since 2002. All ozone measurements show the well-established behaviour of spring maximum and autumn minimum in the southern mid-latitudes. Second order Fourier decomposition was used to determine the increasing and decreasing trend of total ozone and UVAI. Both showed a time periodicity illustrating annual oscillations. Cape Town had the highest offset for total ozone while minimum offset was found in Springbok. For UVAI, Springbok had the highest offset of 0.59 while minimum offset of 0.30 was measured in Johannesburg.

Keywords: absorption, measurement, seasons, variation

4.1 Introduction

Solar radiation is the major source of energy for the Earth's climate. Variation in the amount of energy received at the Earth's surface, therefore has implications for water resources, agriculture, architectural design and thermal devices on global, regional and local scales (Power and Mills 2005). Bryden et al (2005) showed that the average amount of solar radiation reaching the ground reduced globally by about 10 % between 1960 and 1990 with significant reductions over large regions of Africa, Asia, Europe and North America. Research has focused on the possible reasons for this profound global decrease due to its influence on evaporation, the hydrological cycle, surface temperature and ecosystems (Che et al, 2005; Liu et al, 2004; Stanhill and Cohen 2014; Wild et al, 2005). However, Wild et al, (2005) found that the decreasing trend ended in the late 1980s and did not continue into the 1990s. Instead of a decrease, a significant increasing trend was observed when newly available analysis of surface observations analysis was completed which confirmed satellite estimates and statistical analysis (Liang and Xia (2005)). In their book Shinning On, Dunlap et al, (1992) showed that the amount of solar radiation reaching a particular position on the Earth's surface depends on atmopsheric conditions and position of the sun (ie. solar zenith angle). They also stated that clouds are the predominant atmospheric factor determining the amount of solar radiation reaching the Earth's surface. This is because thick clouds reflect large amounts of incoming solar radiation while thin clouds reflect much less radiation. Therefore, for any given location, the amount of solar radiation reduces with increasing cloud cover. It is important to note that mountains, oceans and large lakes influence the formation of clouds. As a result, surface solar irradiance can be directly impacted by local geological features.

Solar radiation can also be affected by aerosol particles which scatter sunlight back into space and in turn reduce surface temperature (Pope et al, 2012). Some aerosol particles such as dust and carbonaceous aerosols can also absorb solar radiation thereby warming the atmosphere and not the surface (Liepert 2002). Solar radiation in the ultraviolet (UV) wavelength range is prevented from reaching the Earth's surface due to absorption by ozone. Maximum ozone concentrations are found in the stratosphere. Here ozone helps to prevent harmful UV radiation from penetrating the Earth's surface while ozone found in the tropospheric region acts as a pollutant and has harmful health impacts (Sivakumar et al., 2007). It is therefore of great importance to examine the changes in atmospheric ozone due to its effect on the Earth's energy budget.

This investigation focuses on the climatology and seasonal variability of ozone, temperature, cloud pressure as well as UVAI over five South African cities. These parameters are chosen with the aim to determine how they influence each other as well as their variabilities over South Africa. The stations selected are due to the availability of data. Based on the Koppen climate type, Cape town (33.9 ^{o}S; 18.4 ^{o}E), lying in the southernmost part of South Africa falls under the semi-arid classification. Springbok (29.7 ^{o}S; 17.9 ^{o}E), is classified under the hot desert; Irene (29.7 ^{o}S; 17.9 ^{o}E) and Johannesburg (26.2 ^{o}S; 28.0 ^{o}E) are classified to be in the subtropical highlands while Durban (29.9 ^{o}S; 31.0 ^{o}E), located in the eastern coast of South Africa is classified as humid subtropical. These locations are representative of the various types of climatic conditions of South Africa. Section 4.2 focuses on the data employed in this study. Results obtained are discussed in section 4.3 while a summary of the work is presented in section 4.4

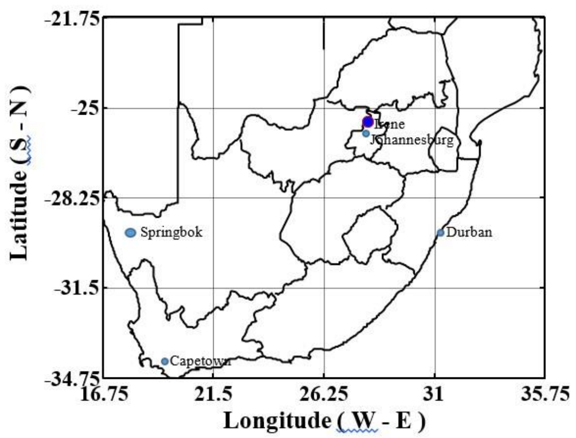

Figure 4.1: Map of South Africa showing the locations of Cape Town, Durban, Irene, Johannesburg and Springbok

4.2 Data and Instrumentation

Data from the Ozone Monitoring Instrument (OMI) was used in this investigation. OMI was launched in July 2004 on a sun-synchronous polar orbit on board the Aura satellite of the National Aeronautics and Space Administration (NASA). The space craft orbits in a 98.2^{o} inclination at about 705 km altitude with an equator crossing time of 13.45 hours. It is a nadir viewing telescope with a field view of 114^{o} used for swath registration and a swath width of 2600 km. OMI combines the advantage of the Global Ozone Monitoring Experiment (GOME) and the Scanning Imaging Absorption Spectrometer for Atmopsheric Chartography (SCIAMACHY) with the advantages of the Total Ozone Mapping Spectrometer (TOMS), measuring the complete spectrum of ultraviolet and visible wavelengths with a very high spatial resolution of 13 km x 24 km and daily global coverage. OMI uses a 2-D charge-couple device to detect radiance and irradiance. One dimension (780 pixels) is used to detect the spectral formation while the other dimension (576 pixels) obtains the spatial information. These 2-D detectors as well as the accompanying optics are probably the most innovative part of this instrument. OMI depolarizes radiation over a complete wavelength range with the use of a polarization scrambler as opposed to GOME and SCIAMACHY which are polarization sensitive instruments. Its measurement accuracy is a function of its in-flight calibration (Levelt et al., 2006). The most important in-flight calibration is the observation of the sun. It observes the sun by opening the sun aperture and rotating a folding mirror and a diffuser in the light path daily. OMI has an internal White Light Source (WLS) which monitors the overall performance of the instrument through a transmission diffuser. The WLS monitors and determines the radiometric degradation, pixel to pixel variation and the nonlinearity of the detector once per week. Depending on the data product, different retrieval techniques are used though the algorithms depend on the experience gained from TOMS, GOME, SCIAMACHY and the Solar Backscatter Ultraviolet Version (SBUV). For the retrieval of total column ozone, TOMS retrieval technique is used as well as the Differential Optical Absorption Spectroscopy (DOAS) technique while the optimal estimation method is used for the retrieval of ozone profile. The Raman scattering technique is used for retrieving cloud pressure while aerosol retrievals are based on changes in reflectance over long wavelength ranges. Ozone and Ultraviolet UVAI datasets are obtained from

OMI. UVAI is calculated based on changes in Rayleigh scattering in the UV range.

Temperature data was obtained from the South African Weather Service (SAWS). This data is in the form of averaged daily data recorded from the early 1990s onwards. However, for this study, only measurements taken from 2004 are considered for comparison with selected atmospheric parameters.

4.3 Results and Discussion

4.3.1 Seasonal variation in Temperature

Figure 4.2a shows the average monthly maximum temperature for Cape Town, Durban, Irene, Johannesburg and Springbok from 1993 to 2016. The figure was obtained by grouping the data in terms of monthly measurements irrespective of the year the measurement was taken. The data quality was very good as they all fell within a standard deviation of 2σ. The figure illustrates the variation in incoming radiation over five cities in South Africa. Temperatures in Durban during winter were considerably higher compared to other locations. This effect may be because of the land and sea breeze in Durban as it is near the Indian Ocean. However, this effect is not observed in Cape Town as both the Indian Ocean and the Atlantic Ocean lie on adjacent sides of the coast and its temperature trends are similar to other experimental stations. According to learnxtra, there are three basic factors that affect weather patterns in South Africa namely, the influence of the oceans, influence of latitudinal position and altitude of the subcontinent as well as the effect of the interior plateau. For Durban, relatively high winter temperatures compared to other locations can be attributed to the influence of the warm Agulhas current flowing along the east coast. The Agulhas current is formed due to the confluence of warm Mozambique and East Madagascar currents. Along the west coast, the influence of the cold Benguela current can also be seen. The Benguela current originates from the upwelling of water from the cold depths of the Atlantic Ocean against the west coast of the continent. The effect of these ocean currents has been seen to contribute to about 6^{o}C temperature difference especially during winter in Cape Town and Durban. Different researchers have documented the role of Agulhas current (Beal and Bryden 1999; Bryden et al 2005; Lutjeharms 2006). Jones (1987), observed high temperatures in Springbok which they attributed to the sheet like intrusion of the Concordia granite gneiss derived from the partial melting of lower crustal rocks. The desert nature of Springbok could also be responsible for high temperature measurements in this location. Irene and Johannesburg are located about 50 km apart and have a similar overpass. When their monthly minimum temperatures are considered their monthly maximum is within 2^{o}C. Irene's temperature measurement was higher than that of Johannesburg throughout the year although both values have same standard deviation. One contributing factor to this may be attributed to the number of industries in Johannesburg which release aerosols into the atmosphere, thereby reducing the amount of incoming solar radiation. In terms of their seasonal variability, all locations have a hot summer and a relatively cold winter except Durban. The maximum temperature for Springbok, Durban, Cape Town, Irene and Johannesburg are 30 ºC, 28.5 ºC, 27.5 ºC, 27.5 ºC and 25.7ºC respectively. Temperature during winter months may be as high as 23 ºC, 19 ºC, 18 ºC, 17ºC and 17ºC for Durban, Irene, Cape Town, Springbok and Johannesburg and they may be as low as 11ºC, 8ºC, 7ºC, 4ºC and 3ºC for Durban, Springbok, Cape Town, Irene and Johannesburg. However, there are days the average temperatures will so much exceed the monthly average and there are days that the locations will experience extremely cold temperatures.

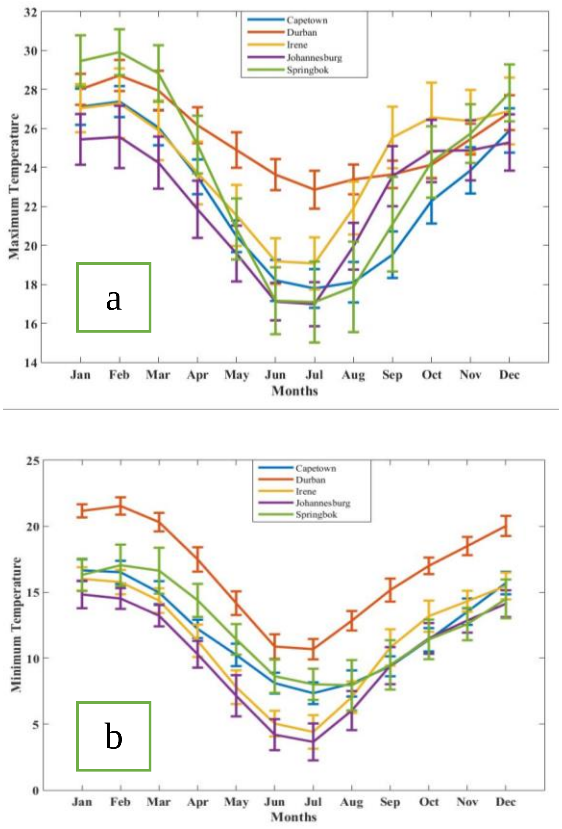

Figure 4.2 Average monthly temperature for Cape Town, Durban, Irene, Johannesburg and Springbok (a) maximum (b) minimum

4.3.2 Interannual variability of total ozone

Figure 3(a) shows the interannual variation in total column ozone for the five selected South African cities. For all locations, relatively high yearly average total column ozone was recorded in 2004. In 2016 low yearly average total column ozone was recorded for the locations under study. The high total column ozone measured in 2004 can be attributed to properties of this data set. This will create the possibility of an artificially high yearly average for 2004. By comparison, data used for the 2016 average was only available for the first six months of the year due to when this research was carried out corresponding to the period when ozone has not yet reached its maximum in the seasonal cycle. This may create the possibility of a low yearly average for 2016. Furthermore, for all locations ozone values were relatively low in 2006, 2008 and 2013. Low total column ozone levels measured in 2006 correspond to the largest ozone hole observed in recorded history. The temperature of the Antarctic stratosphere is the major source of year to year ozone variability in that warm stratospheric Antarctic temperatures reduce the size of the ozone hole. In 2008 and 2013, there were also relatively large ozone holes, and these are most likely responsible for the low average total column ozone measurements obtained for those years.

To identify the increasing or decreasing ozone trend from the measurement, the second order Fourier decomposition was applied to the measured values. This produces a smooth total ozone variation though with similar variations as seen in Figures 4.3a and 4.3b). The obtained Fourier decomposition coefficient shows high ozone for Cape Town corresponding to about 282 DU while Irene and Johannesburg have an offset value of about 265DU. This high ozone concentration in Cape Town can be attributed to maritime sources from dominant winds from SE-W as well as high photochemical reactions taking place there (Zunckel et al, 2004). The decadal trend estimation reveals 1.84 DU, 3.60 DU, 5.23 DU, 5.15 DU and 1.32 DU for Cape Town, Durban, Irene, Johannesburg and Springbok respectively.

4.3.3 Seasonal variation in Total Ozone

Figure 4.3c shows the monthly average ozone variation for the five cities. All cities showed the same seasonal variability of spring maxima and autumn minima which has been well documented for stations in the southern hemisphere subtropics (Diab et al, 2004). Cape Town record an early maximum in September although total column ozone remains approximately constant for the month of October. All other locations show peak ozone levels recorded in October. For all stations, minimum ozone concentrations were recorded in April, except for Irene and Johannesburg whose minima occurred in May. Compared to the four other locations, Cape Town has the highest total column ozone recorded over all seasons. Its values when compared with other locations are within the same standard deviation during summer months while larger deviations are observed during the remaining seasons. Irene and Johannesburg had the lowest total column ozone for all months of the year. Although these locations are highly industrialised and emit carbon monoxide, a strong ozone precursor, more ozone is expected in the lower part of South Africa due to Brewer-Dobson circulation (Butchart 2014). Due of photochemical reactions, though more ozone is produced around the equator, ozone rich air is transported to higher latitudes. It is therefore expected that locations in the southern region of South Africa (Cape Town) will have more total ozone concentration compared to locations in the northern region of the country (Irene and Johannesburg). Irene and Johannesburg show very similar behaviour in terms of their ozone variability while measurements for Springbok and Durban are within the same standard deviation, perhaps due to their similar latitudes.

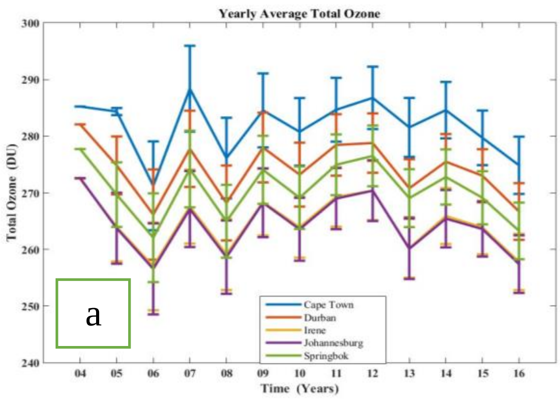

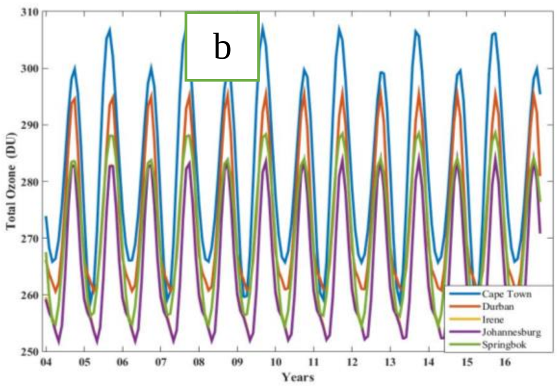

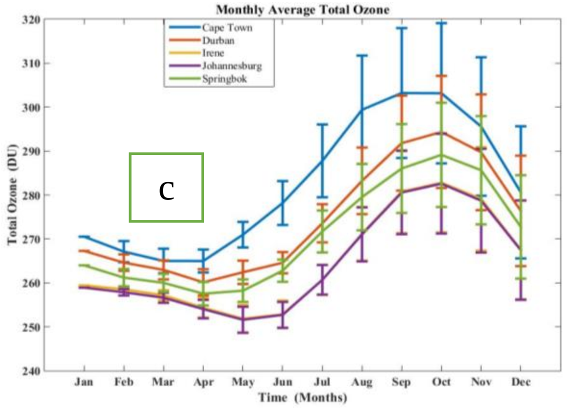

Figure 4.3(a): Interannual variation in total ozone for Cape Town, Durban, Irene, Johannesburg and Springbok (b) after second order Fourier decomposition

Figure 4.3(c): Monthly average total column ozone variation and their corresponding standard deviation for Cape Town, Durban, Irene, Johannesburg and Springbok

4.3.4 Interannual Variation in UVAI

Interannual variation in UVAI (2004 - 2016) for the five selected locations is shown in Figure 4.4(c). The UVAI is a qualitative metric based on the difference between the ratio of absorbing and non-absorbing spectral radiance ratios provided by model calculations and satellite observations. High values of UVAI correspond to high concentrations of strongly absorbing aerosols such as smoke, mineral dust, ultraviolet absorbing soot and brown carbon. When there is little light attenuation in the atmosphere, the Aerosol Optical Depth (AOD) value is low. This is characterised by relatively clean conditions with low particle concentrations, few large particles and an aerosol number distribution comprising of small non-absorbing particles.

Fourier decomposition was also used in identifying the increasing and decrease trend of UVAI. The time periodicity of this decomposition illustrates an annual oscillation. Irene, Johannesburg and Cape Town reveal the lowest absorption properties with offsets of 0.32, 0.30 and 0.34 respectively while the aerosol index for Durban and Springbok correspond to 0.46 and 0.59. Hersey et al (2015) characterised aerosol properties in urban areas using both ground-based and satellite observations for a ten-year period between 2000 and 2009. According to their study in Cape Town, AOD is lowest compared to other metropolitan cities due to the frequent air-mass origin over clean marine areas as well as minor influence by large or absorbing aerosols. Measurements in Springbok were in the range 0.3 and 0.8 for all years except 2015 when levels were approximately 1.1. The presence of strongly absorbing aerosols in Durban in 2007 and 2015 is indicated by a UVAI in the range 1.3 and 1.6. Highest UVAI recorded in Cape Town can be seen in 2010 and 2011 at levels of 0.7 and 0.6 respectively. The interannual variation in Irene and Johannesburg indicate similar levels of UVAI although Irene's absorption tendencies are slightly stronger than those observed in of Johannesburg with increments of about 0.1 for every year of measurement recorded in Irene. The decadal trend reveals 0.16, 0.27, 0.28, 0.25 and 0.01 for Cape Town, Durban, Irene, Johannesburg and Springbok respectively.

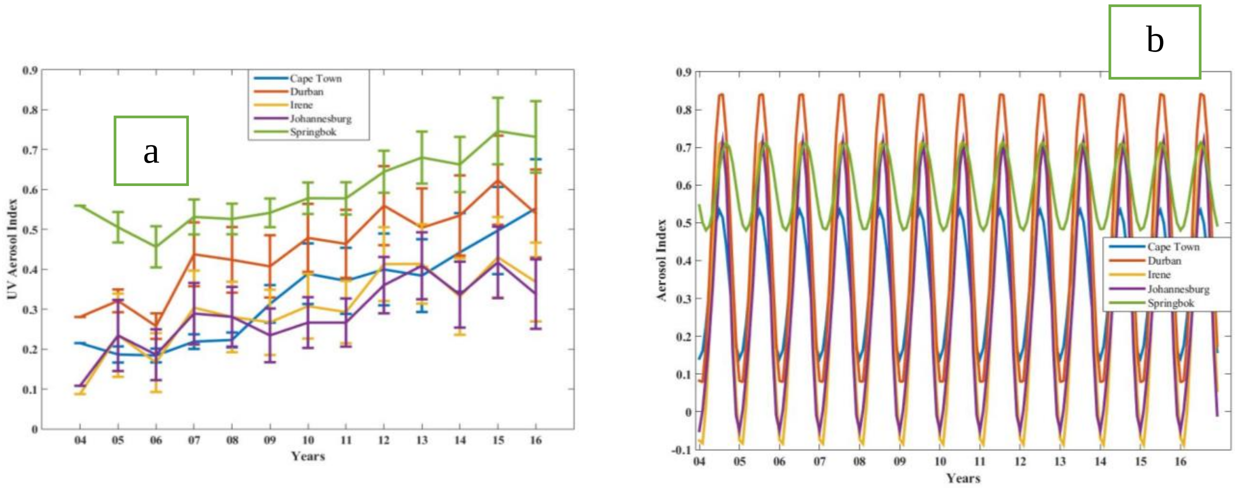

Figure 4.4(a): Yearly average UVAI and corresponding standard deviation for Cape Town, Durban, Irene, Johannesburg and Springbok

Figure 4.4(b): Fourier fitted interannual variation in UVAI for Cape Town, Durban, Irene, Johannesburg and Springbok

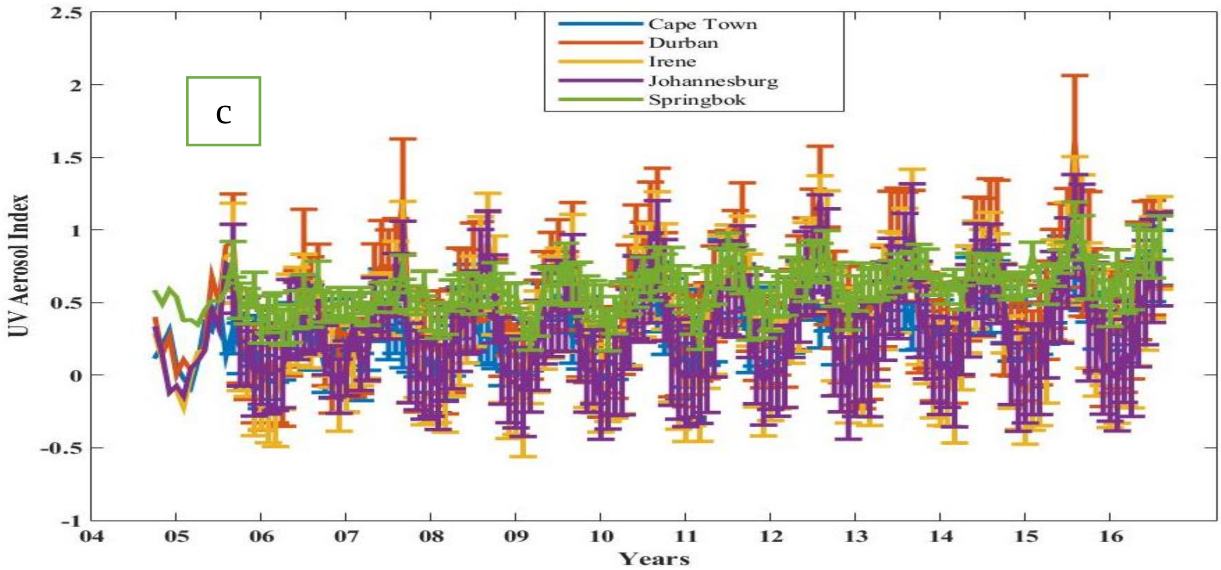

Figure 4.4(c): Temporal trend (2004 - 2016) in UVAI for Cape Town, Durban, Irene, Johannesburg and Springbok

4.3.5 Seasonal variation in UVAI

Figure 4.4(d) shows monthly average UVAI and corresponding standard deviation for the five selected cities. Tesfaye et al (2011) divided South Africa into three classifications in terms of aerosol load level spatial variations. Based on their classifications, Irene and Johannesburg are in the upper South Africa category while Durban and Spingbok lie in the central part, Cape Town is in the lower part of the classification. The seasonal trend illustrated in Figure 4(d) can be considered in terms of biomass burning and dust generation in the five cities under study. All measurements peak in September which is the month with the highest biomass burning in South Africa, a precursor to high aerosol levels. The only exception is Cape Town which peaks in June. Hersey et al (2015) showed that Gauteng (location of Irene and Johannesburg) has the highest density of anthropogenic emissions with mine tailings and waste dumps from refineries prevalent. High turbidity in Cape Town in late winter as observed by Power and Willmott (2001) was also shown to be responsible for maximum UVAI observed in June.

In spring, dust aerosol and biomass burning are strongly prevalent. High UVAI in Durban is attributed to the significant emission of strongly absorbing biomass burning products from local sugar cane burning (Wallace 1999). For Cape Town, low UVAI is observed as marine aerosols appear to dictate column aerosol properties. Maximum UVAI is observed in spring where there is a substantial contribution due to strong absorbing dust and biomass burning particles except Cape Town. During summer, UVAI is less than 0.2 for all locations except Springbok. In Springbok, the UVAI is high for all seasons though with lower values in summer. This may be due to the desert nature of the Northern Cape. A small peak is observed in September and may be attributed to transportation of absorbing aerosol from neighbouring cities.

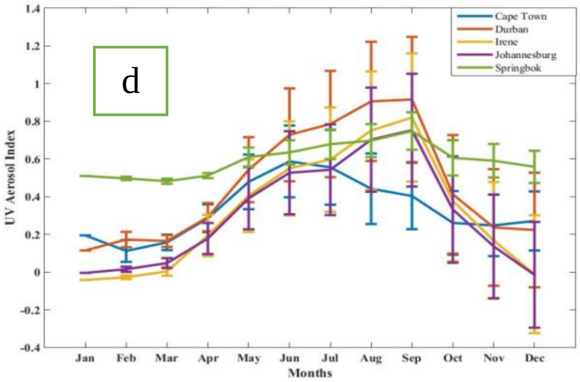

Figure 4.4(d): Monthly average UVAI and corresponding standard deviation for Cape Town, Durban, Irene, Johannesburg and Springbok

4.4 Summary

The seasonal variability of temperature, total ozone and UVAI for Cape Town, Durban, Irene, Johannesburg and Springbok were investigated in this study. The results may be summarised as follows:

Low yearly average total column ozone was recorded in 2006 and can be attributed to the size of the Antarctic ozone hole which was the biggest in recorded history. Conversely, high yearly average total column ozone recorded in 2012 can be attributed to the small size of the Antarctic ozone hole, the second smallest in history. The highest yearly average total column ozone levels were recorded in Cape Town with minimum levels recorded in Irene and Johannesburg for all seasons. The reason for this behaviour is due to the latitudinal positioning of the locations and is explained by the Brewer-Dobson circulation. All monthly average total column ozone measurements confirm the well-established spring time maximum and autumn minimum behaviour pattern that is characteristic of total column ozone levels for southern mid latitudes. Annual oscillation and an offset of 282 DU was obtained for Cape Town while minimum offset of 265 DU was obtained for Irene and Johannesburg when second order Fourier decomposition was used to determine the increasing and decreasing ozone trend. Highest decadal trend of 5.23 was obtained for Irene while the minimum was 1.32 obtained for Spingbok.

In Durban temperatures are relatively high throughout the year compared to other locations. These high temperatures may be due to the influence of the warm Agulhas current flowing along the east coast formed by the confluence of warm Mozambique and east Madagascar currents. Cold winter months in Cape Town may be due to the cold Benguela current originating from the upwelling of water from the cold depths of the Atlantic Ocean against the west coast of the African continent. Temperatures recorded in Irene and Johannesburg have same standard deviation for all months perhaps due to the close proximity of these two locations. Maximum average summer temperatures are 30 ºC, 28.5 ºC, 27.5 ºC, 27.5 ºC and 25.7ºC for Springbok, Durban, Cape Town, Irene and Johannesburg respectively. Minimum values recorded during winter are 11ºC, 8ºC, 7ºC, 4ºC and 3ºC for Durban, Springbok, Cape Town, Irene and Johannesburg though there are days that the monthly maximum and minimum exceeds the average values

Consideration of the UVAI shows that there is an increase in the amount of absorbing aerosols by 0.2 for Springbok, 0.25 for Irene, Johannesburg and Durban and 0.35 for Cape Town. High UVAI observed in Durban can be attributed to the significant emissions of strongly absorbing aerosols from local sugar cane burning while Low values of UVAI are observed in Cape Town and this appears to be due to marine aerosols. UVAI peaks in spring due to the presence of strong absorbing dust and biomass burning particles. This effect is seen in all locations except Cape Town. Time periodicity of UVAI indicates annual oscillation. Springbok had an offset of 0.59 while Johannesburg had an offset of 0.30 when second order Fourier decomposition was used to determine the increasing and decreasing trends.

References

Beal, L. M., & Bryden, H. L. (1999). The velocity and vorticity structure of the Agulhas Current at 32 S. *Journal of Geophysical Research: Oceans, 104*(C3), 5151-5176.

Bryden, H. L., Beal, L. M., & Duncan, L. M. (2005). Structure and transport of the Agulhas Current and its temporal variability. *Journal of Oceanography, 61*(3), 479-492.

Butchart, N. (2014). The Brewer-Dobson circulation. *Reviews of Geophysics, 52*(2), 157-184.

Che, H., Shi, G., Zhang, X., Arimoto, R., Zhao, J., Xu, L., . . . Chen, Z. (2005). Analysis of 40 years of solar radiation data from

China, 1961–2000. *Geophysical Research Letters, 32*(6).

Diab, R., Thompson, A., Mari, K., Ramsay, L., & Coetzee, G. (2004). Tropospheric ozone climatology over Irene, South Africa, from 1990 to 1994 and 1998 to 2002. *Journal of Geophysical Research: Atmospheres, 109*(D20).

Dunlap, M., Cook, G., Marion, B., Riordan, C., & Renne, D. (1992). Shining on: A primer on solar radiation data: National Renewable Energy Lab., Golden, CO (United States).

Hersey, S., Garland, R., Crosbie, E., Shingler, T., Sorooshian, A., Piketh, S., & Burger, R. (2015). An overview of regional and local characteristics of aerosols in South Africa using satellite, ground, and modeling data. *Atmospheric chemistry and physics (Print), 15*, 4259.

Jones, M. (1987). Heat flow and heat production in the Namaqua mobile belt, South Africa. *Journal of Geophysical Research: Solid Earth, 92*(B7), 6273-6289.

Levelt, P. F., van den Oord, G. H., Dobber, M. R., Malkki, A., Visser, H., de Vries, J., . . . Saari, H. (2006). The ozone monitoring instrument. *IEEE transactions on Geoscience and Remote Sensing, 44*(5), 1093-1101.

Liang, F., & Xia, X. (2005). *Long-term trends in solar radiation and the associated climatic factors over China for 1961-2000.* Paper presented at the Annales Geophysicae.

Liepert, B. G. (2002). Observed reductions of surface solar radiation at sites in the United States and worldwide from 1961 to 1990. *Geophysical Research Letters, 29*(10).

Liu, B., Xu, M., Henderson, M., Qi, Y., & Li, Y. (2004). Taking China's temperature: Daily range, warming trends, and regional variations, 1955-2000. *Journal of Climate, 17*(22), 4453-4462.

Lutjeharms, J. R. (2006). The agulhas current: Taylor & Francis.

Pope, F., Braesicke, P., Grainger, R., Kalberer, M., Watson, I., Davidson, P., & Cox, R. (2012). Stratospheric aerosol particles and solar-radiation management. *Nature Climate Change, 2*(10), 713-719.

Power, H., & Mills, D. (2005). Solar radiation climate change over Southern Africa and an assessment of the radiative impact of volcanic eruptions. *International journal of climatology, 25*(3), 295-318.

Power, H. C., & Willmott, C. J. (2001). Seasonal and interannual variability in atm--ospheric turbidity over South Africa. *International journal of climatology, 21*(5), 579-591.

Sivakumar, V., Portafaix, T., Bencherif, H., Godin-Beekmann, S., & Baldy, S. (2007). *Stratospheric ozone climatology and variability over a southern subtropical site: Reunion Island (21 S; 55 E).* Paper presented at the Annales geophysicae.

Stanhill, G., & Cohen, S. (2001). Global dimming: a review of the evidence for a widespread and significant reduction in global radiation with discussion of its probable causes and possible agricultural consequences. *Agricultural and forest meteorology, 107*(4), 255-278.

Wallace Michael Grant (1999). Towards the achievement of environmental standards in the South African sugar industry: The role of GIS. Masters in Science in the Institute of Natural Resources, university of Natal, PMB.

Wild, M., Gilgen, H., Roesch, A., Ohmura, A., Long, C. N., Dutton, E. G., . . . Tsvetkov, A. (2005). From dimming to brightening: Decadal changes in solar radiation at Earth's surface. *Science, 308*(5723), 847-850.

Zunckel, M., Venjonoka, K., Pienaar, J.J., Brunke, E.G., Pretorious, O., Koosialee, A., Raghunandan A. & van Tienhoven, A.M. (2004). Surface ozone over southern Africa: synthesis of monitoring results during the Cross border Air Pollution Impact Assessment project. Atmos.Environ.38,6139-6147.

http://learn.mindset.co.za/sites/default/files/resourcelib/emshare-show-note-asset/859_fdoc.pdf

(Last visited on ????)

Tesfaye, M., Sivakumar, V., Botai, J., & Mengistu Tsidu, G. (2011). Aerosol climatology over South Africa based on 10 years of Multiangle Imaging Spectroradiometer (MISR) data. *Journal of Geophysical Research: Atmospheres, 116*(D20).

CHAPTER FIVE

INTERANNUAL AND SEASONAL VARIATION IN SURFACE SOLAR RADIATION, OZONE AND AEROSOL OVER AFRICA

This Chapter is to be cited as

Ogunniyi, J. & Sivakumar, V. (2018). Interannual and Seasonal Variation in Surface Solar Radiation, Ozone and Aerosol over Africa (*In revision – Atmosfera*)

Manuscript URL:

https://www.revistascca.unam.mx/atm/index.php/atm/author/submission/52609

Interannual and Seasonal Variation in Surface Solar Radiation, Ozone and Aerosol over Africa

Jeremiah OGUNNIYI* and Venkataraman SIVAKUMAR

Discipline of Physics, School of Chemistry and Physics, University of KwaZulu Natal, P.O. Box 54001, Durban 4000, South Africa

* Corresponding author; jerryogunniyi@yahoo.com

Abstract

This study presents an analysis on the variation of downwelling surface incident shortwave flux of the Ozone Monitoring Instrument (OMI) over Africa over a ten-year period (2006 to 2015). Locations close to the equator had higher solar radiation as seen in Central Africa as expected. The climatological mean of shortwave flux shows minimum values of 370 Wm^{-2}, 532 Wm^{-2}, 542 Wm^{-2}, 340 Wm^{-2} and 518 Wm^{-2} in 2010, 2011, 2011, 2010 and 2013 Wm^{-2} and maximum mean of 403 Wm^{-2}, 578 Wm^{-2}, 564 Wm^{-2}, 378 Wm^{-2}, 541 Wm^{-2} were obtained in 2009, 2010, 2010, 2013 and 2012 for North, South, East, West and Central Africa respectively. This study also reveals high potential for solar energy application in Africa for exploration. The interannual variation in ozone reveal an increasing trend over the last decade across Africa. High total ozone in Morocco was attributed to the presence of volatile organic compounds while high ozone in Mozambique was linked with high CO concentration methane and biomass burning. There was an increase of about 6 DU in total ozone in east and west Africa over the last decade. Low ozone in Algeria was attributed to the injection of cold air from higher latitudes which creates a vortex on the Algerian coast. The seasonal variation in ozone reveal a spring time maximum and winter minimum. Seasonal variation between Nairobi and Uganda were within 1 DU. The variation in aerosol index shows that Ethiopia has low absorbing index. Aerosol index was lowest in east Africa and highest in west Africa. Senegal, Gambia, Nigeria, Namibia and Congo have absorbing index greater than 1 for almost all years.

Keywords: downwelling surface radiation flux, energy, equator, transport, season.

5.1. Introduction

The amount of energy reaching the surface of the earth has implications on climate change, agriculture, solar thermal devices, architectural design on global, regional and local scale (Power and Mills, 2005). This amount of solar irradiance observed at ground level on horizontal surfaces is called surface solar irradiance (SSI) which is the sum of direct irradiance – directly from the sun and the diffuse which are either absorbed or reflected (Dahlback and Bjertness, 2008). This direct solar radiation depends on scattering by air molecules (Lefevre et al., 2013). Changes in the amount of tropospheric cloud cover can have a great effect on the penetration of solar radiation due to strong scattering (Dahlback and Bjertness, 2008). It is therefore important to accurately determine the amount of solar radiation penetrating the earth. This knowledge which depends on good measurements is highly essential. Ground based measurements are sparse and the data quality cannot be ascertained (Aksoy, 2011). Moreover, long-term solar radiation data from ground based instruments are grossly insufficient (Lefevre et al., 2013). Several studies have showed the superiority of satellite data over interpolation methods applied to ground based measurement within the radiometric network (Lefevre et al., 2013). The quantity of the radiative energy in the solar wavelength range reaching the earth's surface per time and surface unit is referred to as the downwelling surface shortwave radiation flux (DSSF). DSSF is often the most important quantity used in the characterization of the surface energy budget, hence, the need for reliable and accurate measurement. According to Geiger et al (2008), satellite observations showed improved precision in the measurement of DSSF due to higher spatial resolution as they can exploit the information contained in the images about the precise location of clouds as well as their properties. This downwelling shortwave radiation flux depends on the cloud coverage, solar elevation, atmospheric absorption, scattering as well as the surface albedo. (Liang and Xia, 2005) studied the amount of solar radiation between 1960 and 1990 and found it to have decreased over the three decades. They also studied the regional trends in annual global irradiance using datasets from the Global Energy Balance Archive (GEBA). Their result showed that significant reductions have taken place over large portions of Africa with an average decrease of 2 % per decade. Over similar years, between 1961 and 1990, in the United States of America, (Liepert, 2002) observed a very strong decline in surface solar radiation of about 19 Wm^{-2} or 10 %. Soni et al (2012) also pointed out the decreasing trend in long-term measurements of surface global radiation in many parts of the world. (Stanhill and Cohen, 2001) referred to the phenomenon of the decreasing trend in global solar radiation as global dimming. They evaluated the annual global irradiance over the last 50 years using global irradiance data from 854 sites and estimated a global average of 0.51 Wm^{-2} equivalent to 2.7 % per decade. A 3.4 % decrease was observed in Turkey by Aksoy (2011) while from the former Soviet Union, Abakumova et al (1996) reported a statistically significant decline in global radiation from 60 % of the stations out of the 94 % of the stations where a reduction was observed. They found out that in Russia, an estimate of 7.1% decrease in total global solar radiation was observed between 1955 and 1993 while in Estonia, 6.7 % decrease was observed which they attributed to the influence of increased urbanization on solar radiation transfer. (Long et al., 2009) used data from the department of energy Atmospheric Radiation Measurement (ARM) as well as the National Oceanic and Administration Surface Radiation (SURFRAD) to analyse all-sky and clear sky surface downwelling shortwave radiation and bulk cloud properties from 1995 to 2007. Their result showed widespread brightening averaging about 8 Wm^{-2} for all sky shortwave and 5 Wm^{-2} for clear sky shortwave. They then used their result to explain that changes in dry aerosols or direct aerosols alone cannot explain the changes observed in surface shortwave radiation. However, they stated that changes in cloudiness could play a significant role. (Liang and Xia, 2005) however found that the decreasing trend stopped in the early 1990s as a pronounced increasing trend was observed after. (Soni et al., 2012) also observed that measurements of surface global radiation have shown evidence of transition from dimming to brightening over many parts of the world since the 1990s. This increase, also observed by satellite instruments can be attributed to cloud cover, aerosols, volcanic eruptions or even problems with the measurements. Also, the causes of dimming or brightening may be different from one area to another. (Soni et al., 2012) found a relationship between the reduction in solar radiation and increase cloud optical thickness between 1960 and 1980. However, not in all stations does the increase in cloud cover brings about decrease in surface solar radiation showing that change in solar radiation cannot only be attributed to changes in cloud cover. They also pointed out that the variation in surface solar radiation can also be attributed to extraterrestrial changes in the amount of solar radiation incident at the top of the atmosphere which depends on the Earth's orbital parameters and the solar input, although their contributions appear to be minimal. Solar energy been an alternative source of energy when properly utilised can reduce the pressure on other non-renewable natural sources of energy (Jyotsna and Sivakumar 2014). Aerosol particles in the atmosphere affects the amount of solar radiation that reaches the earth. Some aerosol particles scatter sunlight back into space which reduces the earth's surface temperature while some other particles such as dust and carbonaceous aerosols absorb solar radiation thereby warming the atmosphere (Liepert, 2002; Pope et al., 2012). The amount of solar radiation in the ultraviolet region is reduces as it is absorbed by ozone. This study examines the interannual and seasonal variations in solar radiation, aerosol index and ozone.

5.2 Site, Instrument, Data and Methodology

Though solar radiation is an important factor in global warming, most studies have focused on other continents with very little studies on the African continent. Power and Mills (2005) observed the solar radiation climate change in Southern Africa but only studied two countries Namibia and South Africa. The unavailability of long-term measurements as well as adequate ground-based measurements have made solar radiation studies in the African continent quite challenging. Since there are not enough ground-based measurements over South Africa, measurements from Ozone Monitoring Instrument (OMI), a satellite-based instrument is used for this study. Though a global dataset is made available, due to the focus of this present study, the datasets used are limited to the African co-ordinates. The OMI is a nadir viewing spectrometer which measures both the ultraviolet (UV) and visible reflected and backscattered light in a selected range of the UV and visible spectrum in the wavelength range of 270 nm to 500 nm (Tanskanen et al 2006). For its measurement of solar radiation, the measurement consists of two parts. It first uses an algorithm to determine clear sky surface solar irradiance which subsequently corrects for both cloud as well as absorbing and non-absorbing aerosols. However, when the absorbing effect of aerosols can be estimated which means that the absorbing effect exceeds a certain threshold level, aerosol correction is used to determine the amount of surface solar irradiance. Datasets are available from October 2004 when OMI measurements started operational till date, however, for this study, surface radiation datasets used for this study was restricted to measurements taken between 2005 and 2015 while ozone and aerosol index datasets used are between 2004 and 2016. Eight daily measurements were provided at three-hour interval, however, for this study, the data used were limited to measurements taken at 09.00, 12.00 and 15.00. It is expected that there will be little or no irradiance before and after this time. We divided Africa into five (North, South, East, West and Central) using a 2° x 2° grid for solar radiation while for ozone and aerosol index, countries were selected based on their latitudinal and longitudinal positioning as well as the availability of data.

5.3 Results and Discussion

5.3.1 Interannual Variation in Surface shortwave radiation over Africa

Figure 5.1 shows the interannual variation in DSSF over Africa from 2006 to 2015 at 09.00, 12.00 and 15.00. The east experience more solar radiation during this time of the day as the sun would have risen. The climatological mean shows a minimum value of about 370 Wm^{-2} in 2010 in the North while the climatological mean for South and East corresponds to 532 Wm^{-2} and 542 Wm^{-2} in 2011 respectively while the mean values for West and Central Africa are 340 Wm^{-2} and 518 Wm^{-2} in 2010 and 2013 respectively. Maximum surface irradiance across these five zones correspond to 403 Wm^{-2}, 578 Wm^{-2}, 564 Wm^{-2}, 378 Wm^{-2} and 541 Wm^{-2} for North, South, East, West and Central corresponding to 2009, 2010, 2010, 2013 and 2012. This reveals a low shortwave flux after a year of high flux except for West Africa. Locations close to the equator have higher received higher amount of solar radiation compared to other locations as expected. It is however important to note that, this study concentrated on a 2° x 2° grid and does not reveal details of each country in the zone. For instance, Nigeria, located in the western Africa receives about 600 Wm^{-2}. Based on the amount of solar radiation received in this station, Africa has a high-energy potential for solar energy application and should be explored more. This amount of surface solar radiation has been consistent over the last decade.

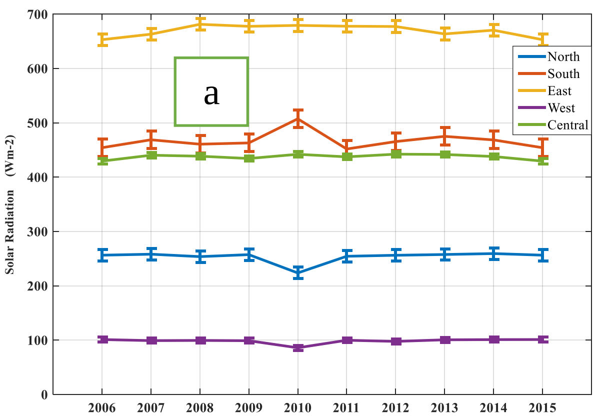

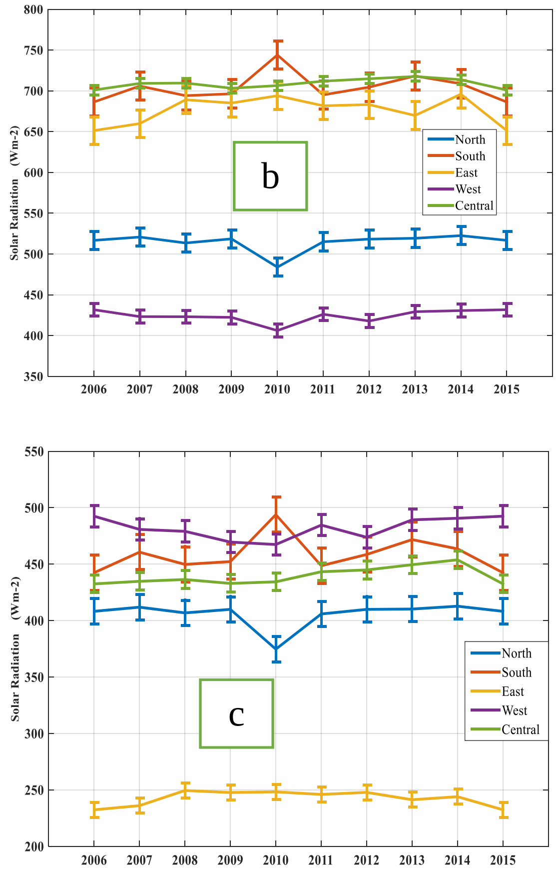

Figure 5.1: Downwelling surface shortwave radiation flux over areas of Africa at (a) 09.00 (b) 12.00 (c) 15.00

5.3.2 Interannual Variation in Ozone

In this section, we present the interannual variation in ozone from 2004 to 2016 over selected regions in Africa. Figure 5.2a shows the variation over Eastern Africa. Total ozone over Malindi was about 8 DU higher than that of Kenya while total ozone in Seychelles, Nairobi and Uganda were all within ±1 DU of each other. High ozone in Malindi may be attributed to its unique location which is just above sea level. The result also reveals that 2013 has the highest total ozone for all countries. Total ozone was also high in 2008 while ozone measurements were considerably low between 2009 and 2012. There has been a systematic increase in total ozone in Ethiopia over the last decade. This ozone increase was not only observed in Ethiopia, but over all locations with about 6 DU over the last decade. Figure 5.2b shows the annual ozone variation over west Africa. Interannual ozone variation over west Africa appears to be similar except for stations that are in the extreme west (Gambia and Senegal). Similar to figure 5.2a, there was high ozone in the atmosphere in 2013, also seen in 2015 while ozone minimum was found in 2007. There was also high ozone in 2006 and 2008. Due to the observed similar trend in total ozone in this region, the major ozone precursor maybe natural sources with little anthropogenic contribution. Over the last decade, ozone has increased by ~6 DU in west Africa. Figure 5.3c shows the interannual variation in ozone over Southern Africa. Interannual ozone variation trend in Southern Africa appears to be different from that of Western Africa with low total ozone in 2006, 2008 and 2013, years in which total ozone were high in west Africa. Also, in 2007 total ozone was high in southern Africa but low in west Africa. Yearly ozone variation is similar for all the stations in southern Africa with Mozambique having the highest overpass, about 11 DU higher compared to Zambia, Namibia, Botswana and about 5 DU higher than total ozone in South Africa. High ozone over Mozambique may be attributed to the Mozambique's atmosphere which has been found to contain high concentrations of carbon dioxide, carbon monoxide, methane, organic and inorganic particles as well as ozone likely caused by biomass burning and the transport of pollutants from South Africa (Mark Cochrane 2010). In South Africa, high ozone may be due to anthropogenic activities from industrial sources, maritime contribution as well as the Brewer-Dobson circulation. Figure 3d shows ozone temporal variation over North Africa and Congo in central Africa. Total ozone over Algeria was much lower compared to other North Africa countries. This may be attributed to the injection of cold and dry air from higher latitudes to southern Spain and Algeria. When there is the presence of this cold air, surface pressure significantly drops, thus, creating vortex on the Algerian coast and the formation of cyclone (Levizzani et al. 2007). High total ozone over Morocco can be attributed to the high-level volatile organic compounds present from forest composed of Eucalyptus and Pine trees (Zaoui et al. 2014). Temporal ozone trend in Alexandria and Cairo are similar with their measurements within 3 DU of each other.

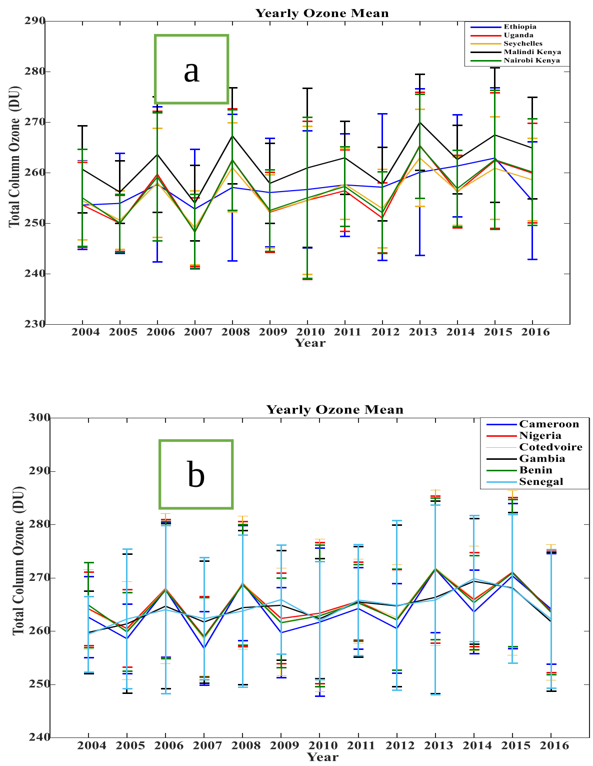

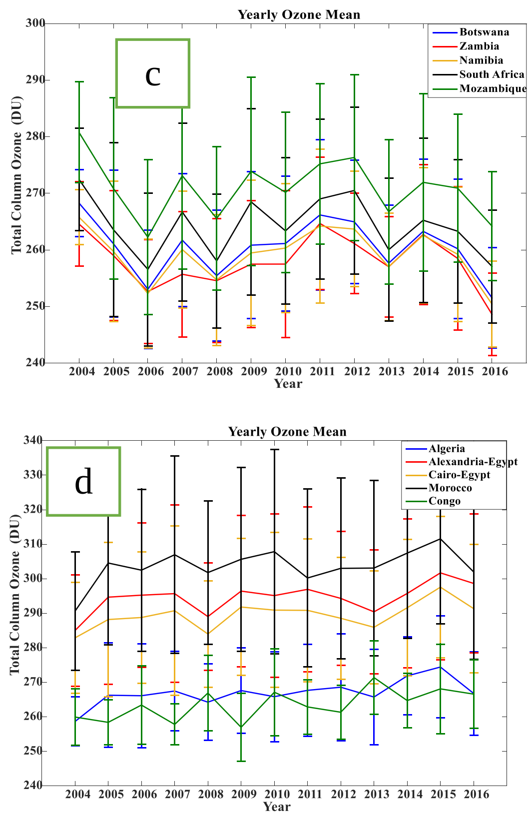

Figure 5.2: Interannual variation in total ozone over (a) East Africa (b) West Africa (c) Southern Africa (d) North and Central Africa

5.3.3 Interannual Variation in Aerosol Index

Figure 5.3a presents the interannual variation in aerosol index over East Africa. The result shows increase aersol index in Malindi.. High aerosol index in Malindi compared to Nairobi may be due to its location as it lies on the Indian ocean coast of Kenya. Ethiopia had the lowest absorbing aerosol index over the decade with less than 0 in 2004 and less than 0.2 in about 8 years and a value above 0.3 in 2012, 2013 and 2016. Aerosol index over Uganda and Nairobi are similar for most years while that of Seychelles is about 0.1 higher than aerosol index over Uganda and Nairobi, Kenya. This may have an effect on the ozone concentration in this region as discussed in section 5.3.2. Figure 5.3b shows the interannual variation in aerosol index over west Africa. Aerosol index over west Africa appears to be steady. Aerosol index in Gambia and Senegal was about 0.2 to 0.4 higher than other west African countries. Aerosol index was lowest in Cameroon over the decade, while in Nigeria and Cotedvoire, the measurements were similar for the decade with Nigeria having a negligibly higher value except for 2016 when the difference was greater than 0.2. The aerosol index over southern Africa is presented in figure 5.3c. Very high aerosol index is observed over Namibia. Botswana's aerosol index was also high compared to other countries. According to NASA, Namibian coast is one of the three places on earth with persistent low-level cloud and the only location that has a steady supply of tiny aerosol particles from inland fires which mix with clouds. Increased biomass burning may also be responsible for the high Aerosol index observed in Namibia (Tesfaye et al. 2011). High aerosol index observed in Botswana can be attributed to the transport of aerosol rich air from Namibia to Botswana and then to Mozambique. Figure 5.3d shows the aerosol index over northern and central Africa. Algeria, noted for desert fire had the highest value for the northern region. Abdessamad (2015) stated four causes of increase in air pollution in Algeria, road traffic which releases nitrogen oxides and carbon monoxide to the atmosphere, public waste dumps, forest fires and emissions from industries as most Algeria's industrialization took place under conditions that did not comply with environmental standards. The trend in interannual variation over Alexandria, Egypt and Morocco are similar while aerosol index over Congo have been on a steady increase over the decade. Karydis et al (2016) presented the effects of mineral dust on global atmospheric nitrate concentrations and showed that the nitrate aerosol fraction is about 20 % to 60 %, with the highest values predicted to be over the equatorial region. They suggested the high mineral dust concentration from the Sahara as well as high nitric acid concentrations from biomass burning in the Congo basin as possible reasons for high aerosol in the region.

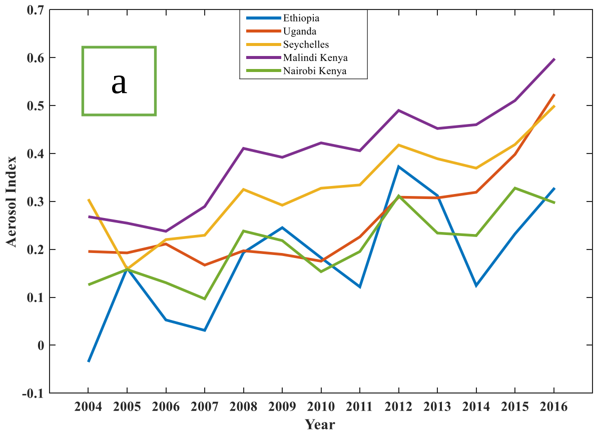

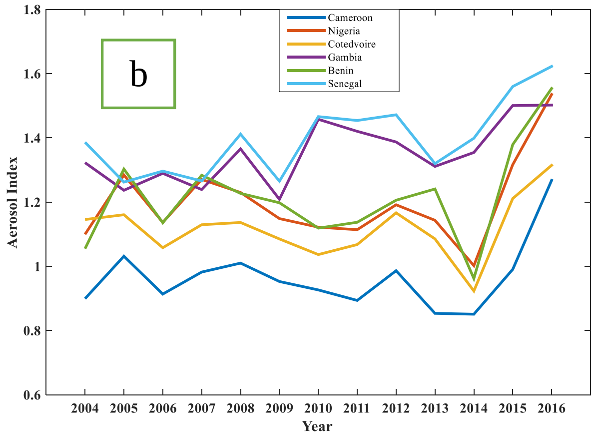

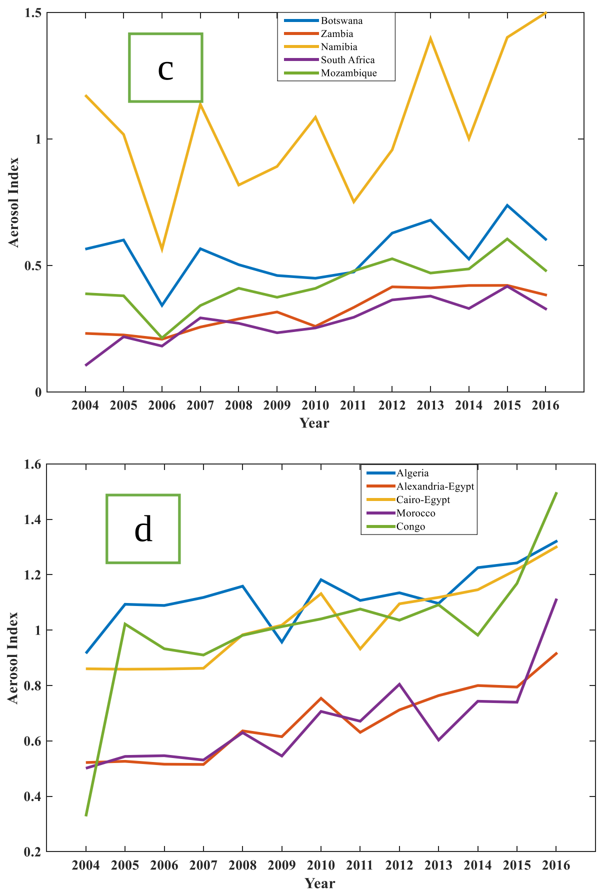

Figure 5.3: Interannual variarion in ozone over (a) East Africa (b) West Africa (c) Southern Africa (d) North and Central Africa

5.3.4 Seasonal Variation in Ozone

The seasonal variation in total ozone over east Africa is presented in figure 5.4a using Kenyan seasons: Spring (September, October, November), Summer (December, January and February), Autumn (March, April and May), Winter (June, July and August). Maximum ozone variation is seen to peak in September for all countries except Seychelles where it is a month early and Ethiopia where maximum ozone variation is found in autumn. This seasonal variation shows similar trend for all countries with a summer minimum, a gradual increase through autumn and winter before it peaks in Spring except Ethiopia which peaks in June. Seasonal mean over Nairobi and Uganda are within ±1 DU of each other while seasonal mean over Malindi is about 5 DU higher than those of Nairobi, Uganda and Seychelles. Figure 5.4b shows the seasonal variation in total ozone over west Africa. Similar to results obtained in sections 5.3.2 and 5.3.3, Gambia and Senegal show a little variation from other west African countries. Total ozone over Cameroon was lower than those of Nigeria and Cotedvoire. Maximum ozone concentration is a month early in July for Senegal and Gambia while for others, maximum ozone is concentration is found in August. Minimum ozone concentration is seen in December and January for all countries. Figure 5.4c shows the seasonal variation in total ozone over southern Africa. All countries show the well-established spring time ozone maximum and autumn minimum in the southern hemisphere. Total ozone over Mozambique was about 12 DU higher than total ozone in South Africa and over 18 DU higher than total ozone in Botswana, Namibia and Zambia. South Africa ozone concentration is about 6 DU higher than other countries in this region. High ozone over Mozambique was attributed to high CO concentration as well as high fire frequency (Leban et al. 2018). Figure 5.4d shows the seasonal ozone variation in northern and central Africa. The seasons here are Spring (March, April, May), Summer (June, July, August), Autumn (September, October, November) and winter (December, January, February). Total ozone in Alexandria was about 4 DU higher that of Cairo during winter and spring but were within ±1 during autumn and summer. Total ozone in Morocco is about 15 DU higher than that of Cairo and about 40 DU higher than Algeria. Inchaouh et al (2017) attributed the high ozone concentration in Morocco to intense solar radiation, high temperature and high relative humidity. The spring maximum observed in East Africa is about 270 DU while those of the west, south and north are 275 DU, 270 DU and 310 DU and minimum are 250 DU, 253 DU, 250 DU and 280 DU for east, west, south and north Africa respectively.

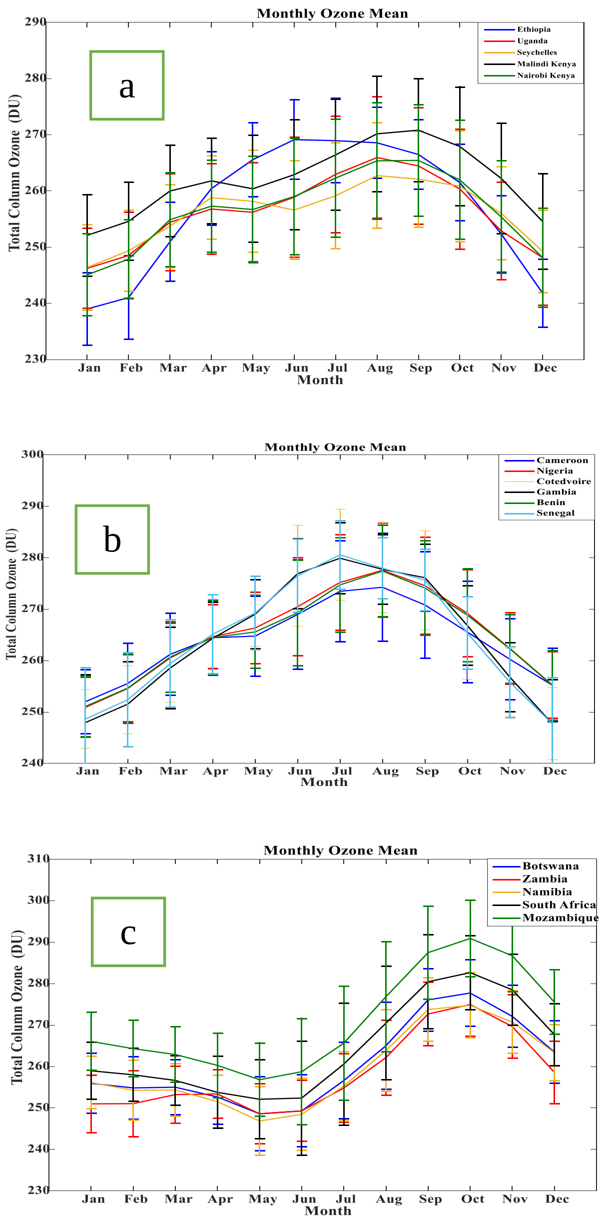

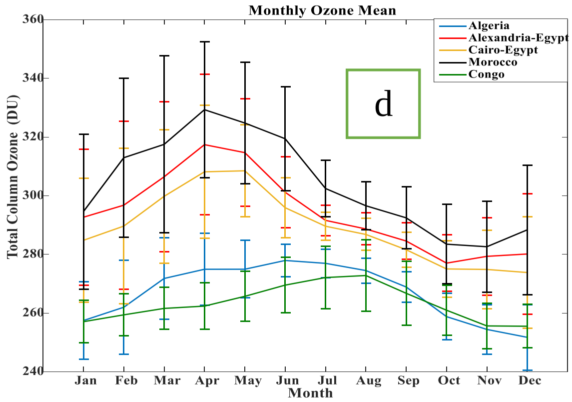

Figure 5.4: Seasonal variarion in ozone over (a) East Africa (b) West Africa (c) Southern Africa (d) North and Central Africa

5.3.5 Seasonal Variation in Aerosol Index

The monthly climatology in aerosol index over east Africa is presented in figure 5.5a. High aerosol index is observed between January and April and then decrease for the remaining part of the year with minimum observed in September and October corresponding to about -0.1 and that of November negligible. High aerosol index is seen in Malindi with no significant seasonal variation. Similar variation is observed in Uganda and Nairobi. The minimum variation in aerosol index is seen in December while maximum aerosol index is observed in February and March. Figure 5.5b shows the seasonal variation in aerosol index in west Africa. Cotedvoire and Senegal have similar variations while aerosol index in Nigeria, Benin and Cameroon were very high in January and February, January corresponding to about 2.6, 2.7, 2.3 respectively. Gambia had an increasing trend in aerosol index for the first six months of the year, before drastically reducing by 0.9 between June and July. Minimum aerosol index is seen between August and October. Figure 5.5c shows the monthly climatology in aerosol index for southern Africa. As presented in section 5.3.3, Aerosol index in Namibia is very high, followed closed by Botswana, Mozambique and South Africa. The climatology presented in 5.5c shows an increasing value from January to October. The aerosol index between Zambia and South Africa are similar from July to October while similar aerosol index is seen between April and July for South Africa and Mozambique. Aerosol index during summer and early autumn is negligible for Zambia and South Africa. The monthly climatology of aerosol index northern and central Africa is presented in figure 5.5d. The result shows an increasing trend from January to June and a decreasing trend from July to December. Aerosol index was highest in Congo corresponding to about 2.3 in June and 2.0 in July. Minimum aerosol index is observed during the winter months and the maximum during the summer months. Aerosol index was above 0.5 for all seasons except Morocco in October.

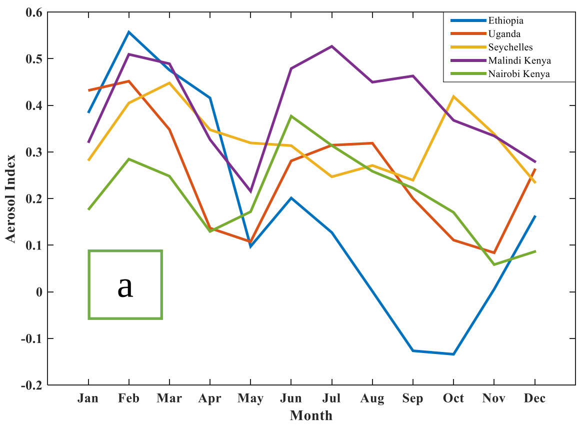

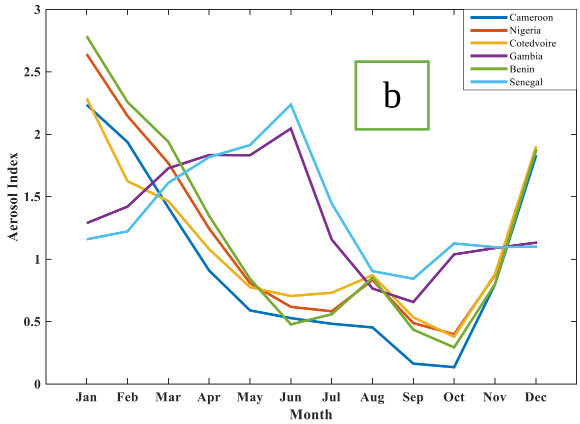

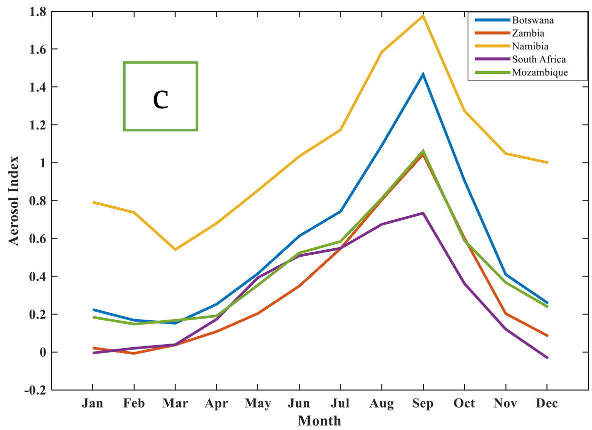

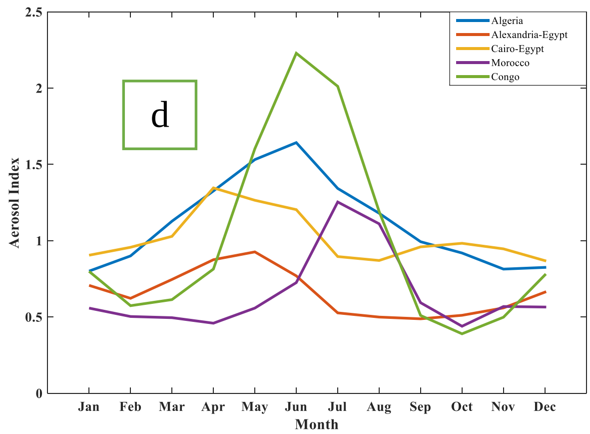

Figure 5.5: Seasonal variation in aerosol index over (a) East Africa (b) West Africa (c) Southern Africa (d) North and Central Africa

5.4. Summary

The interannual and seasonal variability in downwelling surface radiation flux, ozone and aerosol index was studied over Africa. The result showed higher radiation in eastern, southern and central Africa compared to northern and western Africa. However, all regions received good amount of annual radiation which makes Africa viable for solar energy exploration.

The temporal variation in ozone shows an increasing trend across Africa. Total Ozone in Malindi was highest in East Africa corresponding to about 270 DU in 2013 while a minimum of about 250 DU is observed Nairobi, Seychelles and Uganda in 2007. Across Southern Africa, there was a decrease in ozone in 2013 and an increase in 2007. Maximum ozone in southern Africa was observed in Mozambique, corresponding to 280 DU in 2012 and minimum in 2006, corresponding to 250 DU in Zambia. Highest total ozone in Africa is found in the northern part. Total ozone in Morocco was about 310 DU in 2015 while there was a decrease by about 5 DU in 2008 compared to 2007and 2009 in north Africa except Algeria where the decrease is less than 2 DU.

A gradual increase in aerosol index over the last decade was observed. High aerosol index in Congo was attributed to the high dust concentration from the Sahara and high nitric acid concentration from biomass burning while high aerosol index in Algeria was attributed to air pollution majorly from forest fires and increased industrialization. In southern Africa, persistent low-level cloud and tiny aerosol particles mostly smoke mixing with cloud makes aerosol index in Namibia high.

The seasonal trend in total ozone revealed maximum ozone in August for countries in west Africa except Gambia and Senegal whose maximum concentration was a month early. Minimum ozone concentration was observed in December and January. Seasonal ozone variation between Uganda and Nairobi Kenya are within ±1 DU while the seasonal mean over Malindi was about 5 DU higher than other countries for all seasons. The southern hemisphere ozone variation confirmed the spring time ozone maximum and autumn minimum. Monthly ozone over Mozambique was about 20 DU higher than that of Zambia. Total ozone in Morocco was highest in northern Africa, about 15 DU higher than Cairo Egypt and about 40 DU higher than that of Algeria. This high ozone concentration in Morocco was attributed to the intensity of solar radiation, high temperature and high relative humidity.

The seasonal trend in aerosol index over east Africa reveal a gradual increase from January to June and a decreasing trend from July to December. Minimum index was observed in December and maximum in February and March. The highest aerosol index across Africa was seen in west Africa with Nigeria and Benin having values of 2.6 and 2.7 respectively. The highest decrease in aerosol index between consecutive months was seen in Gambia between June and July corresponding to about 0.9. In southern Africa, aerosol index increased from January to October before decreasing in November and December. However, there was negligible index in summer and early autumn for South Africa and Zambia.

References

Abdessamad, B. (2015). Air Pollution in Algeria, Environmental Networking Platform for Children and Youth (http://tunza.eco-generation.org/ambassadorReportView.jsp?viewID=13250).

Abakumova, G., Feigelson, E., Russak, V., & Stadnik, V. (1996). Evaluation of long-term changes in radiation, cloudiness, and surface temperature on the territory of the former Soviet Union. Journal of Climate, 9(6), 1319-1327.

Aksoy, B. (2011). Solar radiation over Turkey and its analysis. International journal of remote sensing, 32(21), 6261-6272.

Dahlback, A., & Bjertness, E. (2008). Global monitoring of atmospheric ozone and solar UV radiation. Solar Radiation and Human Health. Oslo: The Norwegian Academy of Science and Letters, 23-34.

Geiger, B., Meurey, C., Lajas, D., Franchistéguy, L., Carrer, D., & Roujean, J. L. (2008). Near real-time provision of downwelling shortwave radiation estimates derived from satellite observations. Meteorological Applications, 15(3), 411-420.

Inchaouh, M., Tahiri, M., El Johra, B. & Abboubi R. (2017). State of ambient air quality in Marrakech city (Morocco) over the period 2009-2012. International Journal of Geomate, Vol 12, pp, 99-106.

Jyotsna, S. and Sivakumar, V. (2014). Study of surface incidence shortwave flux over two major cities of South Africa. Proc. of 30th Annual conference of South African society for atmosphere science, ISBN 978-0-620-62777-1, 01-02 October 2014, Potchefstroom (South Africa), pp, 58-61, 2014.

Karydis, V.A., Tsimpidi, A.P., Pozzer, A., Astitha, M & Lelieveld, J. (2016). Effects of mineral dust on global atmospheric nitrate concentrations. Atmos.Chem.Phys.,16, 1491-1509.

Leban, T.L., van Zyl, P.G., Beukes, J.P., Vakkari, V., Jaars, K., Borduas-Dedekind,N., Josipovic, M., Thompson, A.M., Kulmala, M. and Laakso, L. (2018). Seasonal influences on surface ozone variability in continental South Africa and implications for air quality. Atmos.Chem.Phys.Discuss

Lefevre, M., Oumbe, A., Blanc, P., Espinar, B., Gschwind, B., Qu, Z., . . . Arola, A. (2013). McClear: a new model estimating downwelling solar radiation at ground level in clear-sky conditions. Atmospheric Measurement Techniques, 6, 2403-2418.

Levizzani, V., Bauer, P. and Joseph Turk (2007). Measuring Precipitaion from Space: EURAINSAT and the Future. Springer Science and Business Media, pp, 522-524.

Liang, F., & Xia, X. (2005). Long-term trends in solar radiation and the associated climatic factors over China for 1961-

2000. Paper presented at the Annales Geophysicae.

Liepert, B. G. (2002). Observed reductions of surface solar radiation at sites in the United States and worldwide from 1961 to 1990. Geophysical Research Letters, 29(10).

Long, C. N., Dutton, E. G., Augustine, J., Wiscombe, W., Wild, M., McFarlane, S. A., & Flynn, C. J. (2009). Significant decadal brightening of downwelling shortwave in the continental United States. Journal of Geophysical Research: Atmospheres, 114(D10).

Mark Cochrane (2010). Tropical Fire Ecology: Climate change, land use and ecosystem dynamics. Springer Science Business Media, chapter 8, page 246

Pope, F., Braesicke, P., Grainger, R., Kalberer, M., Watson, I., Davidson, P., & Cox, R. (2012). Stratospheric aerosol particles and solar-radiation management. *Nature Climate Change, 2*(10), 713-719.

Power, H., & Mills, D. (2005). Solar radiation climate change over Southern Africa and an assessment of the radiative impact of volcanic eruptions. International journal of climatology, 25(3), 295-318.

Soni, V., Pandithurai, G., & Pai, D. (2012). Evaluation of long-term changes of solar radiation in India. International journal of climatology, 32(4), 540-551.

Stanhill, G., & Cohen, S. (2001). Global dimming: a review of the evidence for a widespread and significant reduction in global radiation with discussion of its probable causes and possible agricultural consequences. Agricultural and forest meteorology, 107(4), 255-278.

Tanskanen, A., Krotkov, N. A., Herman, J. R., & Arola, A. (2006). Surface ultraviolet irradiance from OMI. IEEE transactions on Geoscience and Remote Sensing, 44(5), 1267-1271.

Tesfaye, M., Sivakumar, V., Botai, J. & Mengistu Tsidu (2011). Aerosol Climatology over Suth Africa based on 10 years of Multiangle Imaging Spectroradiometer (MISR) data. Journal of geophysical research, vol. 116, D20216

Zaoui, S., Berrabah, M., Azzaoui, K. & Mejdoubi, E. (2014). Monitoring of Tropospheric Ozone in the Peri-Urban area of Oujda city in the East of Morocco. J. Matter. Environ. Sci. 5 (S2), 2504-2509.

https://na.usembassy.gov/nasa-flies-namibia-study-climate-effects-smoke-clouds/ (Last visited ????).

CHAPTER SIX

EFFECTS OF AEROSOL AND CLOUDS ON SURFACE ENERGY BALANCE OVER SELECTED REGIONS OF SOUTH AFRICA

This chapter is to be cited as

Ogunniyi, J. Ruchith, R.D. & Sivakumar, V. (2018). Effects of Aerosol and Clouds on Surface Energy Balance over selected regions of South Africa (Submitted to – Meteorology and Atmospheric Physics)

Submission ID: MAAP-D-18-00171

Effects of Aerosol and Clouds on Surface Energy Balance over selected regions of South Africa

J. Ogunniyi*, R.D. Ruchith, V. Sivakumar

Corresponding author: jerryogunniyi@yahoo.com

Abstract

This study examines the effect of aerosols and clouds on the surface energy balance for selected South African regions. Using the Koppen model of climate classification, eight regions were selected with different surface characteristics. These regions can be described as: warm summer mediterranean, cold desert, hot desert, cold semi-arid, temperate oceanic, humid subtropical, subtropical highland and hot semi-arid. The Modern Era Retrospective analysis for Research and Applications (MERRA 2) data was employed in this study. Shortwave and longwave datasets from MERRA 2 were compared with measurements from Clouds and the Earth Radiant Energy System (CERES). Results obtained showed similar patterns in climatology and interannual variability. Seasonal trends in shortwave and longwave radiation, sensible, latent and ground heat fluxes were examined. A significant trend in shortwave radiation was observed during summer in the warm summer mediterranean, cold and hot desert and subtropical highland regions while during winter, a significant trend was seen in the warm summer mediterranean and hot desert regions. The only significant trend recorded during spring was in the cold semi-arid region. For longwave radiation, significant increases of 1.38 Wm^{-2} and 0.44 Wm^{-2} for warm summer mediterranean and hot desert regions were observed while an increase of approximately 0.54 Wm^{-2} was recorded in autumn for the warm summer mediterranean region. During winter, there was an increase in longwave radiation for the warm summer mediterranean, cold and hot desert regions while in spring, a significant decrease in the cold desert, cold semi-arid and warm summer mediterranean regions was seen. Aerosol seasonal variability was characterized by a spring maximum and winter minimum. Aerosol forcing is also seen to exert more impact on shortwave radiation compared to longwave radiation with a corresponding associated dimming. Finally, variation in Bowen ratio in relation to aerosol effect anomalies is also investigated in this work.

6.1 Introduction

Solar radiation is the main source of energy on Earth and the amount of solar radiation incident on horizontal surfaces directly determines climate variability. The amount of solar radiation received at the surface and recorded by ground-based instrumentation is important, however, sparseness of ground-based stations has proved a constant challenge (Aksoy 2011). Measurements of surface solar irradiance in South Africa can be traced back dated to 1907 in Johannesburg. In subsequent years, a coordinated radiation monitoring network was established. However, continuous monitoring proved challenging due to a number of issues including: remoteness of many sites, difficulties in equipment transportation, influence of climate on instrumentation and differences in infrastructure development between participating African countries. As a result of these difficulties, monitoring programs were established by the South African Weather Bureau and the Meteorological Service of the Belgian Congo (Drummond and Vowinckel 1957). More recently, satellite instrumentation has provided data on a global scale and this has resulted in improved spatial coverage relative to ground-based instrumentation (Singh 2016).

Studies have shown that the level of solar radiation reaching the earth has decreased by approximately10 % over the 30-year period 1960 to 1990 (Liang and Xia 2005; Singh 2016). However, according to Wild et al. (2005), this decreasing trend did not continue into the 1990s, instead they observed a significant increasing trend from the late 1980s. This observation was further confirmed by Pineker et al. (2005) using satellite estimates. By comparison, an investigation by Singh and Kruger (2017) indicated that incident solar radiation declined between 1980 and 2000. They attributed this decline to an increase in the presence of pollutants, particularly aerosols.

The amount of solar radiation reaching the earth is impacted by latitude, cloud cover and the presence of aerosol particles which backscatter radiation thereby reducing surface heating (Liepert 2002). Under clear-sky conditions, atmospheric aerosols are one of the main factors influencing surface solar radiation fluxes. Aerosol levels are enhanced by natural sources such as volcanic eruptions and anthropogenic sources with biomass burning and industrialization being the major contributors. The overall result is that aerosols increase the planetary albedo thereby reducing the amount of solar radiation reaching the surface (Power and Mills 2005). Kim and Ramanathan (2008) showed that absorbing aerosols from anthropogenic sources can reduce the seasonal mean of absorbed solar radiation by as much as 14 Wm^{-2} due to long-range transport of aerosols.

Aerosol-cloud interaction plays a significant role in variability of surface solar radiation. When absorbing aerosols are above the clouds, their radiative impact tends to be highly significant. The amount of cloud cover also has a substantial effect on the penetration of solar radiation due to its strong scattering properties (Dahlback and Bjertness 2008). Soni et al. (2012) examined the relationship between solar radiation and cloud optical thickness for the period 1960 to 1980. They observed that in most of the selected stations, a decrease in solar radiation was recorded when cloud cover increased. They also attributed variation in surface solar irradiance to extraterrestrial factors such as orbital parameters and solar input at the top of the atmosphere. Urankar et al. (2012) noted that large negative bias occurred in areas where large amounts of thick clouds were present.

Most investigations focusing on trends and variability of surface solar irradiance have been carried out in the northern hemisphere while southern hemisphere studies have been mostly limited to a few locations. Power and Mills

(2005) assessed the radiative impact of volcanic eruptions on surface solar radiation and climate change over southern Africa. Their results indicated a decrease in solar radiation from northwest (22.57° S; 17.10° E) to southeast (29.96° S; 30.95° E) and they attributed this decrease to the duration of the annual averaged daily sunshine together with an increase in aerosols from eruptions. Furthermore, they observed approximate decreases in direct irradiance of 8.7%, 5 % and 7.2 % after the volcanic eruptions of Mount Agung in Indonesia, El Chichon in Mexico and Mount Pinatubo in the Philippines. They therefore noted that transport processes conveyed aerosol rich air from the eruption sites around the globe. Singh (2016) ranked levels of surface solar irradiance recorded in various South African provinces using the Modern-Era Retrospective Analysis for Research and Applications MERRA 2D surface incident shortwave flux. Monthly mean results showed that the Northern Cape received the highest levels of surface solar irradiance followed by North West and Free State. The province of KwaZulu Natal surface received minimum surface solar irradiance.

This study focused on an investigation of the effects of aerosols and clouds on the surface radiative budget over South Africa through the use of long-term datasets from MERRA-2. MERRA 2 datasets were then compared with those obtained from CERES. The energy budget for various South African regions was examined as well as aerosol forcing determined.

6.2.1 Data

The Modern Era Retrospective-analysis for Research and Applications (MERRA) 2-D data were employed in this study. This dataset is available from 1979 to the present, however, in this work data from 1979 to 2015 were used. Measurements of monthly net downward shortwave flux (SW), net downward longwave flux (LW), sensible heat flux (H), latent heat flux (LH), ground heat flux (G), cloud fraction (CF) and aerosol optical depth (AOD) were obtained from the Giovanni interactive visualization website https://giovanni.gsfc.nasa.gov/giovanni/. Measurements of longwave and shortwave flux from MERRA were compared with those of Clouds and the Earth Radiant Energy System (CERES). CERES data were used because cloud data are utilized in the calculation of solar radiation incident products and this results in a higher accuracy compared to other gridded products (Zhang et al 2016).

6.2.2 Selected Regions

To determine the effects of aerosol and cloud feedback on the energy budget, South Africa is divided into 8 regions based on the climatic conditions and surface characteristics such as industrialization, vegetation, soil type, precipitation as shown in Figure 6.2. The Koppen-Geiger climatic classification of South Africa was used in the selection of regions. For each selected region, latitude and longitude together with climate type are shown in Table 6.1. Figure 6.1 presents the selected regions for the study.

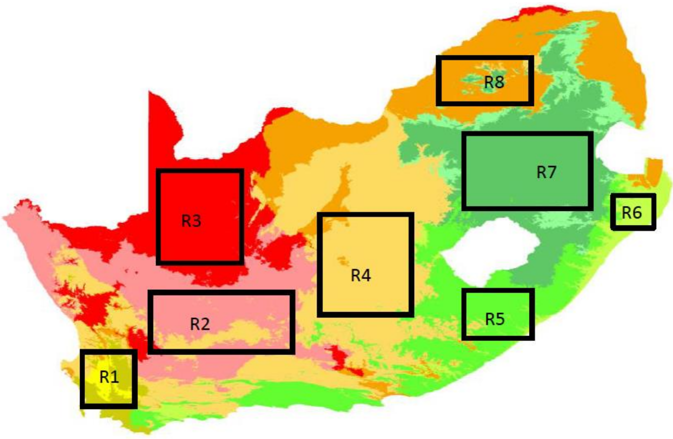

Figure 6.1: Study regions

Table 6.1: Latitude, longitude information and their climate type of the selected regions

Region	Position	Climate type
R1	18 °E - 19 °E, 33 °S – 34 °S	Warm summer Mediterranean
R2	20 °E - 24 °E, 31 °S – 32 °S	Cold dessert
R3	21 °E - 22 °E, 27 °S – 30 °S	Hot dessert
R4	24 °E - 26 °E, 28 °S – 32 °S	Cold semi-arid
R5	28 °E - 29 °E, 31 °S – 32 °S	Temperate oceanic
R6	32 °E - 33 °E, 28 °S – 29 °S	Humid subtropical
R7	27 °E - 31 °E, 26 °S – 27 °S	Subtropical highland
R8	27 °E - 29 °E, 24 °S – 25 °S	Hot semi-arid

6.3 Results and Discussion

6.3.1 Comparison of MERRA and CERES

Figure 6.2a shows a comparison of seasonal variation in shortwave flux measurements as obtained from MERRA and CERES for the period 1997 to 2015. RMSE and correlation values were obtained with respect to MERRA datasets. For R1 to R4, measurements were in good agreement with little deviation from September to December. R2 and R3 showed the best correlation of almost 100 % and RMSE values of 10.12 Wm^{-2} and 10.90 Wm^{-2} respectively (as shown in Table 2) while R6 had the greatest bias in RMSE. The reason for this may be attributed to the arid nature of these regions where the amount of cloud cover may be lower compared to tropical and subtropical regions (Carreras et al, 2015). In more cloudy regions such as R5 to R8, the bias was found to be greater. For R1 and R4, measurements of shortwave flux from MERRA 2 and CERES were within 5 Wm^{-2} while for R5 to R8, measurements were within ± 25 Wm^{-2}. The same observation was noted for longwave radiation. In regions of reduced cloud cover such as R1 to R4, there was a better correlation between MERRA and CERES compared to regions where there are more clouds. This is consistent with the work of Lee et al. (2015). In their investigation, they compared the outgoing longwave radiation with datasets from Atmospheric Infrared Sounder (AIRS), CERES and MERRA and observed bias in their measurements over cloudy regions. They noted that MERRA 2 measurements were lower over tropical mid-high cloud covered regions compared to measurements from CERES. They attributed this to the fact that CERES takes cloud cover into consideration in its measurements. Despite these biases, both MERRA 2 and CERES showed similar patterns of climatology and interannual variability. Loginov et al (2014) assessed the relationship between surface air temperature, surface heat balance and radiative balance at the top of the atmosphere over Russia using reanalysis data. They compared surface radiative fluxes for clear sky using MERRA and CERES and found very good agreement between the two datasets.

For R1 and R4, Figure 6.2b illustrates that measurements of longwave radiation from MERRA 2 and CERES were within 5 Wm^{-2} while for R5 and R8, measurements were within 20 Wm^{-2}. In a similar manner seen in the analysis of shortwave radiation data, the best correlation between measurements from MERRA 2 and CERES was found in R1 and R2 while the least agreement was in R6. For longwave radiation in the R1 to R4 regions, there is more radiation in the second half of the year compared to the first half of the year while for regions between R5 and R8, there is more longwave radiation in the first half of the year than the second half. Both measurements showed a similar seasonal pattern in longwave radiation. This pattern was also observed by Hatzianastassiou and Vardavas (2001) who estimated the longwave radiation budget of the Southern Hemisphere using ISCCP C2 climatological data.

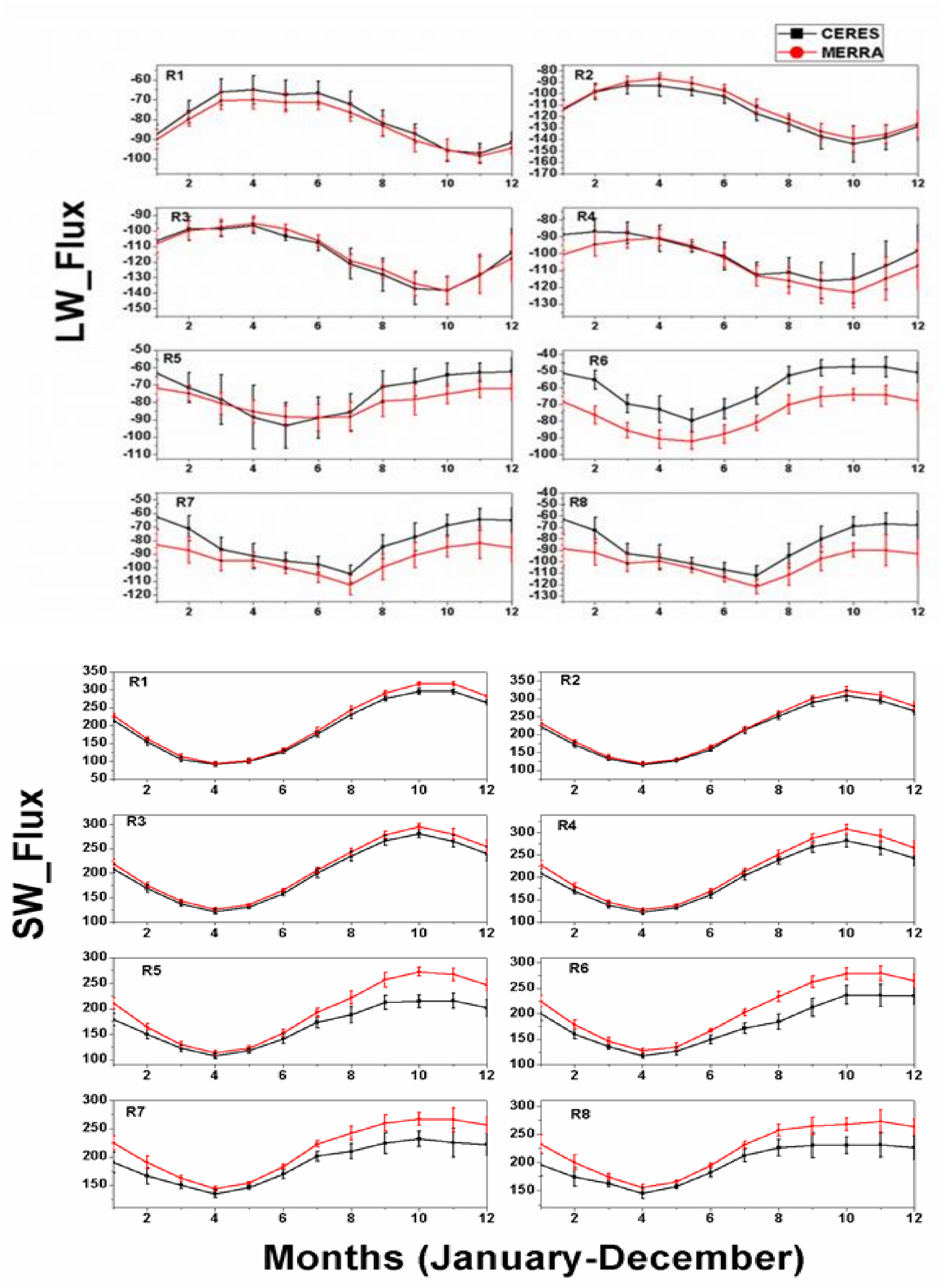

Figure 6.2: Comparison of CERES and MERRA data sets of (a) net shortwave flux (b) longwave flux over selected regions

6.3.2 Total Surface Energy Balance

Figure 6.3 shows the seasonal variation in shortwave, longwave, sensible, latent and ground heat flux as well as variation in cloud fraction and aerosol optical depth. For all regions, net downward shortwave radiation at the surface was observed to be a maximum in summer. It then decreased through autumn and reached a minimum in winter before increasing through spring. The amount of shortwave radiation reaching the surface depends on the amount of aerosol optical depth as well as cloud fraction. Over RI, SW radiation corresponded to approximately 280 Wm^{-2} during summer and approximately 120 Wm^{-2} in June. A similar pattern was observed for all other locations. When AOD is high it absorbs a portion of incident solar radiation incident in a similar manner to the cloud fraction. However, when the sky is clear, more radiation reaches the surface. As expected, shortwave radiation was highest in R2 due to its hot climate. Seasonal values corresponded to over 300 Wm^{-2} during summer and in excess of 150 Wm^{-2} in June. This June minimum was attributed to both increased aerosol optical depth and cloud fraction.

The negative values of longwave radiation show the loss of heat from the Earth's surface. For western regions of South Africa, net downward longwave radiation peaked during winter and this was attributed to increased cloudiness during the study period (Hatzianastassiou and Vardavas 2001)]. This amount of longwave flux emitted may be dependent on the latent heat flux. This is due to the removal of heat from the surface. Similarly, the presence of aerosols and clouds influence the amount of longwave flux. For large numbers of particulates in the atmosphere, there is an increase in longwave radiation due to reflection and emission. Contrary to what was observed over the western regions, there was increased longwave radiation in summer compared to other months in R5 and R6. This may be due to their unique location as they are both situated on the eastern portion of South Africa, along the Indian Ocean.

Observed variations in sensible and ground heat flux revealed a summer maximum and a winter minimum. This is expected as both sensible and ground heat fluxes depend on the amount of solar radiation received. Maximum latent heat flux was observed during spring and the minimum recorded in autumn. Sensible heat flux was higher than latent heat flux in regions bounded by oceans. In R1, sensible heat was higher than latent heat for all months except the period between June and September when there was greater latent heat. The amount of latent and sensible heat flux over R6 was similar for the first half of the year, however, from August to December, there was a significant difference in measurements. Over R5, latent heat flux corresponded to approximately 120 Wm^{-2} in summer. High latent heat over R5 can be attributed to the influence of the warm Agulhas current from the Indian Ocean (Dlomo 2014). For R7, there was a negligible decrease in the amount of sensible heat flux from January to June after which there was an increase for the remaining part of the year. For R8, the difference in the amount of sensible and latent heat flux in late winter and spring was very large. Sensible heat flux was as high as 120 Wm^{-2} in spring while a maximum latent heat of 80 Wm^{-2} occurred in the summer months.

A linear regression was carried out to determine the seasonal trend in shortwave, longwave, sensible, latent and ground heat fluxes was well as the planetary boundary layer (PBL) for all the selected regions and the results presented in Table 6.5. Long time PBL measurements from 1979 to 2015 were obtained from the MERRA. During summer, results showed that there was a signicant decrease in sensible heat over R1, R2 and R3 of approximtely -0.87 Wm^{-2}, -0.47

Wm^{-2}, -0.57 Wm^{-2} respectively while there was a significant increase of approximately 0.34 Wm^{-2} for R7. For R1 and R3 during summer, there was a significant increase in longwave radiation and this corresponded to 1.38 Wm^{-2} and 0.44 Wm^{-2} respectively. For shortwave radiation, there was a significant decrease over R3 of approximately -0.67 Wm^{-2} and a significant increase of 0.25 Wm^{-2} and 0.35 Wm^{-2} for R6 and R7 respectively. Results of longwave flux over the regions reveal that only R3 and R5 showed significant increases of 0.42 Wm^{-2} and 0.34 Wm^{-2} respectively. For all seasons, there was no significant variation in the ground heat flux.

During autumn, there was no significant change in shortwave radiation while over R1, there was a significant increase of approximtely 0.54 Wm^{-2}. Furthermore, there was an increase in sensible heat for R1 and R5 corresponding to 0.82 Wm^{-2} and 0.75 Wm^{-2}, while over the same regions, there was a decrease in latent heat of approximately -0.84 Wm^{-2} and -0.64 Wm^{-2}. During winter, there was a significant decrease in shortwave radiation of approximately -0.98 Wm^{-2} and -1.29 Wm^{-2} for R1 and R3 while a significant increase in longwave radiation corresponding to 1.15 Wm^{-2}, 1.02 Wm^{-2} and 1.36 Wm^{-2} was observed for R1, R2 and R3 respectively. Only R5 showed a significant change in sensible and latent heat.

For R4 during summer, there was a significant increase in sensible heat radiation of approximately 0.50 Wm^{-2} while there was a decrease in longwave radiation over R2, R4 and R7 corresponding to -0.68 Wm^{-2}, -0.73 Wm^{-2} and -0.44 Wm^{-2} respectively. There was a significant increae in sensible heat over R2, R4 and R5 while a significant decrease in the trend of latent heat was observed over R2 and R4.

The annual mean of the different surface fluxes was analyzed and results presented in Table 6.3. Results showed that R8 received the greatest amount of shortwave radiation corresponding to 223.88 Wm^{-2} while R5 received the least shortwave radiation corresponding to 195.82 Wm^{-2}. This is consistent with the earlier work of Ogunniyi and Sivakumar (2018) which showed that the northwestern region of South Africa received more radiation compared to the southeastern region. Other regions also received high levels of shortwave radiation. The annual mean of longwave radiation revealed that R3 and R2 had the highest levels and these corresponded to 115.26 Wm^{-2} and 112.12 Wm^{-2} respectively. The lowest levels were recorded for R5 and R6 and these corresponded to 80.36 Wm^{-2} and 75.69 Wm^{-2} respectively. As expected, sensible heat flux was highest in R2 and R8 and corresponded to 88.35 Wm^{-2} and 83.80 Wm^{-2} while for R5, sensible heat flux was approximately 45.92 Wm^{-2}. Minimum latent heat levels corresponding to 20.55 Wm^{-2} and 16.10 Wm^{-2} were measured over R2 and R3 respectively while the highest levels of 69.43 Wm^{-2} were observed over R5. For ground heat flux, 0.03 Wm^{-2} was measured over R3 and 0.12 Wm^{-2} over R6.

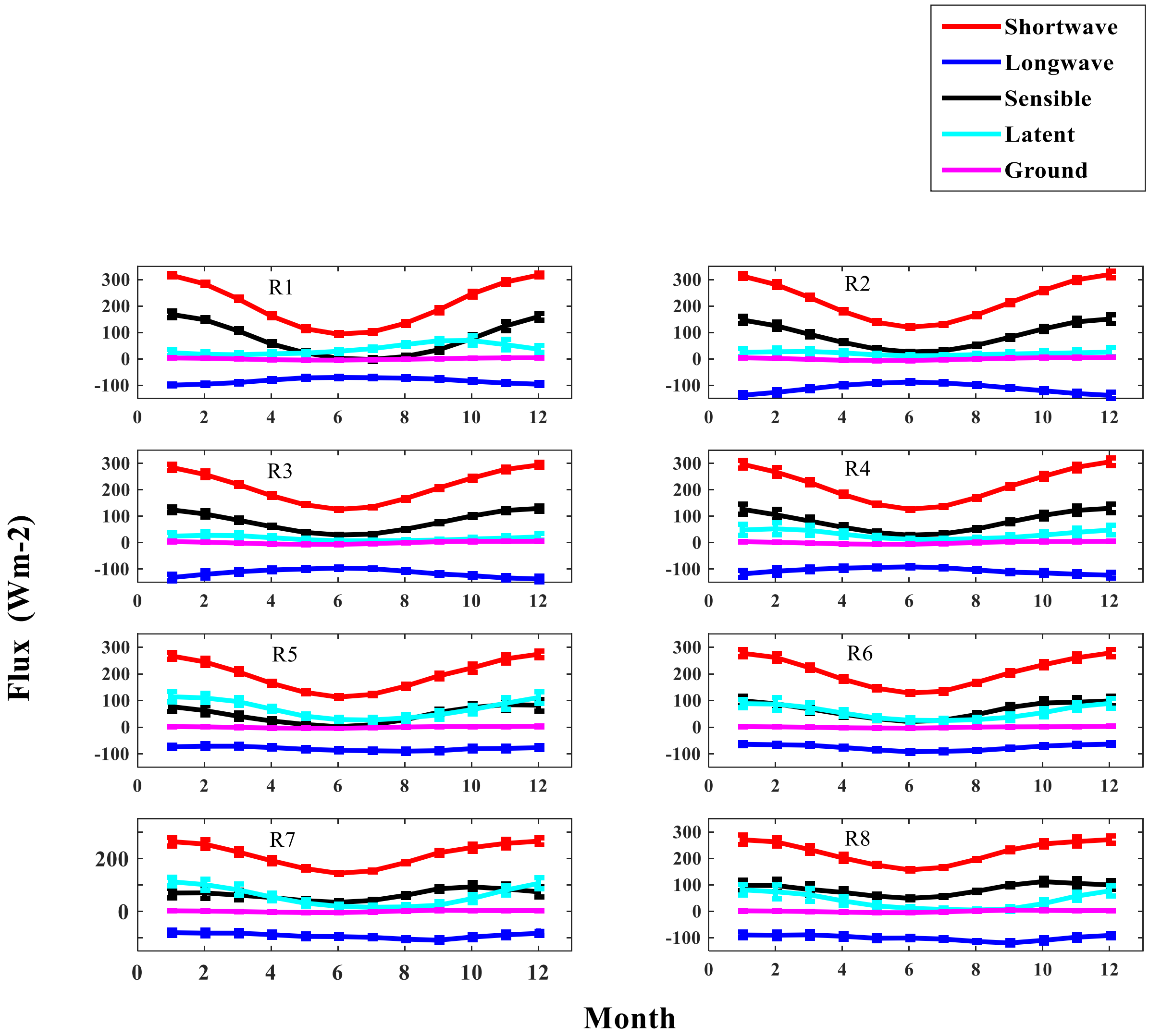

Figure 6.3: Monthly variation of surface fluxes over selected regions

Table 6.2: RMS error and correlation between MERRA and CERES data sets over the selected regions

Region	Long wave radiation		Short wave radiation	
	RMS error	Correlation	RMS error	Correlation
R1	5.581	0.935	13.76	0.987
R2	5.896	0.97	10.12	0.9997
R3	9.298	0.868	10.90	0.995
R4	8.14	0.90	16.57	0.989
R5	10.57	0.801	33.24	0.979
R6	17.26	0.93	32.60	0.964

R7	14.77	0.884	28.20	0.972
R8	17.76	0.878	28.85	0.956

Table 6.3: Annual mean of different surface flux components over the selected regions

Regions	Shortwave	Longwave	Sensible	Latent	Ground
R1	206.02	-83.23	75.57	37.34	0.08
R2	221.08	-112.12	88.35	20.55	0.04
R3	211.07	-115.26	79.68	16.10	0.03
R4	217.33	-106.46	79.68	30.98	0.05
R5	195.82	-80.36	45.92	69.43	0.06
R6	207.94	-75.69	65.67	56.27	0.12
R7	213.52	-92.39	63.69	57.29	0.06
R8	223.88	-100.88	83.80	39.58	0.08

6.3.3 Cloud and Aerosol Radiative Forcing

Figure 6.4 shows seasonal variation in cloud fraction and AOD for the selected regions. Results indicated that AOD reaches a maximum in spring and this maximum is associated with biomass burning. Sinha et al. (2004) studied the transport of biomass burning emissions from southern Africa using ground-based instrumentation, ozonesondes and data recorded using aircraft. They reported an eastward transport of biomass burning emissions from southern Africa towards the Indian ocean which peaks in September. They suggested that this transport may contribute to increased aerosol levels in R5 and R6.

The major source of aerosols in R1, R5 and R6 are marine aerosols. Marine aerosols can be coarse mode or fine mode particles. Tesfaye et al (2011) reported a decline in wind induced coarse mode aerosol production and an increase in fine mode production through inter-coagulation and humidification processes. In R3 and R4, they reported an increase in AOD values but a decrease in wind speed when compared with R1 and R2. Regions R7 and R8 are considered to be industrialized and the population in R7 is quite high. This region is expected to have higher aerosol levels compared to other regions due to industrialization and long-range transport process from surrounding countries.

For the regions R1, R2, R4 and R5, high cloud fraction was observed between May and July and this corresponded to months with low shortwave and sensible heat fluxes. However, over the remaining regions, cloud fraction was a minimum in August and September for R6, R7 and R8 and this corresponded to years of high shortwave and sensible heat flux. However, this did not prove that only cloud fraction and AOD affected the amount of radiation penetrating the atmosphere. For R2 to R8, AOD was high in spring while cloud fraction was low however over R1, both AOD and cloud fraction were high in spring although cloud fraction was higher during early winter.

Estimates of radiative forcing due to anthropogenic aerosols range between -0.3 Wm^{-2} and -2.5 Wm^{-2}. Since there is positive forcing due to greenhouses gases, this negative global climate forcing partially compensates for this effect (Urankar et al, 2012). However, aerosols have a shorter residence time compared to greenhouse gases with the result that atmospheric concentrations respond faster to changes in emission levels (William 2000). Aerosols change the net radiation received at the surface by either scattering or absorbing incoming radiation at the top and bottom of the atmosphere with the consequence of dimming at the surface. If these changes continue over time, this will directly impact the radiative budget as well as surface temperature distribution.

While Figure 6.4 shows the seasonal variation in AOD, Figure 6.5 shows the annual cycle of cloud and aerosol radiative forcing over the selected regions. Both cloud and aerosol forcing are negative and this indicates a reduction in the amount of energy received at the surface resulting in a dimming effect. Since aerosols acts as cloud condensation nuclei, they create cloud droplets. These droplets increase the amount of radiation reflected to space which results in climate cooling. Regions R1 to R8 showed maximum aerosol forcing during spring. Tesfaye et al. (2011) studied aerosol climatology over South Africa using Multiangle imaging spectrometer data and established that the increase in aerosols from June through spring may be linked to air mass transport from southern African countries where biomass burning takes place. However, they noted that the spring maximum was due to pronounced biomass burning in the northeastern and eastern parts of South Africa with little contribution from long range transport process from Namibia, Botswana and Zimbabwe. This may be responsible for high radiative forcing in R6, R7 and R8. With increasing population, vehicular activities and industrialization, South Africa is expected to experience a strong aerosol effect on both shortwave and longwave radiation due to the release of black carbon. Black carbon absorbs shortwave radiation, increases the temperature of the atmosphere and causes dimming effects due to the negative forcing it exerts at the surface (Urankar et al, 2012).

The effect of longwave aerosol forcing was not as significant as that of shortwave aerosol forcing. For all regions, maximum longwave aerosol forcing was observed in summer. High levels of longwave aerosol forcing was observed in R1. Previously Tesfaye et al.

(2011) reported that coarse-mode aerosols dominated the lower parts of South Africa, this coincides with the region R1. Urankar et al. (2012) showed that coarse-mode aerosols exerted direct longwave forcing at the surface. High longwave aerosol forcing in R1, R5 and R6 may therefore be due to their location near the coast. All regions showed low longwave forcing between May and August.

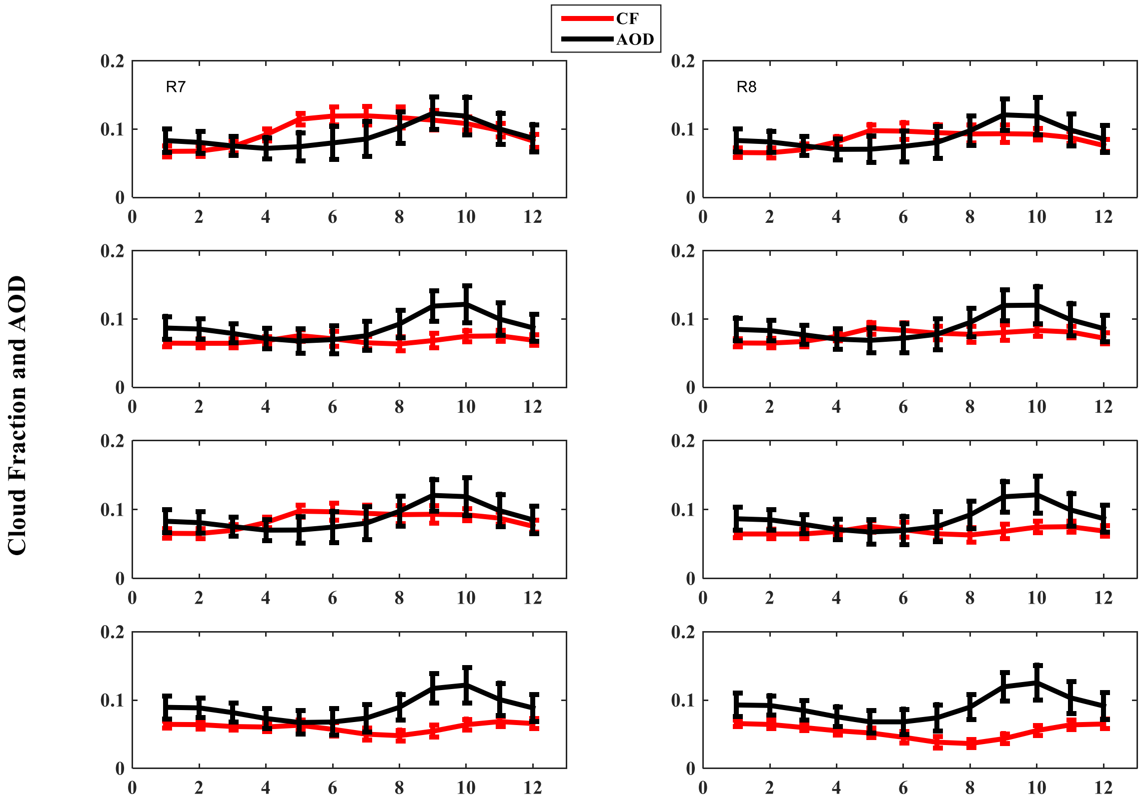

Figure 6.4: Monthly variation of Cloud fraction and Aerosol optical depth over the selected regions

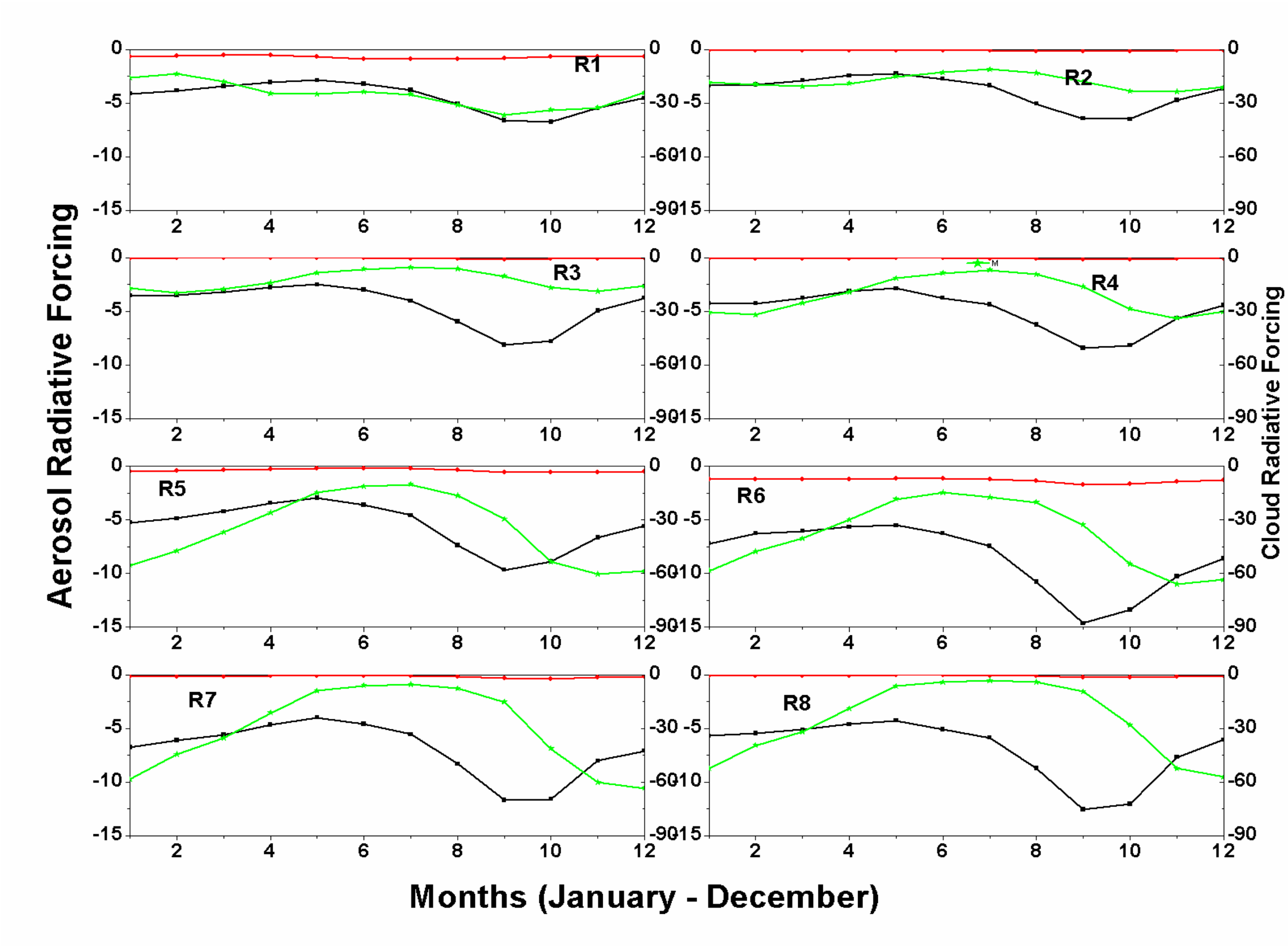

Figure 6.5: Monthly variation of Aerosol and cloud radiative forcing over selected regions

6.3.4 Aerosol effect on Bowen Ration

Bowen ratio is the ratio of sensible heat flux to latent heat flux. When the Bowen ratio is greater than 1, this indicates that the surface has limited water available. However, when the Bowen ratio is less than 1, it indicates that the amount of latent heat in the atmosphere is greater than sensible heat. To obtain the effect of aerosol on Bowen ratio, the annual cycle is removed from the datasets. The difference between the annual cycle and the original datasets gives the anomaly. For R5, R6, R7 and R8, the anomaly in Bowen ratio and aerosol radiative forcing over winter and spring is presented in Figure 6.6. Regions R1 to R4 were excluded as their anomalies were negligible. Furthermore, winter and spring were characterized by higher anomalies. In the results presented here, there was a strong negative correlation between aerosol radiative forcing and Bowen ratio for all regions during both winter and spring. When aerosol radiative forcing increases, the Bowen ratio decreases and vice versa. When aerosol radiative forcing decreases, more radiation reaches the surface thereby increasing the amount of sensible heat. This results in an increase in the Bowen ratio. Table 6.4 shows the estimated slope and correlation between aerosol radiative forcing

(ARF) and Bowen ratio for R5, R6, R7 and R8 for winter and spring seasons. For R6, the decrease in aerosol forcing was greater in both winter and spring. R7 had the highest correlation coefficient of -0.78 and -0.61 for both winter and spring while the smallest correlation between aerosol radiative forcing and Bowen ratio occurred during winter for R8 and during spring for R5. This corresponded to values of -0.44 and -0.24 respectively. This result showed that for the selected study period, the aerosol forcing anomaly was strongly correlated in the eastern part of south Africa. It is suggested that this may due to the presence of high amounts of absorbing aerosols.

Table 6.4: Slope and correlation between aerosol radiative forcing and Bowen ratio for the regions R5, R6, R7 and R8 during winter and spring seasons

Region	Winter		Spring	
	Slope	Correlation	Slope	Correlation
R5	-1.01	-0.46	-0.66	-0.24
R6	-1.45	-0.63	-2.23	-0.53
R7	-0.25	-0.78	-0.94	-0.61
R8	-0.03	-0.44	-0.11	-0.50

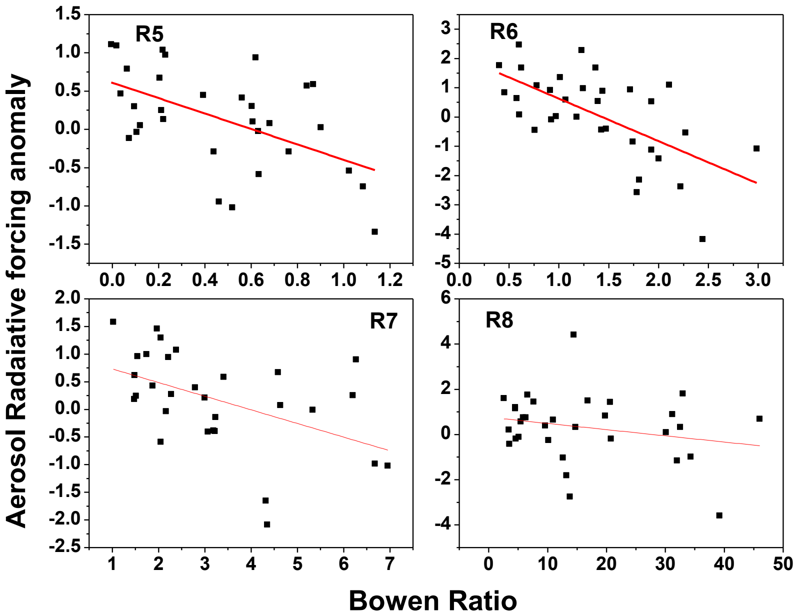

Figure 6.6a: Scatter plot between Bowen ratio and ARF anomaly over the regions R5, R6, R7 and R8 during winter season

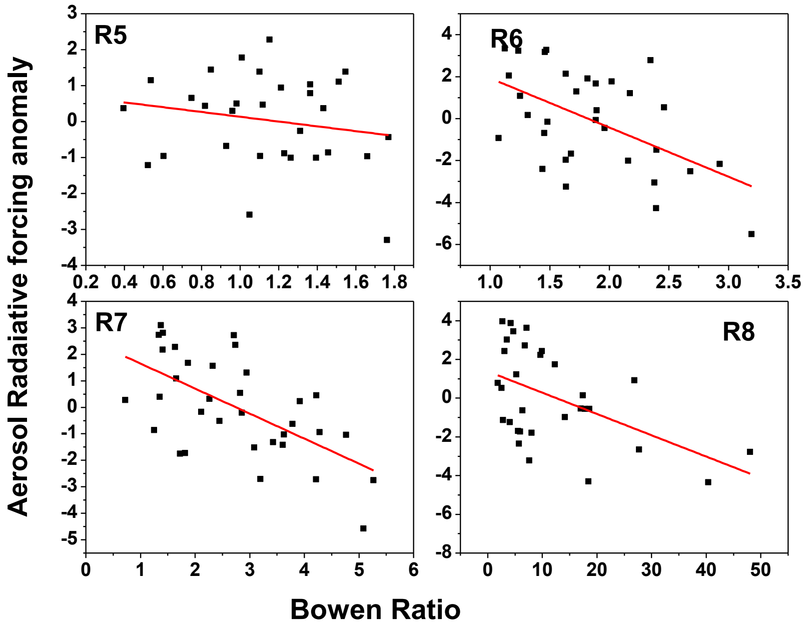

Figure 6.6b: Scatter plot between Bowen ratio and ARF anomaly over the regions R5, R6, R7 and R8 during spring season

Table 6.5: Trend values of different surface flux components for all the four seasons over the selected regions. * indicates statistically significant trend.

		Shortwave	Longwave	Sensible	Latent	Ground	PBL
Summer	R1	-0.87**	1.38**	-0.06	-0.02	4.70	0.28***
	R2	-0.47*	0.33	-0.04	0.13	3.77	0.32***
	R3	-0.57*	0.44*	-0.67*	0.42*	-0.48	0.36***
	R4	-0.26	0.27	-0.22	0.15	1.58	0.36***
	R5	-0.11	0.43	-0.34	0.34*	2.72	0.32***
	R6	0.14	-0.45	0.25*	-0.17	3.95	0.36***
	R7	0.34*	-0.53	0.35*	-0.25	3.28	0.24*
	R8	0.13	-0.16	0.28	-0.25	2.76	0.06
Autumn	R1	-0.40	0.54*	0.82*	-0.84*	-4.13	0.14
	R2	-0.49	0.11	0.09	-0.29	-1.51	0.11
	R3	-0.29	-0.11	0.19	-0.47	1.29	0.10
	R4	-0.08	-0.11	0.28	-0.25	0.56	0.12
	R5	-0.20	-0.06	0.75*	-0.64*	-1.42	0.12
	R6	-0.22	-0.36	-0.11	-0.02	-0.24	0.10
	R7	-0.45	0.47	-0.19	-0.01	-1.52	0.01*
	R8	-0.24	0.20	-0.13	0.04	-2.98	-0.02
Winter	R1	-0.98*	1.15*	-0.30	0.15	-6.47	-0.13*
	R2	-0.95	1.02*	0.86	0.69	-1.29	-0.14*

	R3	-1.29*	1.36*	-0.75	1.75	-0.38	-0.30**
	R4	-0.34	0.69	-0.32	0.71	0.57	-0.20*
	R5	-0.33	0.41	-0.69*	0.54*	-0.20	-0.15*
	R6	-0.31	0.14	0.37	-0.22	3.46	-0.30**
	R7	0.50	-0.38	0.19	0.14	1.87	-0.44***
	R8	0.04	-0.52	0.33	-0.06	-1.97	-0.51***
Spring	R1	-0.09	0.42	-0.16	0.17	-0.91	-0.15*
	R2	0.43	-0.68*	0.55*	-0.59**	6.81	-0.26**
	R3	0.35	-0.48	0.28	-0.39	2.06	-0.27*
	R4	0.50*	-0.73**	0.46*	-0.45*	7.39	-0.31**
	R5	0.13	-0.31	0.28*	-0.26	0.84	-0.25**
	R6	0.09	0.10	0.10	-0.16	2.40	-0.25*
	R7	0.29	-0.44*	0.21	-0.29	6.14	-0.58
	R8	0.18	-0.34	0.09	-0.16	3.90	0.05

6.4 Summary

The effects of aerosols and clouds on surface energy balance over eight selected regions of South Africa were studied using MERRA 2 reanalysis data. The selected regions were based on the Koppen-Geiger classification of climate. A comparison of MERRA 2 and CERES datasets was undertaken.

Comparison of MERRA 2 and CERES shows very good agreement with a correlation of approximately 100 % for shortwave radiation over cold and hot desert regions and a RMSE of 10.12 Wm^{-2} and 10.90 Wm^{-2} respectively. The greatest bias in the measurements for both longwave and shortwave radiation was observed in R6. Furthermore, results indicated that CERES was more accurate compared to MERRA-2 for cloudy regions.

The bias in CERES and MERRA 2 was approximately 5 Wm^{-2} for warm summer mediterranean, cold desert, hot desert and cold semi-arid regions while there was a bias of approximately 25 Wm^{-2} for temperate oceanic, humid subtropical, subtropical highland and hot semi-arid regions in shortwave flux. It was observed that the pattern of climatology and interannual variability for both datasets was similar.

The hot semi-arid region received the highest levels of shortwave radiation while the cold desert regions had the highest amount of longwave and sensible heat flux. The lowest levels of shortwave and sensible heat fluxes were recorded over the temperate oceanic region which also had the highest latent heat flux. All regions received a substantial amount of radiation throughout the year.

The seasonal variability in shortwave, sensible and latent heat indicated a summer maximum and late autumn, early winter minimum. For longwave radiation, a summer minimum and late autumn, early winter maximum was observed, this was linked with increased cloudiness over the study period.

There was negative trend in shortwave radiation over warm summer mediterranean, cold desert, hot desert, cold semi-arid and temperate oceanic regions. A significant decrease over warm summer mediterranean cold and hot desert regions was observed while there was an increase humid subtropical, subtropical highland and hot semi-arid during summer. There was no significant change during autumn, however, during winter, there was a significant decrease in warm summer mediterranean and hot desert regions while during spring, the only significant trend was for the cold semi-arid region.

There was an increase in longwave radiation for the warm summer mediterranean, cold desert, hot desert, cold semi-arid and temperate oceanic regions while decreasing trends were observed for the humid subtropical, subtropical highland and hot semi-arid regions during summer. However, significant trends were only observed for the warm summer mediterranean and hot desert regions. There was a significant trend for the warm summer mediterranean region during autumn while during winter there were increasing trends for the warm summer mediterranean, cold and hot desert regions corresponding to 1.15 Wm^{-2}, 1.02 Wm^{-2}, 1.36 Wm^{-2}. During spring, there were significant decreasing trends in the cold desert, cold semi-arid and subtropical highland regions.

For sensible heat flux, a decreasing trend of -0.67 Wm^{-2} was observed during summer for the hot desert region while increasing trends of 0.25 Wm^{-2} and 0.35 Wm^{-2} were recorded for the humid subtropical and subtropical highland regions in summer. Significant trends of 0.82 Wm^{-2} and 0.75 Wm^{-2} were measured for the warm summer mediterranean and temperate oceanic regions during autumn while the only significant trend in winter was observed in the temperate oceanic region and this corresponded to -0.69 Wm^{-2}. Increasing trends of 0.55 Wm^{-2}, 0.46 Wm^{-2} and 0.28 Wm^{-2} were measured in spring for the cold desert, cold semi-arid and temperate oceanic regions respectively.

For latent heat measurements, increasing trends of 0.42 Wm^{-2} and 0.34 Wm^{-2} for the hot desert and temperate oceanic regions were measured in summer. During autumn, decreasing trends of -0.84 Wm^{-2} and -0.64 Wm^{-2} were observed for the warm summer mediterranean and temperate oceanic regions while in winter, an increasing trend of 0.54 Wm^{-2} was measured for the temperate oceanic region. During spring, trends of -0.59 Wm^{-2} and -0.45 Wm^{-2} were observed for the cold desert and cold semi-arid regions. No significant trend in ground heat flux was seen.

Seasonal variation in AOD showed a spring maximum and winter minimum while that of cloud fraction varied from one region to another. The result of aerosol radiative forcing on shortwave radiation showed significant impact on the temperate oceanic, humid subtropical, subtropical highland and hot semi-arid regions while its effect on longwave radiation was not as pronounced as that on shortwave radiation.

The Bowen ratio showed a strong negative correlation with aerosol effect anomaly during winter and spring for the temperate oceanic, humid subtropical, subtropical highland and hot semi-arid regions. This illustrated that as aerosol effect increased, less radiation reached the surface resulting in a reduction in the Bowen ratio.

References

Aksoy, B. (2011). Solar radiation over Turkey and its analysis. International journal of remote sensing, 32(21), 6261-6272. doi:10.1080/01431161.2010.508056

Carreras, L.G., Marsham, J.H. and Spracklen, D.V. (2017). Observations of increased cloud cover over irrigated agriculture in an arid environment. Journal of hydrometeorology, Vol. 18, 2161-2172. https://doi.org/10.1175/JHM-D-16-0208.1

Dahlback, A., and Bjertness, E. (2008). Global monitoring of atmospheric ozone and solar UV radiation. Solar Radiation and Human Health. Oslo: The Norwegian Academy of Science and Letters, 23-34.

Dlomo, X. (2014). Sea surface temperature trends around Southern Africa (Focusing on the Benguela current system and the Agulhas retroflection area). Dissertation submitted to the department of Oceanography, University of Cape Town.

Drummond, A.J. and Vowinckel, E. (1957). The distribution of solar radiation throughout southern Africa. Journal of meteorology 14(4):343-353.

Hatzianastassiou, N. and Vardavas, I. (2001). Longwave radiation budget of the Southern Hemisphere using ISCCP C2 climatological data. Journal of geophysical research, Vol. 106, 785-798. https://doi.org/10.1029/1999JD900477

Kim, D., and Ramanathan, V. (2008). Solar radiation budget and radiative forcing due to aerosols and clouds. Journal of geophysical research, Vol. 113. doi:10.1029/2007JD008434

Lee, J.N., Susskind, J., Iredell, L., Loeb, N. and Lim, Y.K. (2015). Comparison of OLR datasets from AIRS, CERES and MERRA 2. NASA

Liang, F., and Xia, X. (2005). Long-term trends in solar radiation and the associated climatic factors over China for 1961-2000. Paper presented at the Annales Geophysicae. doi:10.5194/angeo-31-795-2013

Liepert, B. G. (2002). Observed reductions of surface solar radiation at sites in the United States and worldwide from 1961 to 1990. Geophysical Research Letters, 29(10). doi:10.1029/2002GL014910

Loginov, S.V., Ippolitov, I.I. and Kharyutkina, E.V. (2014). The relationship of surface air temperature, heat balance at the surface and radiative balance at the top of atmosphere over the Asian territory of Russia using reanalysis and remote sensing data. International journal of remote sensing, Vol. 35, 5878-5898.

Ogunniyi, J. and Sivakumar, V. (2018). Seasonal variations in global, direct, diffuse radiations over South African cities and Namibia. International conference for solar power systems for Namibia.

Power, H. and Mills, D. (2005). Solar radiation climate change over Southern Africa and an assessment of the radiative impact of volcanic eruptions. International journal of climatology, 25(3), 295-318. https://doi.org/10.1002/joc.1134

Pineker, R.T., Zhang, B. and Dutton, E.G. (2005). Do satellites detect trend in surface solar radiation? Science 308, 850-854. doi: 10.1126/science.1103159

Singh, J., and Kruger, A. (2017). Is the summer season losing potential for solar energy applications in South Africa? Journal of energy in southern Africa, 28(2):52-60.

Singh, J. (2016). Ranking South African provinces on the basis of MERRA 2D surface incident shortwave flux. Journal of energy in Southern Africa 27(3):50-57.

Sinha, P. Jaegle, L. Hobbs, P.V. and Liang, Q. (2004). Transport of biomass burning from southern Africa. Journal of geophysical research 109, D20204. doi:10.1029/2004JD005044

Soni, V., Pandithurai, G., and Pai, D. (2012). Evaluation of long-term changes of solar radiation in India. International journal of climatology, 32(4), 540-551. https://doi.org/10.1002/joc.2294

Tesfaye, M. Sivakumar, V. Botai, J. Tsidu, G.M. (2011). Aerosol climatology over South Africa based on 10 years of Multiangle Imaging Spectroradiometer (MISR) data. Journal of geophysical research 116, D20216. http://dx.doi.org/10.1155/2013/237483

Urankar, G., Prabha, T.V., Pandithurai, G., Pallavi, O., and Achuthavarier, D. (2012). Aerosol and cloud feedbacks on surfaxe energy balance over selected regions of the Indian subcontinent. Journal of geophysical research 117, D04210. doi:10.1029/2011JD016363

Wild, M., Gilgen, H., Roesch, A., Ohmura, A., Long, C.N., Dutton, E.G., Forgan, B., Kallis, A., Russak, V., and Tsvetkov, A. (2005). From dimming to brightening: decadal changes in solar radiation at earth’s surface. Science 308 (5723), 847-850. doi:10.1126/science.1103215

William, C. Conant. (2000). An observational approach for determining aerosol surface radiative forcing: Results from the first field phase of INDOEX. Journal of Geophysical Research. Vol. 105, 347-360.

Zhang, X., Liang, S., Wang, G., Yao, Y., Jiang, B. and Cheng, J. (2016). Evaluation of the reanalysis surface incident shortwave radiation products from NCEP, ECMWF, GSFC, and JMA using satellite and surface observations. Remote sensing, 8. https://doi.org/10.3390/rs8030225

CHAPTER SEVEN

SUMMARY AND FUTURE WORK

Summary

In this work, the intensity of solar radiation received on the earth surface in relation to the total ozone column and aerosol present was examined using both ground-based and satellite instruments for the study. The study focused on South Africa but was also extended to Southern Africa and Africa. We selected 5 different regions in South Africa (Alexander Bay, Bloemfontein, Pretoria, Durban and Port Elizabeth) and Windhoek in Namibia to determine the seasonal variation on global, direct and diffuse irradiance. Using these surfaces, we also examined the variations in shortwave radiation and total cloud fraction. We observed that solar radiation decreased from north-western regions to south-eastern regions. The result also showed higher solar energy potential in South Africa and Namibia when compared with the United States and many parts of Europe. We then divided South Africa into four, the Northern region (Irene and Johannesburg), Eastern region (Durban), Western region (Springbok) and Southern region (Cape Town) to determine the variation in temperature, ozone and ultraviolet aerosol index. High temperature and ultraviolet aerosol index were observed in Durban while in Cape Town, absorbing aerosol was low but with high total ozone. We made use of second order Fourier decomposition to determine the increasing and decreasing trend in total ozone and ultraviolet aerosol index. Using South African climatic type, we divided South Africa to eight (warm summer Mediterranean, cold desert, hot desert, cold semi-arid, temperate oceanic, humid subtropical, subtropical highland and hot semi-arid) to examine the effects of aerosol and clouds on the surface energy balance. The results reveal that aerosol radiative forcing had significant effect on temperate oceanic, humid subtropical, subtropical highland and hot semi-arid regions. Also, for these regions, Bowen ration showed a strong negative correlation with aerosol effect anomaly during winter and spring. Over Africa, we studied the interannual and seasonal variation in shortwave flux, ozone and aerosol index. The result showed that Africa received adequate amount of solar radiation. We observed that the injection of cold air from higher latitude resulted in Algeria having low total ozone while the presence of volatile organic compounds from forests in Morocco resulted in high total ozone. With high desert fires in Namibia, aerosol index was very high.

In conclusion, we were able to achieve the research objectives of this work. The relationship between ozone and solar radiation over various surfaces of South Africa was determined as well as the relationship between ozone and aerosol index. This study also provided broader understanding on the climatology and variation of ozone and aerosol over Africa as well as the effects of aerosol and cloud forcing on different South African surfaces. The solar potential of South African cities was examined and the earth’s radiation budget over South Africa was estimated.

Future Work

In the future, it is necessary to use more instruments for study and validation. It would be of great importance to the research community if a ten-year model of solar radiation can be done as well as other atmospheric parameters. The Aerosol Indirect Effect on solar radiation over South Africa is an area yet to be explored.